UNIVERSITÀ
POLITECNICA
DELLE MARCHE

Università Politecnica delle Marche
Corso di Dottorato in Ingegneria Civile, Ambientale, Edile ed Architettura

---

The role of soil-structure interaction in interpretation of vibration measurements on continuous viaducts

Ph.D. Dissertation of:

Marco Regni

Advisor:

Prof. Ing. Luigino Dezi

Co-Advisor:

Prof. Ing. Fabrizio Gara

Curriculum Supervisor:

Prof. Ing. Stefano Lenci

XXXI ciclo

Università Politecnica delle Marche
Facoltà di Ingegneria
Dipartimento di Ingegneria Civile, Edile ed Architettura

Via Brecce Bianche – 60131 – Ancona, Italia

Acknowledgments

I wish to thank Professor Fabrizio Gara, Sandro Carbonari and Francesca Dezi for their time and patience and for the great opportunity to work with them during these years.

I would like to thank Francesca Dezi for her important support in the geotechnical issues.

I am thankful to Davide Roia for his support during all my PhD activity.

I would like to thank Professor Luigino Dezi and Fabrizio Gara for giving me the chance to accomplish this PhD course.

I would like to thank the laboratory technicians (Enzo D'Aria, Stefano Bufarini, Franco Rinaldi and Andrea Conti) for their skills and support during these years.

Finally, I would like to thank all the PhD of the Department I.C.E.A for supporting me through these years (Michele Morici, Maria Chiara Capatti, Vanni Nicoletti, Laura Gioiella, Fabrizio Scozzese, Lucia Minnucci, Fabio Micozzi, Claudia Canuti and Davide Arezzo).

Contents

List of Figures

List of Tables

Abstract

The scope of this thesis is to identify the significance of soil-structure interaction and site response on the dynamic behaviour of continuous multi-span r.c. viaducts, based on ambient vibration measurements and numerical simulations with finite element models.

For this purpose, an 875 m long bridge, located in Central Italy, founded on piles in eluvial-colluvial soil deposit was instrumented and ambient vibration tests together with geophysical investigations were performed. Experimental modal properties were evaluated by means of operational modal analysis on accelerometric data and the role of soil-structure interaction in the interpretation of the tests was detected by means of finite element models characterised by different accuracy in addressing the interaction problem. In the soil-structure-interaction models the local site condition in correspondence with each bridge piers (determined by geotechnical and geophysical investigations) were taken into account in the definition of the soil-foundations impedances. Comparison between the experimental results obtained from ambient noise measurements on the free-field and on the viaduct deck, permits the identification of both predominant period of the site and the fundamental periods of the structure. In addition, comparisons between results obtained from the different numerical models with the measured dynamic response of the viaduct, in terms of fundamental frequencies and mode shapes, allow the identification of the contribution of different soil-structure interaction aspects such as the pile-soil-pile interaction, the radiation problem, the pile cap embedment as well as the variability of the soil stratigraphy along the longitudinal direction of the viaduct.

Referring to the transverse behaviour, some tests were performed in correspondence with one pier, measuring accelerations of the foundation cap (both translational and rotational components) and the pier bent, in order to identify the contribution to the transverse modal displacement due to the elastic deflection of the pier and the foundation rocking. The test results are compared with those obtained from a 3D finite element model of the viaduct, considering or not the soil-structure interaction problem.

In addition, other two case studies of viaducts, with different characteristics respect to the previous one, were presented, with the aim of extending the study of soil-structure interaction also for foundations with different geometrical characteristics: the first one called “Paglia bridge” is a three-spans continuous deck bridge with steel-concrete composite structure, composed by four steel beams with variable height and a r.c. slab with uniform thickness; the second one, called “Cesano bridge”, is a three-span continuous bridge with steel-concrete composite deck composed by a steel box-girder and a r.c. slab with uniform thickness.

Keywords: r.c. viaduct; Soil-Structure Interaction; dynamic identification; Operational Modal Analysis; finite element model; Foundation rocking.

Sommario

L’oggetto della tesi è lo studio dell’effetto dell'interazione terreno-fondazione-struttura e della risposta del sito sul comportamento dinamico di viadotti continui su più campate, sviluppato sia sperimentalmente tramite misurazioni di vibrazioni ambientali sia numericamente con l’ausilio di modelli raffinati agli elementi finiti.

A tal fine, si sono eseguite misure di vibrazione ambientale su un ponte multi campata di lunghezza 875 m, situato nell'Italia centrale, fondato su pali in un deposito eluviale-colluviale e per caratterizzare dinamicamente il terreno circostante si sono eseguite indagini geofisiche. Le proprietà modali sperimentali sono state valutate mediante l'analisi modale operativa su dati accelerometrici e il ruolo dell'interazione terreno-struttura nell'interpretazione dei test è stato riscontrato mediante modelli agli elementi finiti caratterizzati da diversa accuratezza nella modellazione delle fondazioni e dell’interazione con il terreno. Nei modelli di interazione terreno-struttura, è stata presa in considerazione la condizione locale del sito in corrispondenza di ciascun pilastro del ponte (derivante da indagini geotecniche e geofisiche) nella definizione delle impedenze tra fondazioni e terreno. Il confronto tra i risultati sperimentali ottenuti dalle misure di rumore ambientale sul campo libero e sull’impalcato consente di identificare sia il periodo predominante del sito che i periodi fondamentali della struttura. Inoltre, il confronto tra i risultati ottenuti dai diversi modelli numerici con la risposta dinamica misurata del viadotto, in termini di frequenze fondamentali e forme modali, consente l'identificazione del contributo di diversi aspetti di interazione tra struttura del suolo come l’interazione tra le pile, il problema della dissipazione per radiazione, l'ingombro della zattera e la variabilità della stratigrafia del suolo lungo la direzione longitudinale del viadotto.

Inoltre, con riferimento al comportamento trasversale, sono stati eseguiti alcuni test in corrispondenza di una pila del viadotto per misurare le accelerazioni del pulvino (componenti traslazionali e rotazionali) e della zattera in modo da identificare il contributo allo spostamento modale trasversale dovuto alla deformazione elastica delle pile e alla rotazione della fondazione. I risultati del test sono confrontati con quelli ottenuti dai modelli 3D del viadotto, includendo o meno il problema dell'interazione terreno struttura.

In aggiunta, vengono presentati altri due casi studio di viadotti con caratteristiche diverse al precedente, allo scopo di ampliare lo studio dell’interazione terreno-struttura anche per fondazioni con diverse caratteristiche geometriche; in particolare il ponte sul Paglia si tratta di un ponte ad impalcato continuo su tre campate avente struttura composta, con quattro travi di acciaio ad altezza variabile ed una soletta in c.a. di spessore uniforme, mentre il ponte sul Cesano si tratta di un ponte ad impalcato continuo su tre campate avente struttura composta, con travi di acciaio ‘a cassone’ ed una soletta in c.a. di spessore uniforme.

Parole chiave: Interazione terreno-struttura; identificazione dinamica degli edifici; analisi modale operativa; Modello agli elementi finiti; Rotazione della fondazione.

Introduction

The high Italian seismicity in conjunction with the existing dense transport infrastructure network require the seismic assessment and upgrading of key components of the network links (i.e. bridge, tunnels, earth-retaining system) to improve the overall earthquake resilience of communities. In this framework, system identification and structural health monitoring of structures have recently drawn attention within the civil engineering community for developing real time assessment tools and reducing uncertainties involved within the risk assessment procedure of existing structures. Estimation of the dynamic properties of structures using recorded vibration data allows the calibration of numerical models for the assessment of the structural safety and for the design of seismic retrofit. In this framework, many works are available in the literature, both for buildings (Luco JE. et al 1988, Foti D. 2014, Mirshafiei F. et al 2016, Omenzetter P. et al 2016, Ubertini F. et al 2017, Behmanesh et al 2016, Ranieri C. et al 2012) and for bridges, for which the previous considerations, especially holds since effects of non-structural components on the modal properties are very limited (Cabboi A. et al 2017, Omenzetter P. et al 2013, Cunha A. et al 2006, Zhang J. et al 2013, Zonta D. et al 2014, Polanco NR. et al 2014, Prendergast LJ. et al 2016, Chen GW. et al 2017, Li Y. et al 2017). Various testing techniques, differing for the involved equipment, time-consuming, costs, and dynamic input, can be adopted. The Ambient Vibration Test (AVT) is one of the most attractive methods for the evaluation of the dynamic properties of existing constructions in elastic range since it uses natural vibrations as input (e.g. micro tremors, wind, anthropic activities). Furthermore, small, light, and portable instrumentation is required. On the other hand, because of the low amplitude range of the ambient accelerations, the method requires the use of expensive low-noise wired accelerometers.

It is generally common practice to perform AVTs and then to calibrate finite element models by changing the mechanical properties of materials, achieving the best fit of the model results with the experimental data, especially when materials laboratory tests are not available. On the contrary, geometry of structural components is generally assumed in a deterministic way (assessed or determined through inspections) and the structure restraints at the base are assumed to be fixed. However, with reference to the latter hypothesis, it is well-known in the literature, from both numerical (Capatti MC et al 2017, Carbonari S. et al 2017, Dezi F. et al 2012, Carbonari S. et al 2011, Kappos AJ. et al 2002, Elgamal A. et al 2008, Sextos AG. et al 2003 [Part 1-2], Mylonakis G. et al 2000, Dezi F. et al 2016) and experimental studies (Safak E. 1995, Trifunac MD. et al 2001, Faraonis P. et al 2015), that Soil-Structure Interaction (SSI) may play an important role in the dynamic structural response, especially for medium or soft soil conditions and for existing bridges, which are generally characterised by foundations with relatively low dynamic stiffnesses, mainly deriving from the adoption of dated code prescriptions. In this topic, numerical models developed to interpret results of vibrational measurements should include the modelling of the soil-foundation dynamic compliance before the calibration process, essentially based on

the variation of the material mechanical properties to account for uncertainties related to the material heterogeneity and ageing effects.

The objective of this research work is to address the significance of soil-structure interaction and site response in the interpretation of vibrational tests performed on bridges. For this reason, the Chiaravalle viaduct, that is founded on piles and is connects the SS76 with the airport of Ancona (in Central Italy), is considered. Detailed experimental campaigns and surveys on both the soil deposit and the superstructure were performed to characterise the soil stratigraphy and the mechanical properties of the lithotypes, as well as the geometry of structural elements (e.g. girders, deck slab, piers, etc…) and the relevant mechanical characteristics of materials. Furthermore, AVTs were performed on both the free-field soil and the structure, to evaluate the presence of potential resonance effects between the site and structure and to identify the modal parameters of the bridge, usefull for the assessment of the finite element model to be used for the seismic upgrading design. As for the bridge, the measurement approach required acquisitions of data from more than one configuration of the sensors and the Covariance driven Stochastic Subspace Identification (SSI-Cov) approach (Magalhães F. et al 2011, Cantieni R. 2005) as well as the Post Separate Estimation Re-scaling (PoSER) technique (Dohler E. et al 2010) are adopted to perform the Operational Modal Analysis (OMA). At first, a refined 3D finite element model of the bridge is firstly developed starting from results of the experimental campaign on the superstructure and assuming the hypothesis of fixed base, obtaining fundamental frequencies and mode shapes rather different from the experimental ones. Considering the high level of knowledge of the structural geometry and the material properties, various numerical models accounting for the soil-foundation compliance are developed to improve the matching with the experimental data. The SSI is modelled according to the sub-structure approach, simulating the frequency-dependent soil-foundation impedances through Lumped Parameter Models (LPMs) (Wolf JP. 1988). In detail, the LPM developed (Carbonari S. et al 2018) in is adopted and calibrated to reproduce the dynamic impedances of soil-foundation systems obtained with models with different accuracy in accounting for the pile-soil-pile interaction, the radiation problem, the pile cap embedment as well as the variability of the soil stratigraphy along the longitudinal direction of the viaduct. Modal parameters obtained from the OMA are compared with those derived from all the finite element models of the bridge revealing the significance of SSI in the interpretation of vibrational tests performed on bridges.

For the sake of completeness, two more viaducts case studies with different geometrical characteristics are investigated, to expand the study to a larger case series. In particular, the work deals with some interesting aspects concerning the contribution of the foundation compliance on the dynamic measured response of the structure subjected to ambient vibrations. To this purpose, the Paglia bridge in Orvieto and Cesano bridge, in Corinaldo, are considered.

The present thesis work is subdivided into six chapters (in addition to the present introduction), and their contents are summarized hereinafter.

Chapter 1 describes the ambient vibration tests and their possible uses, the adopted instrumentation and the analysis methodology performed.

Chapter 2 presents the problem of soil-structure interaction (SSI) from a theoretical point of view; the formulation and the solution of the relevant dynamic problem of a superstructure, elastic-linear, supported by a rigid foundation on viscoelastic means are exposed. The direct method is presented, while the method for substructures is explained in a more rigorous way, through the study of the various problems from which it is constituted. The motion equations of the interacting system and the different solution methods are then formulated. Finally, a theoretical description of LPMs is provide.

Chapter 3 is dedicated to the general description of the viaducts. In addition to the description of all the structural elements of “Chiaravalle viaduct” (deck, stacks, abutments and foundations); the geological and geotechnical aspects of the area on which the structure is located are presented, from which the geotechnical model of the subsoil is defined; finally, a short description of “Paglia bridge” and “Cesano bridge”, useful as case studies to evaluate the contribution of the foundation rocking on transversal behaviour is presented.

Chapter 4 presents the results obtained from experimental data in terms of modal parameters with the operative modal analysis (OMA). The results are showed for all the viaducts investigated both for the overall behaviour of the deck and the behaviour of the piers.

Chapter 5 describes in detail the develop of the viaducts finite element model with different details level able to consider the soil-structure interaction problem. First of all, a fixed base model of the viaduct is presented, then how to insert an LPM in the model is shown, the different types of analysis that are carried out and the methodology of data extrapolation after a "Steady State" analysis are reported. In the final part, the conventional finite element model with springs along the piles is presented. Finally, analytical results of the foundation rocking are shown.

Chapter 6 contains all the comparisons and considerations on the obtained results.

Chapter 1.
Ambient Vibration Tests (AVTs)

In a country with a high seismic risk such as Italy, the problems related to the design of new buildings as well as the assessment of seismic vulnerability of the built, especially with strategic importance such as hospitals, bridges and schools, constitute a research field of extreme actuality. In this sense, the knowledge of the dynamic characteristics of the construction, and therefore the methods for experimental modal analysis play a fundamental role for the calibration of the finite element models of the constructions on which to base any safety assessments, design of seismic upgrading interventions, or to correctly interpret the aspects that may cause changes in the dynamic characteristics of buildings over the time. Ambient vibration measurements are performed to evaluate modal parameters of the structures in order to develop and validate a numerical finite element models for the design of the seismic upgrading, but in the case of viaducts or bridges, these tests can be used also to evaluate the soil-structure interaction effects, through the foundation rocking of the piles in the viaducts, or a possible effect of the reduction in the depth of excavation around the piles in the bridges (Figure 1.1).

Figure 1.1 Fields of application of Ambient Vibration Tests

AVTs are performed with the aim of evaluating the modal parameters of the structure (vibration frequencies, modal shapes and damping ratios). To this purpose, piezoelectric monoaxial accelerometers PCB model 393B31 are placed at suitable configurations to capture both translational and rotational components of displacements. Sensors have been connected through coaxial cables to acquisition cards (24-bit NI 9234 acquisition cards and one chassis NI cDAQ-9178) coupled to a laptop equipped with dedicated software.

In ambient vibration tests, the input is not controlled and is assumed to have a flat spectrum such as a white noise. This assumption is not exactly true, and the input magnitude can be of a certain importance when, because of the limited number of available sensors and/or the

insufficient number of channels of the acquisition system, the structural response cannot be measured in just one test. In these cases, tests must be repeated in different times, considering different configurations (i.e. varying the sensor positions) and finally a merging operation of the recorded data is necessary. The Post Separate Estimation Re-scaling (PoSER) approach (Dohler E. et al 2010) is used to process data from non-simultaneous acquisitions; this method requires that a group of sensors, called reference sensors, are left in the same place for all the test configurations so that they can be used to scale the data of different tests, acquired by sensors moved in different places (roving sensors).

For the acquisitions, a time equal to 1000÷2000 times the period of the first mode is recommended and usually, if no more information are available, the fundamental frequency of the structure was preliminary estimated to be 1 Hz and therefore recordings with a duration of 1800 seconds (30 minutes) were made, dividing each time histories into 90 samples of 20 seconds. The analogical signal is sampled at 2048 Hz and all the frequency components in the analogic signal above the Nyquist frequency are removed through a low-pass filter to avoid aliasing.

All the recorded data were processed with standard signal processing techniques before performing the modal analyses. Initially, data were carefully inspected in order to cut those parts characterized by anomalous behaviours (signal clipping, intermittent noise, spikes and so on) due to sensor or measurement chain malfunctioning or due to signal saturation. Then, the contributions of spurious trends were eliminated through a baseline correction (adopting a second order polynomial) and the high frequency content was eliminated by filtering with a Butterworth low pass filter characterized by order 4 and a cut-off frequency of 20 Hz. Finally, signals were down-sampled at 51.2 Hz to decrease the number of data and make the successive analyses faster.

Different techniques were available to elaborate the recorder data, both in the time domain (Random Decrement, Least-Square Complex Exponential (LSCE), Ibrahim, ARMA and SSI-Cov) or in the frequency domain (Peak Picking, Averaged Normalized Power Spectral Density (ANSPD), Enhanced Frequency Domain Decomposition (EFDD) and Least-Square Complex Frequency (LSCF)).

In this thesis, the Stochastic Subspace Identification (SSI) technique (Magalhães F. 2011, Cantieni R. 2005) was used to identify the dynamic properties of the structure from the recordings.

In the case of the bridges, in addition to the tests carried out for the overall identification of the deck, experimental investigations can be performed to evaluate possible contributions of the soil-foundation compliance on the dynamic response of the bridge. For this purpose, some tests were performed in the piers with the aim of identifying the foundation translation and rocking.

Chapter 2.
Soil Structure Interaction (SSI)

Site geomorphology and interaction with the soil can significantly influence the seismic response of structures, as evidenced by post-earthquake investigations and in situ experiences (Sextos et al. 2003, Lupoi et al. 2005). The fixed-base structural models, commonly used for design, fail to capture the actual structural dynamic behaviour as they are not able to describe the deformability and dissipative capacity of the soil-foundation system. Moreover, in the case of motorway or railway viaducts, foundations of piers can be placed on non-homogeneous soils and, consequently, the seismic shaking can be variable at the different piers. In these cases, the Soil-Structure Interaction (SSI) and the non-synchronous seismic inputs must be considered in the analyses. Modern European codes such as EC8, require specific analyses to include these effects. The level of accuracy adopted to model the SSI problem may vary depending on the importance of the structure. However, even if models and analytical procedures are available, an integrated methodology is not yet available.

The procedure to include the effect of SSI in the non-linear response of bridges is based on the technique of decomposing the domain: the kinematic interaction analysis is performed in the frequency domain, with a procedure that considers radiation damping, pile-soil interaction and pile-soil-pile interaction; non-linear inertial interaction analysis, on the other hand, is performed in the time domain with the use of a finite element model of the superstructure.

To reproduce the frequency dependence behaviour of the soil-foundation system, Lumped Parameters Models (LPMs) are usually adopted and calibrated to reproduce the soil-foundation behaviour in a selected frequency range of interest. Therefore, from a structural point of view, considering the deformability of the soil-foundation system generally implies:

- a decrease of the overall stiffness of the structure;
- a modification of the seismic input to account for the actual foundation displacements (which are different for the free-field ones, especially in the case of pile foundations, and may be constituted by rotational components);
- the onset of waves that, propagating in the ground, increase the energy dissipation capabilities of the structure (radiation damping).

The general definition of the problem is therefore the evaluation of the mechanical response of a structure to a variable external excitation with time, taking into account the following aspects:

- deformability of the soil and foundation system;
- dissipation of energy in the soil by geometric damping;
- dissipation of energy in the soil due to its inelasticity;
- inability of the foundation to conform to the free-field motion.

2.1. SSI Direct approach

The topic of SSI can be analysed through two different approaches, the first one is known as a "direct approach", in which the structure and the soil (near field) are modelled simultaneously, together with surrounding constraints able to guarantee the radiation conditions. This approach, which usually requires high computational efforts, allows capturing the soil and structural responses simultaneously and must be used if both systems (soil and structure) behave nonlinearly. A sketch of the direct approach is reported in Figure 2.1, where surrounding constraints consisting of spring-viscous dashpot systems are used to account for the far-field compliance and damping.

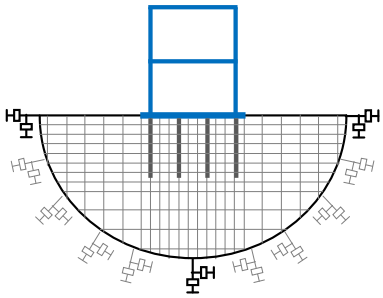

Figure 2.1 Simple scheme of SSI direct approach

To describe the resolving system of an SSI direct approach, for simplicity, the overall soil-foundation-superstructure system can be divided into the following sub-systems

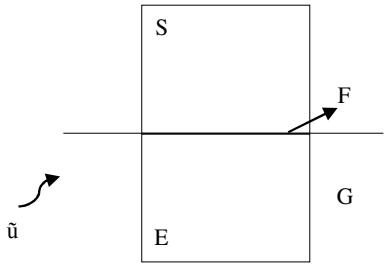

S: Superstructure
E: Embedded
F: Foundation
G: Ground
ũ: Free-field motion

Figure 2.2 Scheme in subsystems of a soil-foundation-superstructure system

The dynamic equilibrium equations for the global system, expressed in the time domain, can be written as

$$\begin{bmatrix} \mathbf{M}_S & 0 & 0 \\ 0 & \mathbf{M}_F & 0 \\ 0 & 0 & \mathbf{M}_E \end{bmatrix} \begin{bmatrix} \ddot{\mathbf{u}}_S \\ \ddot{\mathbf{u}}_F \\ \ddot{\mathbf{u}}_E \end{bmatrix} + \begin{bmatrix} \mathbf{C}_{SS} & \mathbf{C}_{SF} & 0 \\ \mathbf{C}_{FS} & \mathbf{C}_{FF}^S + \mathbf{C}_{FF}^E & \mathbf{C}_{FE} \\ 0 & \mathbf{C}_{EF} & \mathbf{C}_{EE} \end{bmatrix} \begin{bmatrix} \dot{\mathbf{u}}_S \\ \dot{\mathbf{u}}_F \\ \dot{\mathbf{u}}_E \end{bmatrix} + \\ + \begin{bmatrix} \mathbf{K}_{SS} & \mathbf{K}_{SF} & 0 \\ \mathbf{K}_{FS} & \mathbf{K}_{FF}^S + \mathbf{K}_{FF}^E & \mathbf{K}_{FE} \\ 0 & \mathbf{K}_{EF} & \mathbf{K}_{EE} \end{bmatrix} \begin{bmatrix} \mathbf{u}_S \\ \mathbf{u}_F \\ \mathbf{u}_E \end{bmatrix} = \begin{bmatrix} 0 \\ \mathbf{f}_F(t) \\ \mathbf{f}_E(t) \end{bmatrix} \tag{1}$$

where $\boldsymbol{u}$ represents the vector that groups subvectors $\boldsymbol{u}_S$, $\boldsymbol{u}_F$ and $\boldsymbol{u}_E$, collecting displacements of the nodes belonging to the superstructure, the interface and the soil, respectively; $\boldsymbol{M}$, $\boldsymbol{C}$ and $\boldsymbol{K}$ represent the masses, damping and stiffnesses matrix, respectively and $\boldsymbol{f}_F$ and $\boldsymbol{f}_E$ are vectors collecting forces deriving from the pile-soil-pile interactions as a consequence of the seismic wave propagation in the deposit.

If the soil is a viscoelastic medium, the displacements of the soil can be calculated with the relationship

$$\begin{bmatrix} \mathbf{u}_F(t) \\ \mathbf{u}_E(t) \end{bmatrix} = -\int_0^t \begin{bmatrix} \mathbf{h}_{FF}(t-\tau) & \mathbf{h}_{FE}(t-\tau) \\ \mathbf{h}_{EF}(t-\tau) & \mathbf{h}_{EE}(t-\tau) \end{bmatrix} \begin{bmatrix} \mathbf{f}_F(\tau) \\ \mathbf{f}_E(\tau) \end{bmatrix} d\tau + \begin{bmatrix} \tilde{\mathbf{u}}_F(t) \\ \tilde{\mathbf{u}}_E(t) \end{bmatrix} \tag{2}$$

Operating in the field of validity of the overlapping principle of Boltzmann and for the principle of causality, we can note the effects of this force field as the sum of the effects induced by infinitesimal impulses applied in the generic instant τ, exploiting the convolution integral introduced in (2) to obtain the global response in terms of displacement.

This integral, takes into account the effects that an impulsive signal, generated by the effect of $\tilde{\boldsymbol{u}}$ at any point in the foundation, produces around itself by propagating through the surrounding ground. In particular, the terms of the $\boldsymbol{h}$ matrix are Green's elastodynamic functions: they describe the response of a viscoelastic system at a point different from that of the force application, taking into account the phenomena associated with the propagation of a signal in a viscoelastic medium such as internal damping of the ground and radiation damping, the damping associated with the propagation of the signal in the indefinite space.

The problem can be simplified by expressing equation (2) in the frequency domain, through the Fourier transform. By indicating with capital letters, the Fourier Transform of the relevant quantities in the time domain, the following expressions for the force vector can be obtained:

$$\begin{bmatrix} \mathbf{F}_F(\omega) \\ \mathbf{F}_E(\omega) \end{bmatrix} = -\begin{bmatrix} \mathbf{H}_{FF}(\omega) & \mathbf{H}_{FE}(\omega) \\ \mathbf{H}_{EF}(\omega) & \mathbf{H}_{EE}(\omega) \end{bmatrix}^{-1} \left(\begin{bmatrix} \mathbf{U}_F(\omega) \\ \mathbf{U}_E(\omega) \end{bmatrix} - \begin{bmatrix} \tilde{\mathbf{U}}_F(\omega) \\ \tilde{\mathbf{U}}_E(\omega) \end{bmatrix} \right) = \\ = -\begin{bmatrix} \mathbf{K}_{FF}(\omega) & \mathbf{K}_{FE}(\omega) \\ \mathbf{K}_{EF}(\omega) & \mathbf{K}_{EE}(\omega) \end{bmatrix} \left(\begin{bmatrix} \mathbf{U}_F(\omega) \\ \mathbf{U}_E(\omega) \end{bmatrix} - \begin{bmatrix} \tilde{\mathbf{U}}_F(\omega) \\ \tilde{\mathbf{U}}_E(\omega) \end{bmatrix} \right) \tag{3}$$

Taking into account equation (3), system (1) can be re-written in the frequency domain as follows:

$$\begin{bmatrix} \mathbf{K}_{SS}-\omega^2\mathbf{M}_{SS}+i\omega\mathbf{C}_{SS} & \mathbf{K}_{SF}+i\omega\mathbf{C}_{SF} & 0 \\ \mathbf{K}_{FS}+i\omega\mathbf{C}_{FS} & \mathbf{K}_{FF}^{S+E}-\omega^2\mathbf{M}_{FF}+i\omega\mathbf{C}_{FF}^{S+E} & \mathbf{K}_{FE}+i\omega\mathbf{C}_{FE} \\ 0 & \mathbf{K}_{EF}+i\omega\mathbf{C}_{EF} & \mathbf{K}_{EE}-\omega^2\mathbf{M}_{EE}+i\omega\mathbf{C}_{EE} \end{bmatrix} \begin{bmatrix} \mathbf{U}_S(\omega) \\ \mathbf{U}_F(\omega) \\ \mathbf{U}_E(\omega) \end{bmatrix} = \tag{4}$$
$$= \begin{bmatrix} 0 & 0 & 0 \\ 0 & \mathbf{K}_{FF}^{G}(\omega) & \mathbf{K}_{FE}^{G}(\omega) \\ 0 & \mathbf{K}_{EF}^{G}(\omega) & \mathbf{K}_{EE}^{G}(\omega) \end{bmatrix} \begin{bmatrix} 0 \\ \tilde{\mathbf{U}}_F(\omega) \\ \tilde{\mathbf{U}}_E(\omega) \end{bmatrix} = \begin{bmatrix} 0 \\ \tilde{\mathbf{F}}_F(\omega) \\ \tilde{\mathbf{F}}_E(\omega) \end{bmatrix}$$

Collecting the vector of displacements and introducing the matrix of impedances ***Z***, equation (4) can be rewritten in the compact form

$$\begin{bmatrix} \mathbf{Z}_{SS} & \mathbf{Z}_{SF} & 0 \\ \mathbf{Z}_{FS} & \mathbf{Z}_{FF}^{S}+\mathbf{Z}_{FF}^{EG} & \mathbf{Z}_{FE} \\ 0 & \mathbf{Z}_{EF} & \mathbf{Z}_{EE} \end{bmatrix} \begin{bmatrix} \mathbf{U}_S(\omega) \\ \mathbf{U}_F(\omega) \\ \mathbf{U}_E(\omega) \end{bmatrix} = \begin{bmatrix} 0 \\ \tilde{\mathbf{F}}_F(\omega) \\ \tilde{\mathbf{F}}_E(\omega) \end{bmatrix} \tag{5}$$

System (5) represents the solving system according to the SSI direct approach. It is evident that the problem solution is very complex, since all the subsystems in which we have divided the problem are coupled.

2.2. SSI Substructure approach

The second approach is known as "substructures approach" and is consists in a technique where the SSI problem is solved by decomposing the whole soil-foundation-superstructure system into two subsystems (the soil-foundation system and the structural system). The response of the soil-foundation system subjected to the seismic excitation is firstly determined, obtaining the system compliance and the foundation input motion; then the structural response on compliant restraints subjected to the foundation motion is evaluated. The approach allows adopting specific analysis methodologies and tools to study the soil-foundation system (kinematic interaction analysis and impedances determination) and the superstructure system (inertial interaction analysis). The substructure approach is based on the superposition principle, valid for linear systems but can be also adopted to include structural nonlinearities.

The global response is fully determined through the following three steps:

1. solution of the kinematic interaction problem. This step allows capturing the soil-foundation interactions and leads to the evaluation of the foundation input motion (FIM), namely the motion experienced by the foundation subjected to the seismic wave field. Due to the soil-foundation system linearity the problem is solved in the frequency domain in order to easily account for the frequency-dependent behaviour of the system.
2. Evaluation of the soil-foundation system dynamic stiffness. This step leads to the evaluation of the frequency-dependent dynamic impedance matrix of the soil-foundation system, detached from the superstructure. The real part of the impedance matrix, reflects the compliance of the soil-foundation system and it may be represented by a spring with a frequency-dependent coefficient, while the imaginary part captures the energy dissipation occurring in the soil as the foundation vibrates (mainly due to the radiation damping).
3. Calculation of the dynamic response of the structural system subjected to the FIM. Inertial interaction is taken into account in this step. In order to evaluate inertial effects in the soil-foundation system, the inertial contribution to the foundation motion, which may be determined at this step by subtracting the FIM to the inertial foundation displacement, needs to be evaluated and applied to the soil-foundation system at the foundation level. The global soil-foundation response is finally determined superimposing the latter results to those determined in step 1.

The inertial interaction analysis can be performed either through time and frequency domain analyses. Frequency-domain analyses are carried out by implementing the frequency-dependent dynamic impedance matrix previously computed in the finite element model (FEM) of the superstructure, at the foundation level. This generally presents difficulties since commercial structural analysis programs does not include library elements able to introduce fully coupled frequency-dependent matrices. In time-domain analyses, otherwise, it is possible to account for the linear or non-linear behaviour of the superstructure. However, the frequency dependent impedance matrix of the soil-foundation system cannot be used and an implementation strategy must be adopted. Generally, dynamic Lumped Parameter Models (LPMs) having frequency independent parameters are used; parameters are calibrated so that the dynamic impedance of the LPM approximates the soil-foundation one in the frequency range of interest. Figure 2.3 reports a scheme of the "sub-structures approach".

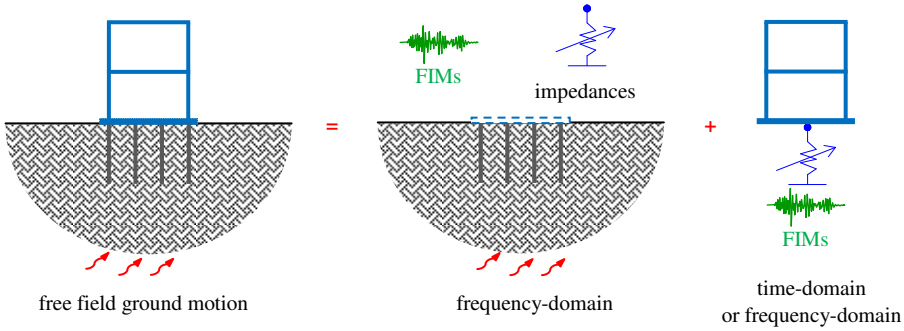

Figure 2.3 Simple scheme of SSI substructures approach

The substructure approach (applicable under the hypothesis of validity of the overlapping effects principle) allows to solve this system of equations by decoupling the soil-foundation system from that of the superstructure and solving two different systems of equations separately. The first phase is called kinematic interaction and analyses the substructure consisting of E and G (Figure 2.4)

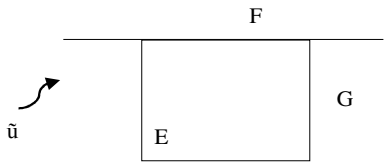

F: Foundation
E: Embedded
G: Ground
ũ: Free-field motion

Figure 2.4 Scheme in subsystems EG in SSI substructure approach

The solving system of this substructure makes it possible to derive the displacements to which the underground foundation is subjected due to the effect of the seismic input, in the absence of superstructure, the motion at the base of the structure (at interface F) and the dynamic impedance of the foundation soil system. This system is:

$$\begin{bmatrix} \mathbf{Z}_{FF}^{EG} & \mathbf{Z}_{FE} \\ \mathbf{Z}_{EF} & \mathbf{Z}_{EE} \end{bmatrix} \begin{bmatrix} \mathbf{U}_{F,K} \\ \mathbf{U}_{E,K} \end{bmatrix} = \begin{bmatrix} \tilde{\mathbf{F}}_F \\ \tilde{\mathbf{F}}_E \end{bmatrix} \tag{6}$$

where $\boldsymbol{U}_{F,K}$ and $\boldsymbol{U}_{E,K}$ are the "kinematic" displacements. Evaluating $\boldsymbol{U}_{E,K}$ from the second equation of (6) and replacing it in the first equation of (6), the following expression is obtained:

$$\left[\mathbf{Z}_{FF}^{EG} - \mathbf{Z}_{FE}^{EG} \left(\mathbf{Z}_{EE}^{EG} \right)^{-1} \mathbf{Z}_{EF}^{EG} \right] \mathbf{U}_{F,K} = \tilde{\mathbf{F}}_F - \mathbf{Z}_{FE}^{EG} \left(\mathbf{Z}_{EE}^{EG} \right)^{-1} \tilde{\mathbf{F}}_E \tag{7}$$

If we indicate with $\Im = \mathbf{Z}_{FF}^{EG} - \mathbf{Z}_{FE}^{EG} \left(\mathbf{Z}_{FE}^{EG} \right)^{-1} \mathbf{Z}_{EF}^{EG}$ the impedance of soil-structure system, the displacements $\boldsymbol{U}_{F,K}$ and $\boldsymbol{U}_{E,K}$ can be determined as follow

$$\mathbf{U}_{F,K} = \mathbf{U}_{FIM} = \Im^{-1} \left[\tilde{\mathbf{F}}_F - \mathbf{Z}_{FE}^{EG} \left(\mathbf{Z}_{EE}^{EG} \right)^{-1} \tilde{\mathbf{F}}_E \right] \tag{8}$$

$$\mathbf{U}_{E,K} = \left(\mathbf{Z}_{EE}^{EG} \right)^{-1} \left\{ \tilde{\mathbf{F}}_E - \mathbf{Z}_{EF}^{EG} \Im^{-1} \left[\tilde{\mathbf{F}}_F - \mathbf{Z}_{FE}^{EG} \left(\mathbf{Z}_{EE}^{EG} \right)^{-1} \tilde{\mathbf{F}}_E \right] \right\} \tag{9}$$

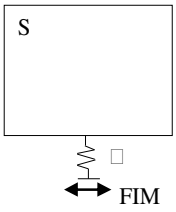

S: Sovrastructure

□: Impedance

FIM: Foundation Input Motion

Figure 2.5 Scheme in subsystems S in SSI substructure approach

Taking into account equations (7) and (8), $\boldsymbol{U}_E$ can be obtained from the third equation of (5). It results

$$\mathbf{U}_E = \left(\mathbf{Z}_{EE}^{EG}\right)^{-1}\left(\tilde{\mathbf{F}}_E - \mathbf{Z}_{EF}^{EG}\mathbf{U}_F\right) \tag{10}$$

From the second equation of (5), it can be obtained:

$$\mathbf{Z}_{FS}\mathbf{U}_S + \left(\mathbf{Z}_{FF}^{S} + \mathfrak{I}\right)\mathbf{U}_F = \mathfrak{I}\mathbf{U}_{FIM} \tag{11}$$

So, the solving system of inertial interaction for the superstructure, is represented in the following form:

$$\begin{bmatrix} \mathbf{Z}_{SS} & \mathbf{Z}_{SF} \\ \mathbf{Z}_{FS} & \mathbf{Z}_{FF}^{S} + \mathfrak{I} \end{bmatrix}\begin{bmatrix} \mathbf{U}_S \\ \mathbf{U}_F \end{bmatrix} = \begin{bmatrix} 0 \\ \mathfrak{I}\cdot\mathbf{U}_{FIM} \end{bmatrix} \tag{12}$$

The system (12), in which the results of the kinematic interaction were highlighted (the influence of the foundation and of the soil on the superstructure), provides displacements and stresses on the superstructure. Determined $\boldsymbol{U}_F$, is also possible to determine the movements of the underground foundation from (10). The difference between the latter and those obtained from the kinematic interaction phase are the so-called inertial displacements of the foundation.

2.3. Lumped parameter model for time-domain analysis

The analysis of the soil-foundation system allows evaluating the soil-foundation dynamic impedances, namely the complex-valued forces-displacements relationships which define the compliant restraints of the superstructure in the subsequent inertial interaction analysis. Different models have been developed over the years to this purpose, however, since foundation impedances are frequency-dependent functions, all procedures furnish results that may be adopted directly only if the inertial interaction analysis of the superstructure is performed in the frequency-domain.

Dezi et al. (2009), recently proposed a numerical model for the analysis of the 3D kinematic interaction of the groups of piles on horizontal-layer plots, based on the BEM-FEM pair where the piles are modelled with beam elements while the ground is schematised with horizontal, independent and infinite layers. The dynamics of the ground layer is described by means of the Green functions, which allow to consider both the pile-soil-pile interactions and the irradiation damping. These derive from a simplification of the Novak plan model, (1978) also developed by Gazetas and Dobry, (1984). The model allows to evaluate all the components of the impedance-dependent matrix of the foundation (eg translational, rotational and roto-translational impedances).

Foundation impedances are frequency-dependent functions, all previous procedures provide results that can be directly adopted in an analysis of the superstructure interaction in the frequency domain (inertial interactions). However, this type of analysis can only be used if the superstructure behaves linearly, moreover it is a typology of analysis less know to professional engineers than to the analysis in the time domain. If the analysis of the inertial interaction are developed in the time domain, as in the case of non-linear behaviour of the structure, the Lumped Parameter Model (LPM) must be introduced, obtained by assembling springs, masses and dampers to reproduce the behaviour dynamic of the foundation.

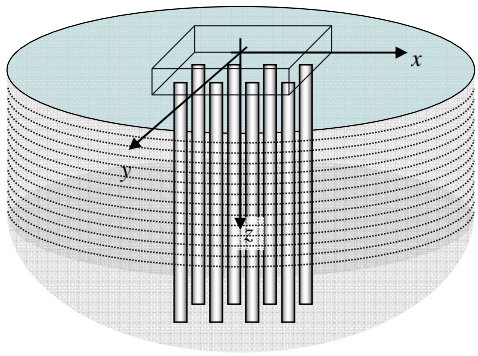

Figure 2.6 Soil-foundation system

A generic set of vertical piles placed in a stratified soil and connected at the head by a rigid cap is considered (Figure 2.6). The group of n piles of length L is modelled with elastic Euler-Bernoulli beam elements embedded in a medium constituted by independent horizontal viscoelastic infinite layers. Under the assumption that no gaps arise between piles and soil during the motion, the problem is linear, and the dynamic equilibrium condition of the system can be derived from the Lagrange-D'Alembert principle. By approximating the displacement field within the piles, according to the finite element approach, the following complex valued system of coupled linear algebraic equations can be obtained

$$\left[\mathbf{K}_P - \omega^2 \mathbf{M}_P + \mathbf{Z}_P(\omega)\right] \mathbf{U}(\omega) = \mathbf{f}(\omega) \tag{13}$$

where $\mathbf{K_P}$, $\mathbf{M_P}$ and $\mathbf{Z_P}(\omega)$ are the stiffness and mass matrices of the piles and the impedance matrix of the soil, respectively, obtained by assembling the contributions of the elements, $\boldsymbol{U}(\omega)$ is the vector grouping the pile nodal displacements and $\boldsymbol{f}(\omega)$ is the vector of the external nodal forces due to the free-field motion.

The cap that connects the pile heads is considered by introducing a rigid body constraint characterised by the geometric matrix $\boldsymbol{A}$ that permits to express the nodal displacement vector as a linear function of the 6 displacements of the rigid body master node F ($\boldsymbol{U}_F$) and the displacements of the sections of the piles embedded in the layered media ($\boldsymbol{U}_E$),

$$\mathbf{U} = \mathbf{A}\begin{bmatrix} \mathbf{U}_F \\ \hline \mathbf{U}_E \end{bmatrix} \tag{14}$$

Taking (14) into account, (13) transforms into

$$\left[\begin{array}{c|c} \mathbf{Z}_{FF} & \mathbf{Z}_{FE} \\ \hline \mathbf{Z}_{EF} & \mathbf{Z}_{EE} \end{array}\right]\begin{bmatrix} \mathbf{U}_F \\ \hline \mathbf{U}_E \end{bmatrix} = \begin{bmatrix} \mathbf{f}_F \\ \hline \mathbf{f}_E \end{bmatrix} \tag{15}$$

Where

$$\left[\begin{array}{c|c} \mathbf{Z}_{FF} & \mathbf{Z}_{FE} \\ \hline \mathbf{Z}_{EF} & \mathbf{Z}_{EE} \end{array}\right] = \mathbf{A}^T\left(\mathbf{K}_P - \omega^2\mathbf{M}_P + \mathbf{Z}_P\right)\mathbf{A} \qquad \begin{bmatrix} \mathbf{f}_F \\ \hline \mathbf{f}_E \end{bmatrix} = \mathbf{A}^T\mathbf{f}_P \tag{16}$$

System (16) can be thus condensed as

$$\mathfrak{I}(\omega)\mathbf{d}_F = \mathbf{f}_F - \mathbf{Z}_{FE}\mathbf{Z}_{EE}^{-1}\mathbf{f}_E \tag{17}$$

Where

$$\mathfrak{I}(\omega) = \left(\mathbf{Z}_{FF} - \mathbf{Z}_{FE}\mathbf{Z}_{EE}{}^{-1}\mathbf{Z}_{EF}\right) \tag{18}$$

is the 6x6 impedance matrix of the soil-foundation system that expresses forces to be applied at F in order to produce unit steady uncoupled vibrations of the node F itself. This matrix is complex-valued and is generically fully populated depending on the piles layout and the position of the reference node; however, in the case of doubly symmetric system, by locating the reference node F at the intersection of the two symmetry axes, the impedance matrix has the form

$$\Im(\omega)=\begin{bmatrix} \Im_x & 0 & 0 & 0 & \Im_{x-ry} & 0 \\ & \Im_y & 0 & \Im_{y-rx} & 0 & 0 \\ & & \Im_z & 0 & 0 & 0 \\ & & & \Im_{rx} & 0 & 0 \\ & sym & & & \Im_{ry} & 0 \\ & & & & & \Im_{rz} \end{bmatrix} \tag{19}$$

If time-domain inertial interaction analyses are performed, as in this case, suitable Lumped Parameter Models (LPMs) must be introduced to reproduce the foundation dynamic behaviour. LPMs are constituted by frequency-independent springs, dashpots and masses, suitably assembled and calibrated in order to reproduce the dynamic behaviour of the soil-foundation system. The numerical model of Dezi et al. (2009), in which piles are modelled with beam elements and the soil is schematized with independent horizontal infinite layers, is used for the definition of the foundation impedances, while the LPM parameters are determined in accordance to the model proposed by Carbonari et al. (2012).

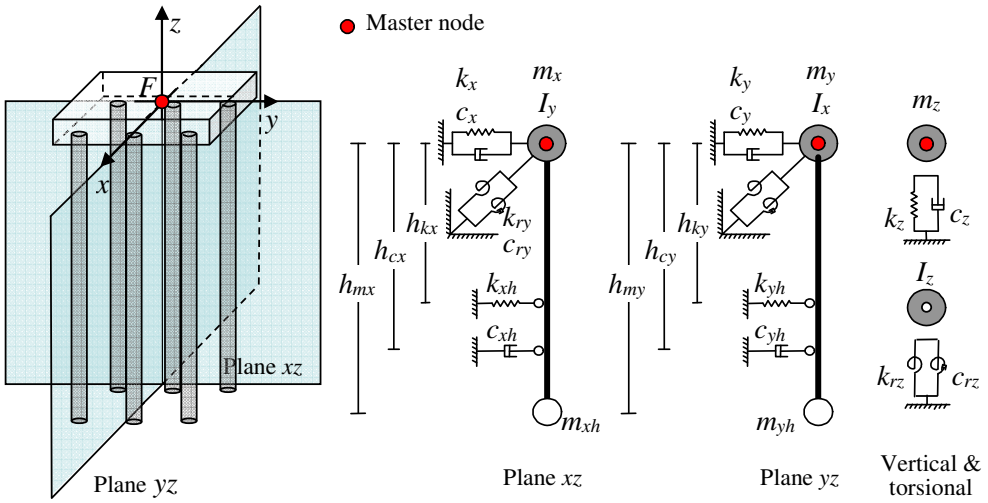

Figure 2.7 Scheme of the adopted LPM

In this thesis the LPM presented by Carbonari et al. (2012) is adopted to simulate the soil-foundation dynamic behaviour of each pier in the CB models (Figure 2.7). Each LPM is characterized by 24 parameters, namely the translational (m_x, m_y and m_z) and rotational masses (I_x, I_y and I_z), lumped at the external node of the LPM, the elastic (k_x, k_y, k_{rx}, k_{ry}, k_z and k_{rz}) and viscous (c_x, c_y, c_{rx}, c_{ry}, c_z and c_{rz}) constants that define the relevant spring-dashpot elements and two additional eccentric masses (m_{xh}, m_{yh}) connected to the external node by stiff links (of lengths h_x and h_y) and to the ground by spring-dashpot elements (k_{xh}, k_{yh}, c_{xh}, c_{yh}). The adopted LPM is capable to reproduce the frequency dependent dynamic impedance

matrix of pile foundations characterised by a double symmetric layout, assuming the external node (i.e. the node representing the interface between the soil-foundation system and the superstructure) located at the intersection of the two symmetry axes (Figure 2.7). By defining by $\mathbf{U}_x$, $\mathbf{U}_y$, $\mathbf{U}_z$, $\mathbf{\Phi}_x$, $\mathbf{\Phi}_y$ and $\mathbf{\Phi}_z$ the displacement and rotations of the external node along and around axes of the reference system frame (Figure 2.7), the dynamic equilibrium equations of the LPM in the frequency domain can be formulated as follows:

$$\begin{bmatrix} \mathbf{F}_x \\ \mathbf{F}_y \\ \mathbf{F}_z \\ \mathbf{M}_x \\ \mathbf{M}_y \\ \mathbf{M}_z \end{bmatrix} = \begin{bmatrix} \Im_x & 0 & 0 & 0 & \Im_{x-ry} & 0 \\ & \Im_y & 0 & \Im_{y-rx} & 0 & 0 \\ & & \Im_z & 0 & 0 & 0 \\ & & & \Im_{rx} & 0 & 0 \\ & sym & & & \Im_{ry} & 0 \\ & & & & & \Im_{rz} \end{bmatrix} \begin{bmatrix} \mathbf{U}_x \\ \mathbf{U}_y \\ \mathbf{U}_z \\ \mathbf{\Phi}_x \\ \mathbf{\Phi}_y \\ \mathbf{\Phi}_z \end{bmatrix} \tag{20}$$

where ω is the circular frequency and $\mathbf{F}_x$, $\mathbf{F}_y$, $\mathbf{F}_z$, $\mathbf{M}_x$, $\mathbf{M}_y$ and $\mathbf{M}_z$ are the external generalised forces applied at the external node. Components of the impedance matrix in equation (20) assume the form

$$\Im_x = \left(k_x + k_{xh}\right) - \omega^2 \left(m_x + m_{xh}\right) + i\omega\left(c_x + c_{xh}\right) \tag{21}$$

$$\Im_y = \left(k_y + k_{yh}\right) - \omega^2 \left(m_y + m_{yh}\right) + i\omega\left(c_y + c_{yh}\right) \tag{22}$$

$$\Im_z = k_z - \omega^2 m_z + i\omega c_z \tag{23}$$

$$\Im_{rx} = \left(k_{rx} + k_{xh}h_{kx}^2\right) - \omega^2 \left(I_x + m_{xh}h_{mx}^2\right) + i\omega\left(c_{rx} + c_{xh}h_{cx}^2\right) \tag{24}$$

$$\Im_{ry} = \left(k_{ry} + k_{yh}h_{ky}^2\right) - \omega^2 \left(I_y + m_{yh}h_{my}^2\right) + i\omega\left(c_{ry} + c_{yh}h_{cy}^2\right) \tag{25}$$

$$\Im_{rz} = k_{rz} - \omega^2 I_z + i\omega c_{rz} \tag{26}$$

$$\Im_{x-ry} = k_{xh}h_{kx} - \omega^2 m_{xh}h_{mx} + i\omega c_{xh}h_{cx} \tag{27}$$

$$\Im_{y-rx} = -\left(k_{yh}h_{ky} - \omega^2 m_{yh}h_{my} + i\omega c_{yh}h_{cy}\right) \tag{28}$$

It is worth noting that the lumped system can account for the translational, rotational and coupled roto-translational behaviour of deep foundations, as well as the vertical and torsional behaviour. According to the LPM assemblage, real part of the impedances matrix components are characterised by second-order parabolas while imaginary parts vary linearly with ω. Further details about the LPM can be found in Carbonari et al (2012).

Chapter 3.
Viaduct descriptions

3.1. “Chiaravalle Viaduct” – Chiaravalle (AN), Italy

3.1.1. Position and main features

The "Chiaravalle Viaduct” in Central Italy connects the SS76 road to the "Raffaello Sanzio" airport (Figure 3.1). The viaduct has a total length of 875 m and is constituted by 4 Kinematic Chains (KC#), separated by structural joints (Figure 3.2). The KCs, involving 13, 10, 3 and 5 spans, respectively, each one of length 27.5 m, are constituted by simply supported girders connected over the piers through post-tension cables at the level of the concrete slab (Figure 3.3a).

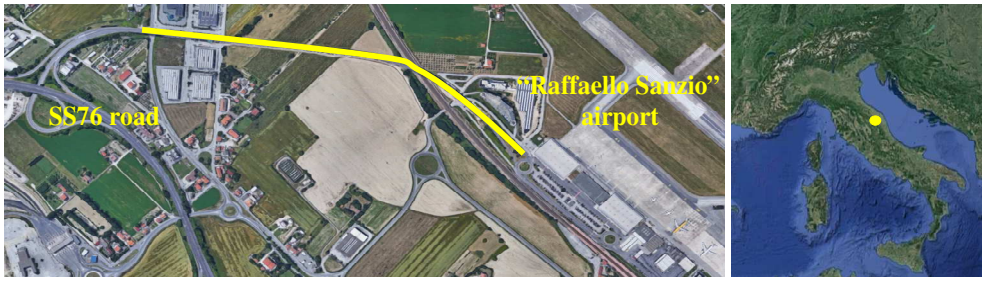

Figure 3.1 Geographic position of the viaduct (from Google Maps)

The deck is 12.10 m wide and is constituted by three simply supported V-shaped r.c. beams underlying a 0.25 m thick concrete slab. The column bent piers are constituted by 2 circular columns with diameter of 1.4 m, with heights (distance between the top of the pile foundation cap and the bottom of the column cap, it is indicate with “var.” in Figure 3.4) ranging between 5.50÷9.47 m for KC1, 9.47÷11.50 m for KC2, 5.25÷9.70 m for KC4 (Table 1).

The length of the V-shaped beams is 26 m calculated in axis supports. The span between the piers 24 and 25, located above the railway line Orte-Falconara Marittima, is an exception, because its deck consists in a box beam in c.a.p., with a total length of 51.80 m, ending with two Gerber saddles, on which the trapezoidal beams of the adjacent spans are connected.

There are expansion joints in flooring at the piers P13 and P23, while the other spans are connected in the slab by inserting Ø40 and Ø50 bars.

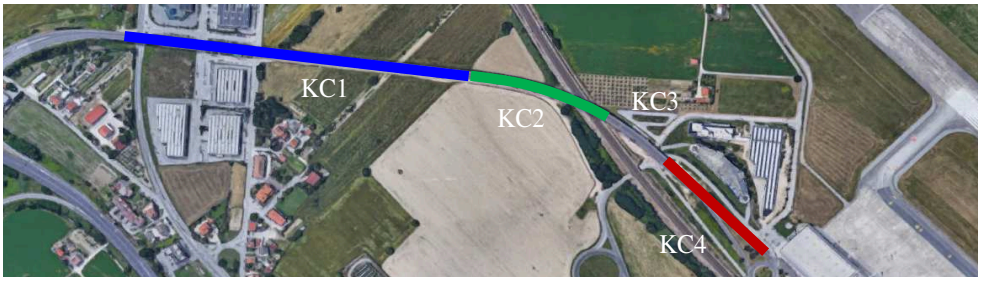

Figure 3.2 Plane location of KCs

It is worth mentioning that only one pier (P17 in Table 1) of the whole viaduct (the 5th of KC2) has a different geometry, since it is characterized by a single column with a rounded rectangular cross section with a maximum size of 7.40 x 1.40 m (Figure 3.3b).

Table 1. Height of the piers

KC1	***P1***	***P2***	***P3***	***P4***	***P5***	***P6***	***P7***	***P8***	***P9***	***P10***	***P11***	***P12***	***P13***
h [m]	5.50	6.50	7.05	7.50	7.50	7.50	8.00	7.97	8.54	8.47	8.96	8.97	9.47
KC2	***P13***	***P14***	***P15***	***P16***	***P17***	***P18***	***P19***	***P20***	***P21***	***P22***	***P23***	-	-
h [m]	9.47	9.50	9.98	9.98	*8.60*	10.5	10.5	11.0	11.0	11.5	11.0	-	-
KC4	***P26***	***P27***	***P28***	***P29***	***P30***	-	-	-	-	-	-	-	-
h [m]	9.70	8.76	7.80	7.25	5.25	-	-	-	-	-	-	-	-

(a) (b)

Figure 3.3 (a) Cross section of the viaduct and column bent pier, (b) wall pier

All foundations are made of plinths on groups of Ø1000 mm bored piles of variable length between 27.0 and 35.5m. The pile foundation cap of the piers, with a thickness of 1.70 m, have a rectangular plan (9.00 x 5.00 m) and connect 6 Ø1000 mm piles, with 3.5 m

wheelbase, arranged on two spaced rows of 3.0 m (Figure 3.4). The pier P17 has a pile foundation cap with a plan of dimensions equal to 10.80x10.00 m and thickness varying from 2.0 m, in the middle of pile foundation cap, at 1.40 m at the ends (Figure 3.5).

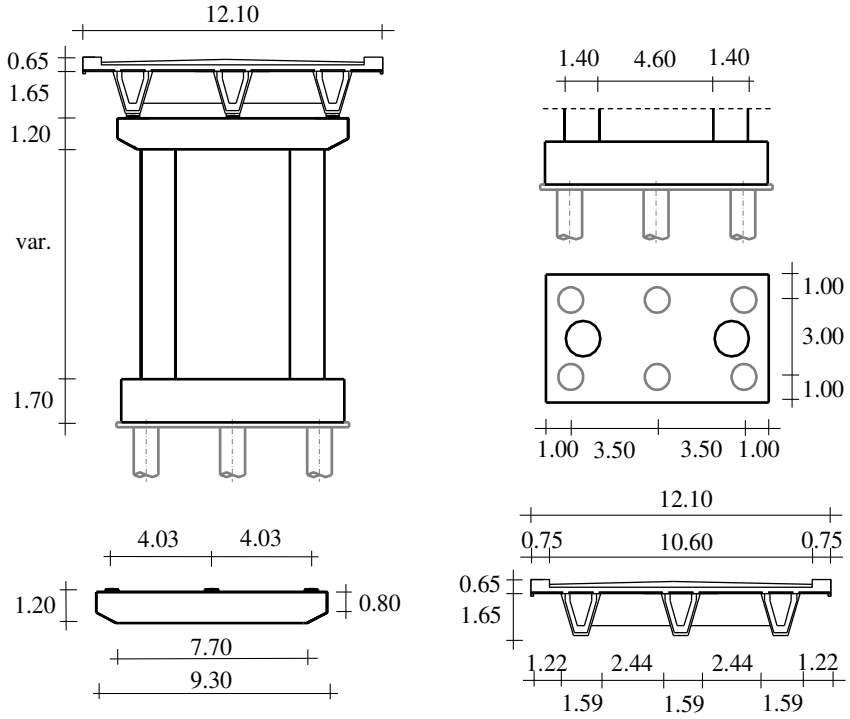

Figure 3.4 Dimensions of the viaduct cross section, including foundations

During construction, 240 concrete samples were taken and tested at the Materials and Structures Testing Laboratory of the Università Politecnica delle Marche. Results of experimental tests are synthetically reported in Table 2 in terms of concrete compressive strength fc and elastic modulus E_c for different structural components. As for reinforcements, rebars FeB44k with nominal yielding strength of 435 MPa were used.

Table 2. Mechanical properties of concrete

Structural element	Number of specimens	f_{cm} [MPa]	f_{ck} [MPa]	R_{ck} [MPa]	E_c [MPa]
Columns	33	17.0	14.3	20.99	25796.3
Foundation piles	20	7.5	4.5	6.63	20180.9
Pile foundation cap	29	12.8	9.6	14.09	23691.1
Columns cap	8	27.1	22.1	32.43	29669.7
Beams	10	40.7	35.7	42.04	33519.8

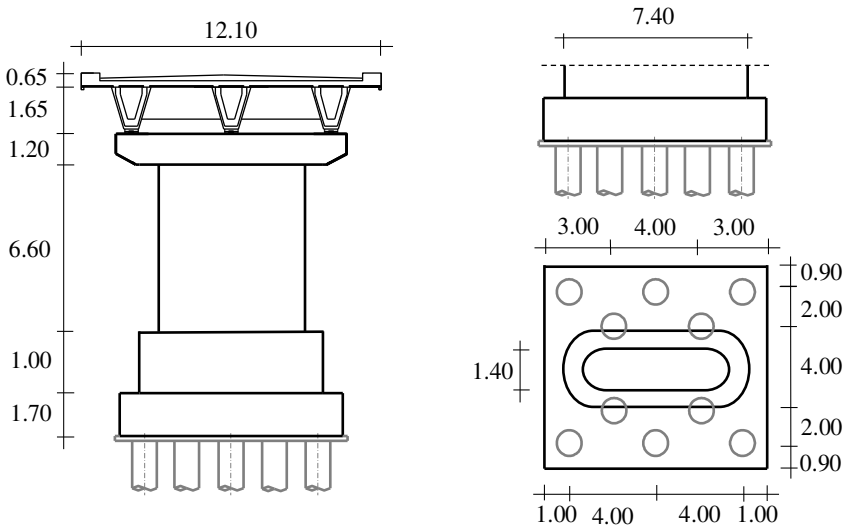

Figure 3.5 Dimensions of the P17 cross section, including foundations

With respect to vertical loads, each span of the viaduct has a simply supported decks static scheme. About the response to horizontal longitudinal actions, it acts as a monolithic element, thanks to the presence of the connections in the slab designed to form a "kinematic chain", connected either to the abutment or to the affine fixed pier.

Each span is arranged on six steel-teflon supports (3 + 3); the lateral beams rest on the 200 t multi-directional ones while the central ones on 30 t longitudinal unidirectional supports of transverse force. There are transverse restraints on each pier consisting of r.c. projections pairs embedded in the pulvinus and placed on the sides of the central beam.

3.1.2. Site characterization

The viaduct is located in the area between Falconara Marittima and Chiaravalle (two towns of the Marche region in Central Italy). From the geomorphological point of view, is a wide almost flat area with low altitudes set at almost 17-20 m above the mean sea level. With reference to Figure 3.7a, the geological configuration of the site is constituted by three main formations: a Plio-Pleistocene marine deposit, prevalently composed of Pleistocene marly, silty clays (AD4) underlying a recent continental covering soil that mainly consists of Quaternary (Pleistocene-Holocene) eluvial-colluvial (sandy and clayey silts, AD1) and Plio-Pleistocene alluvial (mainly sandy gravels with clayey silts lenses, AD2) deposits. Locally, above the Plio-Pleistocene clayey substratum, lenses of sands in clayey-silty matrix can be found (AD3) (Figure 3.6).

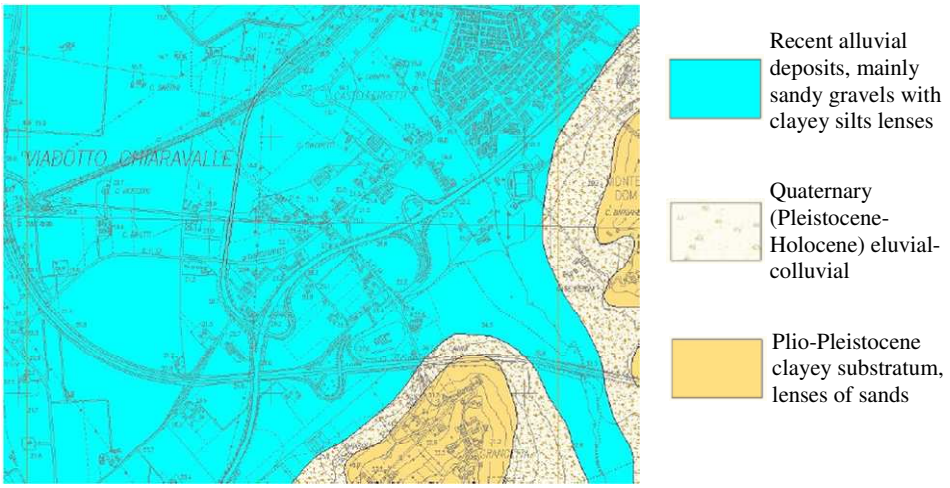

Figure 3.6 Geolithological map

Before the execution of the AVTs, data obtained from previous laboratory and field geotechnical testing performed along the viaduct in 1982 and 1984 were collected, and new geotechnical and geophysical explorations were performed in 2011 and 2012 for the specific purpose of the bridge seismic upgrading. Overall, the area was investigated by means of Boreholes (B), laboratory tests (e.g. triaxial tests, oedometer test) and in-situ Standard Penetration Test (SPT) conducted up to a maximum depth of about 24 m. The geophysical characterisation was performed through a Multichannel Analysis of Surface Waves (MASW), Horizontal to Vertical Spectral Ratio (HVSR) and Down Holes (DH).

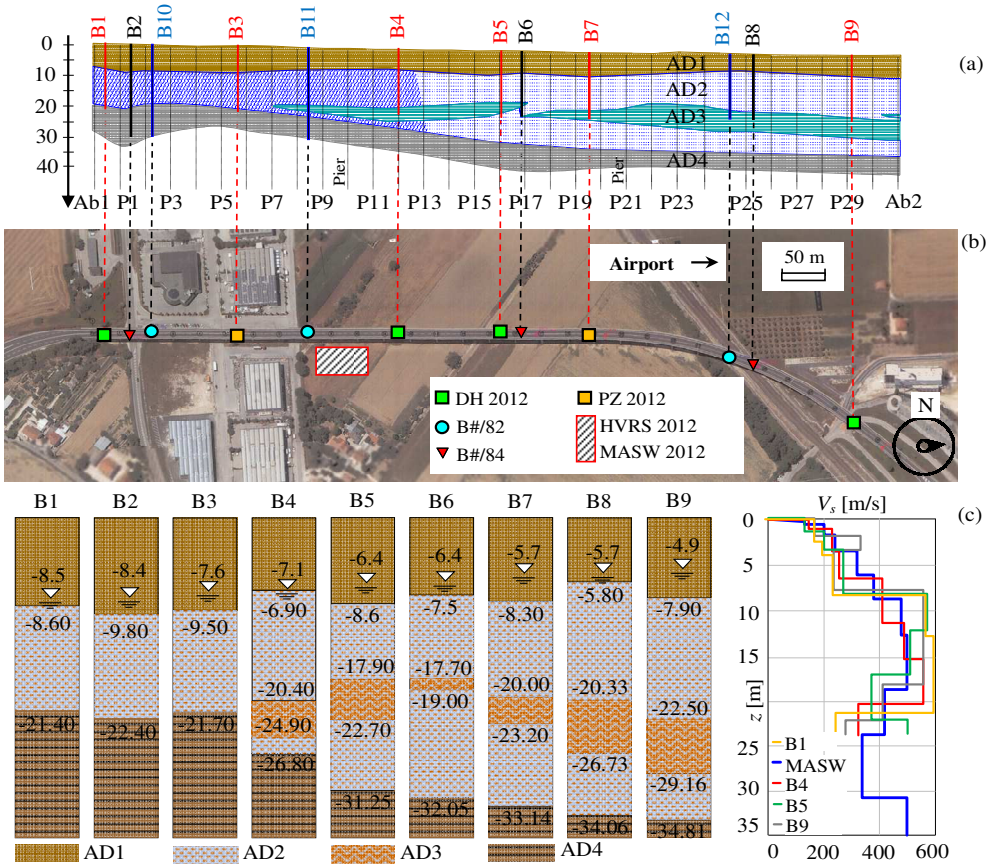

Figure 3.7 (a) Soil geological profile; (b) position of the test site and geotechnical surveys; (c) soil profiles from borehole investigations and shear wave velocities within the deposit.

Locations of above tests are schematically shown in Figure 3.7a, b. Stratigraphies deduced from borehole investigations (Figure 3.7c) lead to the 2D geotechnical model depicted in Figure 3.7a. Furthermore, two Piezometers (PZ) was used to monitor the ground-water level along the viaduct, which was found to be between 7.6 ÷ 5.7 m below the ground level, increasing from S2-PZ to S5-PZ.

Figure 3.7c shows the profiles of shear wave velocity Vs obtained from the geophysical measurements (DHs and MASW) according to the available geological and geotechnical information. Furthermore, Figure 3.8a shows the HVSR plot obtained from registrations of velocities from ambient noises; average spectrum of each velocity component in the North-South (NS), East-West (EW) and Up-Down directions (UD) is shown in Figure 3.8b. Peaks are evident at frequencies of about 1.1 and 9.7 Hz, corresponding to two impedance contrasts of the investigated deposit: the first at a high depth and the second one at the interface between lithotypes AD1 and AD2. 9.7 Hz can be interpreted as the predominant frequency of the shallower layer (AD1).

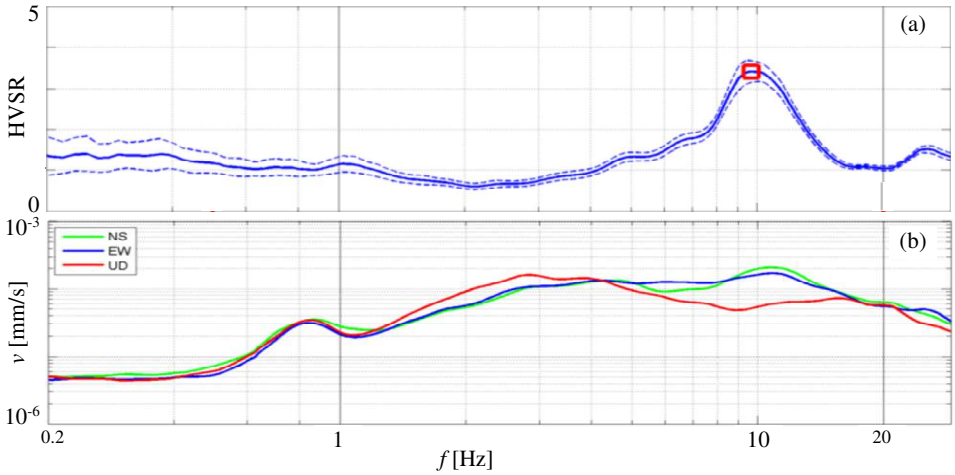

Figure 3.8 HVRS plot obtained from in situ tests

Interpretation of results of geotechnical and geophysical surveys leads to the mechanical and dynamic parameters reported in Table 3 for each lithotype.

Table 3. Mechanical and dynamic parameters

Soil	γ [kN/m³]	I_D [%]	c' [kPa]	c_u [kPa]	Φ' [°]	E_s [kPa]	E_{oed} [kPa]	V_s [m/s]	G_0 [kPa]
DA1	19.02	-	20	20	27	63000	8700	230	92000
DA2	19.60	63	-	-	39	42000	-	540	567000
DA3	20.00	-	7	35	27	15000	-	325	218000
DA4	20.00	-	30	400	26	70000	-	600	770000

I_D = density index — *V_s = shear wave velocity* — *c' = drained cohesion*
γ = unit weight of soil — *G_0 = small strain shear modulus* — *c_u = undrained cohesion*
Φ' = angle of internal friction — *E_s = elastic modulus* — *E_{oed} = oedometric modulus*

Environmental vibration tests were also carried out on two other viaducts in order to evaluate the SSI effect on the foundation rocking for different types of viaducts

3.2. “Paglia bridge” - Orvieto (TR), Italy

Figure 3.9 shows an image of the bridge in the current state; the construction is completed except for the joints near the abutment, the finishing mat of the road surface and the lighting. It is a continuous deck bridge on three spans (about 70 + 100 + 70 m) with a composite structure, with 4 steel beams with variable height and a r.c. deck of uniform thickness.

Figure 3.9 Lateral views of “Paglia bridge”, Orvieto

The 12.10 m deck is supported by two wall piers, having length of 13 m and high of 6 m from ground level to the base of support of the steel beams (Figure 3.10). The height of the steel beams is variable along the development of the bridge, assuming the maximum value at the supports and the minimum value in the middle of spans.

The peculiarity of this viaduct is the stiffness of two wall piers that should not allow pier transverse deflection.

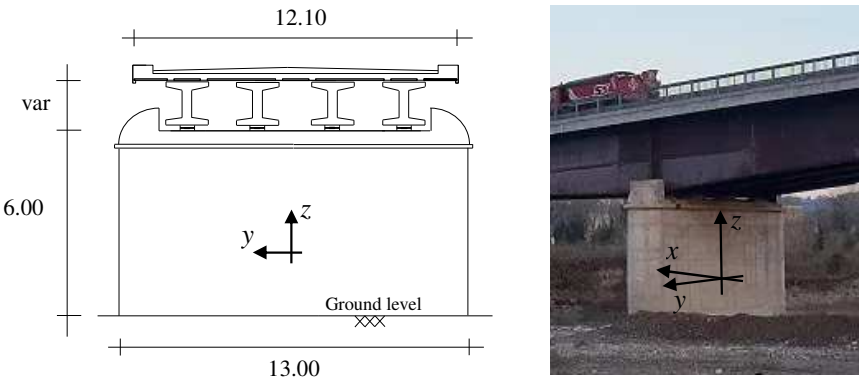

Figure 3.10 Dimensions of the “Paglia bridge” cross section

3.3. “Cesano bridge” - Corinaldo (AN), Italy

The last case study is a bridge rebuilt after a collapse. The bridge connects Corinaldo to San Michele, two villages on the border between the province of Ancona and Pesaro-Urbino, in central Italy (Figure 3.11). The Cesano bridge is a continuous deck bridge on three spans (29.45 + 42 + 29.45 m) with a composite structure, with box steel beams and a concrete slab of uniform thickness (Figure 3.12).

Figure 3.11 Geographic position of the “Cesano bridge” (from Google Maps)

Figure 3.12 Global view of “Cesano bridge”

This bridge was followed from the beginning until the end of the works; this allowed to monitor the bridge with environmental vibration measurements during each step of the construction; in particular it is interesting to study the rotation of the pile at different construction steps (Figure 3.13).

- Step1: underground piers with a height of about 4 meters (H1=3.95m, H2=4.35m)
- Step2: barefoot piers with a height of about 7.80 meters (from ground level)
- Step3: barefoot piers with a height of about 9.20 meters (from ground level)
- Step4: final condition, barefoot piers with a height of about 7.00 meters (from ground level)

Figure 3.13 Images of the “Cesano bridge” piers at different construction steps

Chapter 4.
Description of AVTs on the viaducts

4.1. “Chiaravalle viaduct” tests

4.1.1. Introduction

Ambient vibration measurements were performed to evaluate modal parameters of the viaduct in order to develop and validate a numerical finite element model for the design of the bridge seismic upgrading.

AVTs were carried out with low noise unidirectional piezoelectric accelerometers connected to a 24-bit data acquisition system by means of coaxial cables and a portable PC for data storage (Figure 4.1). Each KC is monitored separately, and different sensor configurations are scheduled to cover the overall length of the KC, due to the limited availability of sensors. In ambient vibration tests, the input is not controlled and it was assumed to have a flat spectrum such as a white noise. This assumption is not completely correct, and the input magnitude can be of a certain importance, in fact, when the structural response cannot be measured in just one test, due to the limited number of available sensors and/or the insufficient number of channels of the acquisition system. In these cases, tests must be repeated in different times, considering different configurations (i.e. varying the position of sensors) and finally merging the recorded data. This method requires that a group of sensors, called reference sensors, are left in the same place for all the test configurations so that they can be used to scale the data of different tests, acquired by sensors moved in different places (roving sensors).

Tests for each KC are performed in different days during the same week of July 2014 in the same timeslot; the overall weather conditions were constant for the entire week and the environmental temperature, measured by a portable thermometer, ranged between 27°-32° during all the tests. Consequently, ambient effects on the estimated modal parameters can be considered negligible (Regni M. et al 2018, Xu YL. et al 2010, Xia Y. et al 2012). It is worth mentioning that KC3 was not investigated due to logistic problems

In order to catch the transverse dynamic behaviour of the bridge, unidirectional accelerometers were placed at each span support and oriented in the transverse direction for each configuration. Bees wax was used to fix accelerometers preventing any relative movements between the deck and the sensors.

For each configuration, 1800 seconds long records sampled at a rate of 2048 Hz (the minimum rate for the used equipment) were acquired; this time length provides enough

frequency resolution to guarantee a good accuracy of identified modal parameters (Cantieni R. 2005).

Figure 4.1 Photos of the instrumentation setup

All the recorded data are processed with standard signal processing techniques before performing the modal analyses. Initially, data were carefully inspected in order to cut those parts characterized by anomalous behaviours (signal clipping, intermittent noise, spikes and so on) due to sensor or measurement chain malfunctioning or signal saturation. Then, the contributions of spurious trends are eliminated through a baseline correction (adopting a second order polynomial) and the high frequency content is eliminated by filtering with a Butterworth low pass filter characterized by order 4 and a cut-off frequency of 20 Hz. Finally, signals are down-sampled at 51.2 Hz to decrease the number of data and make the successive analyses faster.
In this thesis, the Covariance Stochastic Subspace Identification (SSI-Cov) technique was used to identify the dynamic properties of the viaduct from the recordings. For KC1 tests were made at different times, according to different sensors configurations; in operational modal analysis of large structures this often occurs, making necessary the data processing from multiple non-simultaneously recorded measurement setups. The Post Separate Estimation Re-scaling (PoSER) approach is used to process the data in this case.
The modal parameter identification (i.e. the evaluation of natural frequencies, damping ratios and relevant mode shapes) is performed through the SSI-Cov method working in the frequency domain, which has been implemented in Matlab environment. Modal parameters obtained from the AVTs will be presented in a dedicated section (Chapter 6) in which numerical and experimental results are compared.

The tests covered the viaduct in the kinematic chains 1, 2 and 4, and the pier P3. In Figure 4.2, an example of the positioning of the accelerometers for the kinematic chains was reported. In detail, the transverse accelerations, contained in the horizontal plane with direction orthogonal to the axis of the deck, were recorded. They are the most significant from the point of view of the seismic behaviour. To evaluate the behaviour of the joints between the kinematic chains 1 and 2 and the chains 3 and 4, the accelerations were simultaneously monitored before and after the joints, as shown in Figure 4.2. In addition to tests carried out for the overall identification of the structure, experimental investigations were performed to evaluate possible contributions of the soil-foundation compliance on the dynamic response of the bridge. For this purpose, pier P3 of the KC1 was selected, and some tests were performed with the aim of identifying the foundation translation and rocking. In particular, the instrumentation layout reported in Figure 4.15 was considered to capture translational and rotational accelerations of the foundation cap and the pier bent.

Tests carried out will be illustrated in detail below.

4.1.2. Configuration KC1

KC1 is composed by 13 piers and the abutment, so at least 14 accelerometers are required to cover the entire development of the kinematic chain. Since only 8 accelerometers were available, it was necessary to make two configurations (KC1-1 and KC1-2) (Figure 4.2).

The sensor placed in P7, called reference sensor, was left in the same place for all the test configurations so that it can be used to scale the data of different tests, acquired by sensors moved in different places (roving sensors).

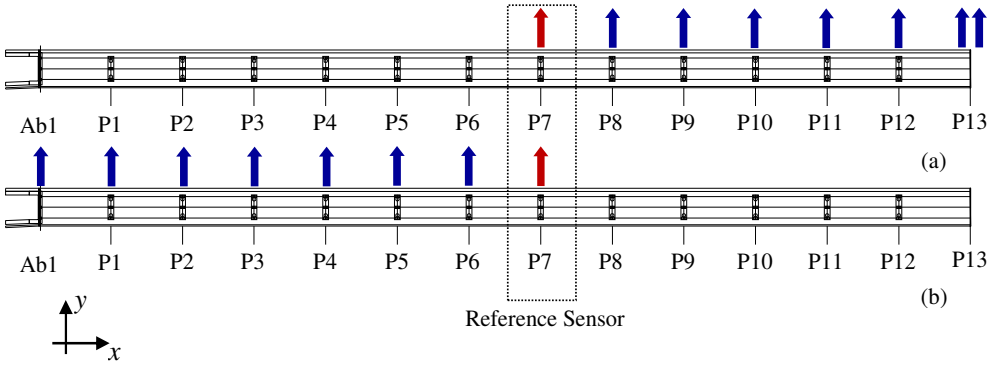

Figure 4.2 KC1 Configurations: (a) KC1-1, (b) KC1-2

For each configuration, all the recorded data were processed with standard signal processing techniques before performing the modal analysis through SSI-Cov method. This method returns a stabilization diagram in which the average of the cross power spectrum density (cpsd) of the signals measured by the 8 accelerometers (blue line) is represented. Furthermore, the procedure with the increase in the order of the model inserts a symbol if there are negligible variations at the level of frequencies, damping and modal forms (MAC), as indicated in the legend (Figure 4.3).

The aim of the tests was to determine the first three mode shapes of the viaduct, for each kinematic chain, except for the KC1, where six mode shapes were selected in the diagram (dashed lines in Figure 4.3) because in the configuration KC1-2 the first three modes are not clear like in KC1-1 (Figure 4.3). This is because the first modes mainly mobilize the piers near to the KC2 than those near the abutment; in addition, we were interested in knowing the modes that mobilize the first piers, in particular the pier P3, in order to compare the displacements with those measured on the pier P3.

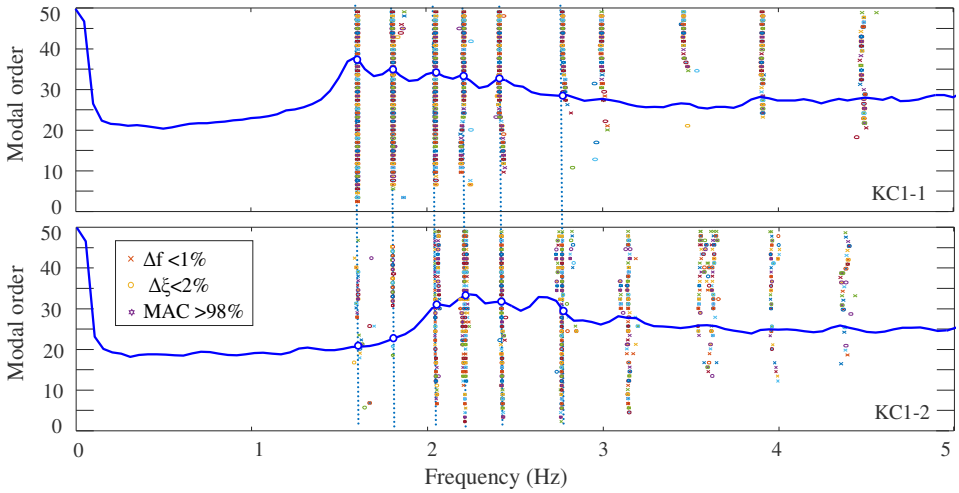

Figure 4.3 Stabilization Diagram of the KC1 Configurations (KC1-1 and KC1-2)

Table 4 and Table 5 shows the frequencies, damping and modal displacements related to the first six modes of the KC1-1 and KC1-2 configurations

Table 4. Modal parameters of KC1-1

f (Hz)	ξ (-)	P7	P8	P9	P10	P11	P12	P13sx	P13dx
1.59	1.78	0.01	-0.01	-0.07	-0.22	-0.45	-0.72	-1.00	-1.00
1.80	1.83	-0.16	-0.44	-0.75	-1.00	-0.97	-0.63	-0.02	0.05
2.03	2.42	-0.66	-1.00	-0.98	-0.49	0.25	0.70	0.60	0.59
2.22	2.42	1.00	0.26	-0.41	-0.63	-0.28	0.37	0.81	0.72
2.44	1.75	-0.79	-1.00	-0.23	0.73	0.83	-0.03	-0.90	-0.96
2.78	7.58	0.55	-0.55	-0.95	-0.02	1.00	0.63	-0.81	-0.77

Table 5. Modal parameters of KC1-2

f (Hz)	ξ (-)	P7	P6	P5	P4	P3	P2	P1	Ab1
1.62	3.66	0.15	0.07	0.68	0.05	-1.00	0.19	-0.18	0.69
1.83	3.34	1.00	0.17	-0.71	-0.75	-0.52	-0.15	0.08	0.03
2.08	1.88	-1.00	-0.77	-0.47	-0.24	-0.06	-0.05	-0.08	-0.04
2.22	1.52	0.63	1.00	1.00	0.69	0.43	0.14	0.06	-0.03
2.48	1.15	0.69	-0.28	-0.97	-1.00	-0.73	0.01	0.16	0.05
2.72	0.96	-0.29	-0.72	-0.36	0.44	1.00	0.77	0.29	-0.06

The two obtained configurations had to be scaled with respect to the reference sensor, in order to have modal displacements comparable between the different configurations.

The Post Separate Estimation Re-scaling (PoSER) approach was used to process the data in this case, and the final modal parameters of KC1 are shown in Table 6.

Table 6. Modal parameters of KC1 (PoSER)

f (Hz)	ξ (-)	P1	P2	P3	P4	P5	P6	P7	P8	P9	P10	P11	P12	P13
1.61	***0.77***	0.25	-0.03	0.08	-0.08	0.06	0.17	-0.02	0.07	-0.07	-0.09	-0.23	-0.49	-0.77
1.81	***2.28***	0.01	0.01	-0.02	-0.08	-0.12	-0.11	0.03	0.16	0.42	0.73	1.00	1.00	0.69
2.05	***2.00***	0.03	0.06	0.04	0.04	0.18	0.35	0.57	0.74	1.00	0.92	0.38	-0.28	-0.71
2.22	***0.92***	0.06	-0.09	-0.22	-0.69	-1.09	-1.58	-1.59	-1.00	-0.39	0.35	0.40	0.10	-0.21
2.46	***1.65***	-0.04	-0.14	-0.01	0.63	0.86	0.84	0.25	-0.59	-1.00	-0.38	0.52	0.91	0.18
2.75	***3.51***	-0.12	0.55	1.46	1.89	0.83	-0.68	-1.36	-0.54	0.58	0.97	-0.01	-1.00	-0.64

Figure 4.4 represents the first three mode shapes of KC1

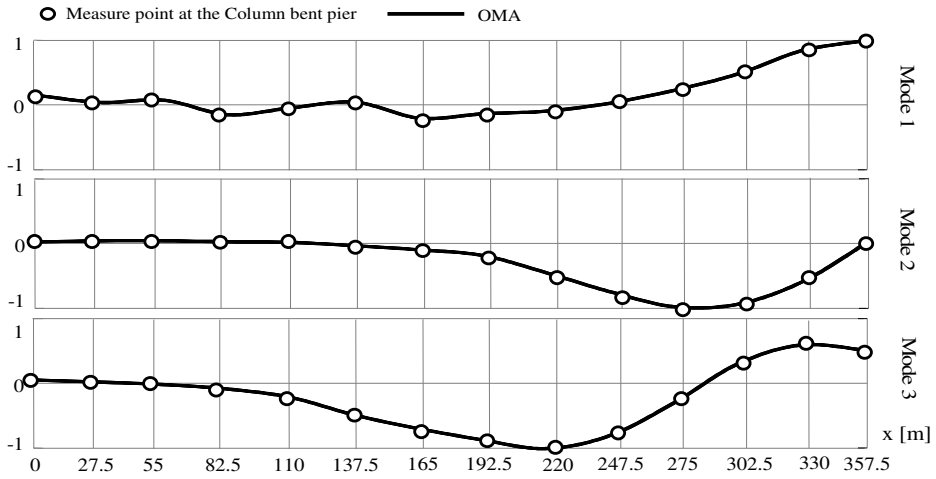

Figure 4.4 First three mode shapes of KC1

Figure 4.5 represents the fourth fifth and sixth mode shape of KC1, where it is clear that the higher modes mobilize more the piers near the abutment, that is pier P3.

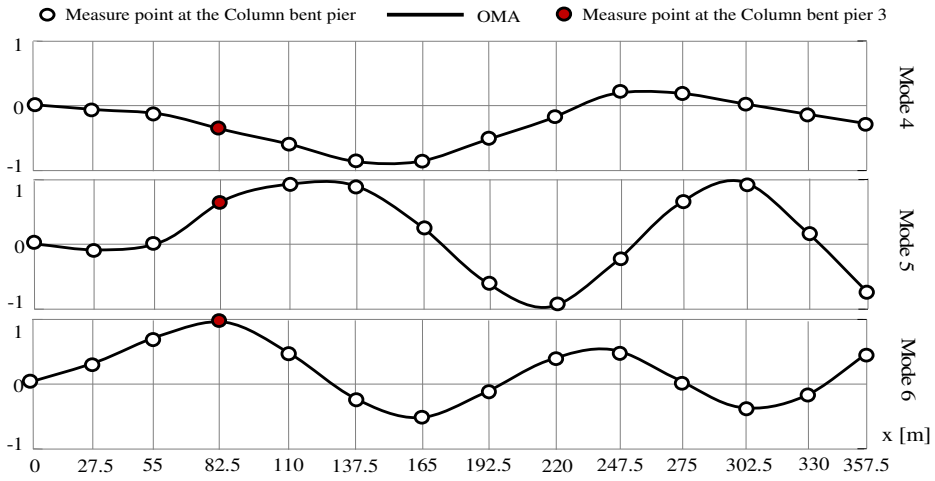

Figure 4.5 Higher mode shapes of KC1 involving pier P3

Figure 4.6 presents the degree of coupling of the experimental mode shapes through the Modal Assurance Criterion (MAC). According to this criterion, a MAC equal to 1 identifies the perfect matching of the experimental mode shapes while a MAC equal to 0 denotes the orthogonality of the two modes. It is worth noting that the experimental data give good results in terms of mode shapes.

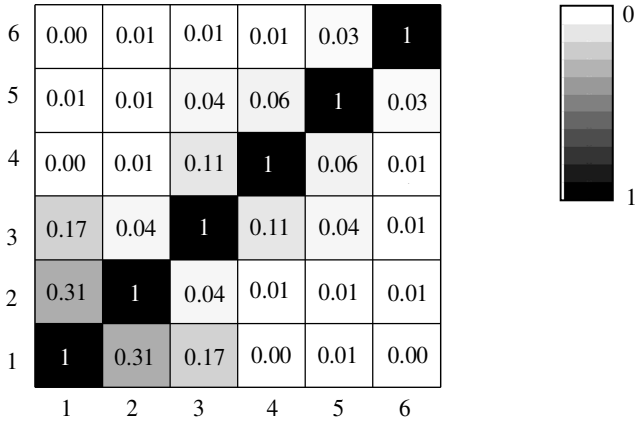

Figure 4.6 Auto MAC of KC1

4.1.3. Configuration KC2

KC2 is composed by 11 piers, so 11 accelerometers were sufficient to cover the entire development of the kinematic chain (Figure 4.7).

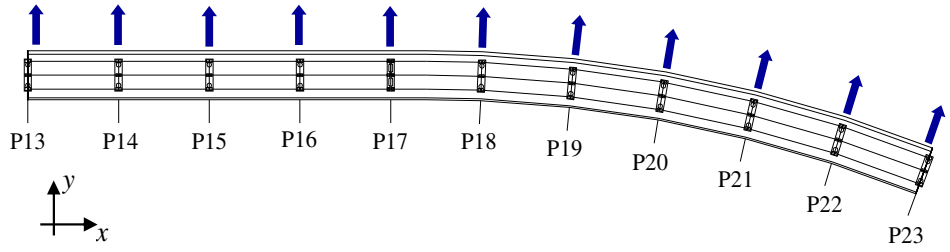

Figure 4.7 KC2 Configuration

All the recorded data were processed with standard signal processing techniques before performing the modal analyses through SSI-Cov method. This method returns a stabilization diagram in which the average of the cross power spectrum density (cpsd) of the signals, measured by the 11 accelerometers (green line), was represented. Furthermore, the procedure, with the increase in the order of the model, inserts a symbol if there are negligible variations at the level of frequencies, damping and modal forms (MAC), as indicated in the legend (Figure 4.8).

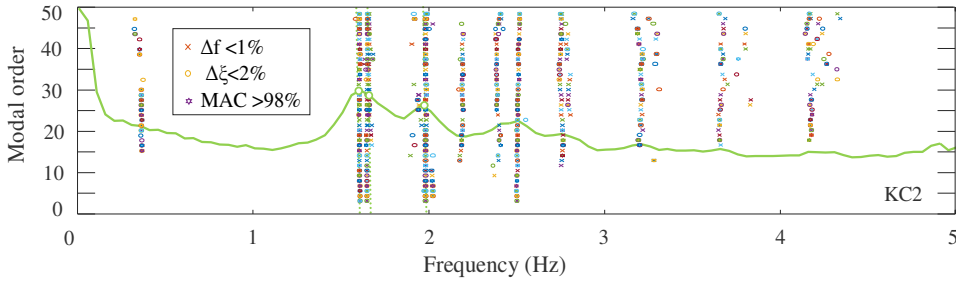

Figure 4.8 Stabilization Diagram of the KC2 Configuration

The first three mode shapes of the KC2, are selected in the diagram (dashed lines in Figure 4.8) Table 7 shows the frequencies, damping and modal displacements related to the first three modes of the KC2

Table 7. Modal parameters of KC2

f (Hz)	ξ (-)	P13	P14	P15	P16	P17	P18	P19	P20	P21	P22	P23
1.58	**0.93**	-0.54	-0.51	-0.42	-0.22	-0.01	0.13	0.22	0.26	0.23	0.15	0.07
1.66	**0.43**	-0.20	-0.16	-0.10	-0.04	-0.03	-0.16	-0.32	-0.49	-0.51	-0.38	-0.19
1.98	**0.60**	-0.07	-0.07	-0.03	-0.01	-0.07	-0.33	-0.44	-0.28	0.16	0.51	0.55

Figure 4.9 represents the first three mode shapes of KC2

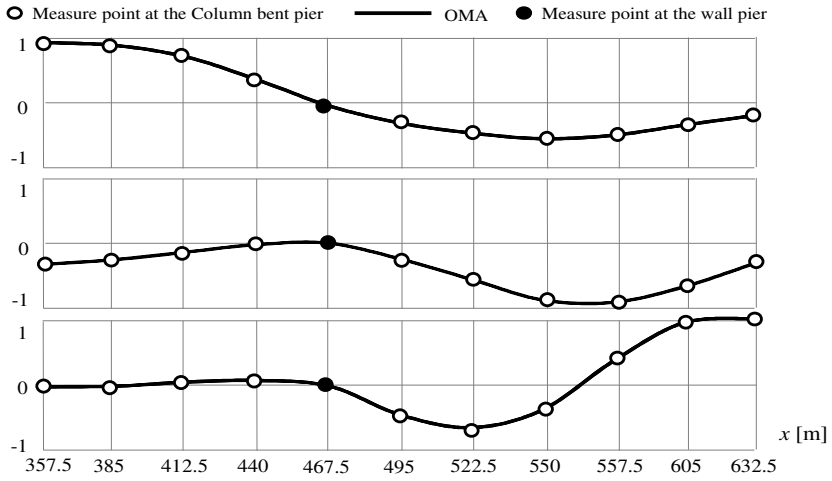

Figure 4.9 First three mode shapes of KC2

Figure 4.10 presents the degree of coupling of the experimental mode shapes through the Modal Assurance Criterion (MAC). According to this criterion, a MAC equal to 1 identifies the perfect matching of the experimental mode shapes while a MAC equal to 0 denotes the orthogonality of the two modes. It is worth noting that the experimental data give good results in terms of mode shapes.

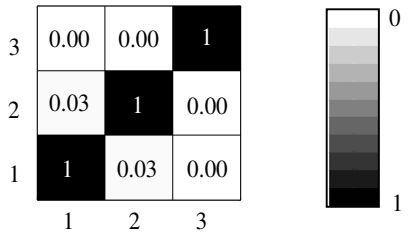

Figure 4.10 Auto MAC of KC2

4.1.4. Configuration KC4

KC4 is composed by 5 piers and the abutment, so 7 accelerometers are sufficient to cover the entire development of the kinematic chain (Figure 4.11).

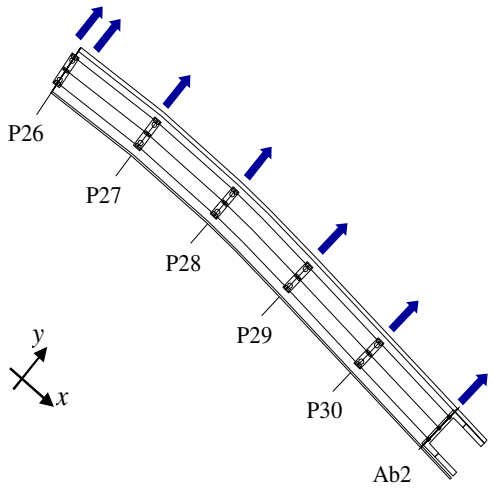

Figure 4.11 KC4 Configuration

All the recorded data were processed with standard signal processing techniques before performing the modal analyses through SSI-COV method. This method returns a stabilization diagram in which the average of the cross power spectrum density (cpsd) of the signals measured by the 7 accelerometers (orange line) is represented. Furthermore, the procedure with the increase in the order of the model inserts a symbol if there are negligible variations at the level of frequencies, damping and modal forms (MAC), as indicated in the legend (Figure 4.12).

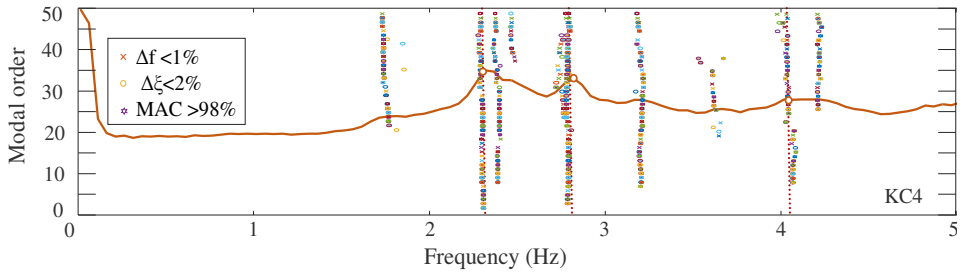

Figure 4.12 Stabilization Diagram of the KC4 Configuration

The first three mode shapes of the KC4, are selected in the diagram (dashed lines in Figure 4.12)

Table 8 shows the frequencies, damping and modal displacements related to the first three modes of the KC4

Table 8. Modal parameters of KC4

f (Hz)	ξ (-)	Ab2	P30	P29	P28	P27	P26 dx	P26 sx
2.26	**0.42**	0.00	0.04	0.17	0.42	0.63	0.56	0.23
2.79	**1.91**	0.00	0.31	0.80	1.00	0.38	-0.76	-0.91
4.04	**1.07**	0.08	0.74	1.00	-0.28	-0.48	0.68	0.33

Figure 4.13 represents the first three mode shapes of KC4

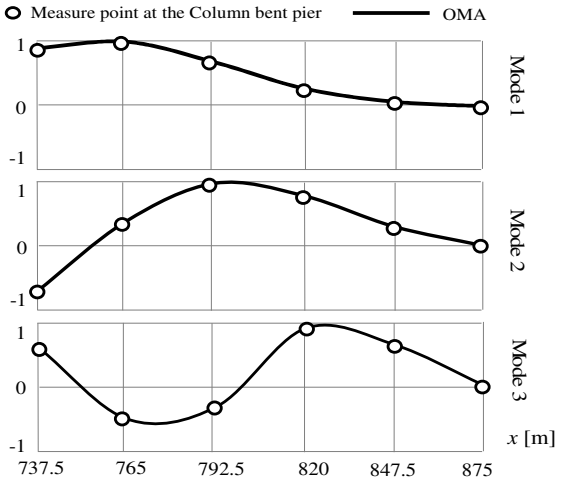

Figure 4.13 First three mode shapes of KC4

Figure 4.14 represents the degree of coupling of the experimental mode shapes through the Modal Assurance Criterion (MAC). According to this criterion, a MAC equal to 1 identifies the perfect matching of the experimental mode shapes, while a MAC equal to 0 denotes the orthogonality of the two modes. It is worth noting that the experimental data give good results in terms of mode shapes.

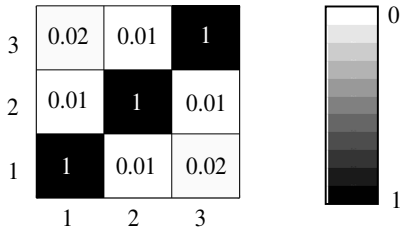

Figure 4.14 Auto MAC of KC4

4.1.5. Configuration P3

In addition to tests carried out for the overall identification of the structure, experimental investigations are performed to evaluate possible contributions of the soil-foundation compliance on the dynamic response of the bridge. For this purpose, pier 3 of the KC1 is selected, and some tests are performed with the aim of identifying the foundation translation and rocking. In particular, the instrumentation layout reported in Figure 4.15 is considered to capture translational and rotational accelerations of the foundation cap and the pier bent. In details, accelerometer Y1 catches the transverse displacement of the foundation cap while accelerometers Z2 and Z3 are positioned to capture the rocking of the cap. Furthermore, accelerometers Y4, Z5 and Z6 are necessary to evaluate displacements due to the pier deflection. (Figure 4.16)

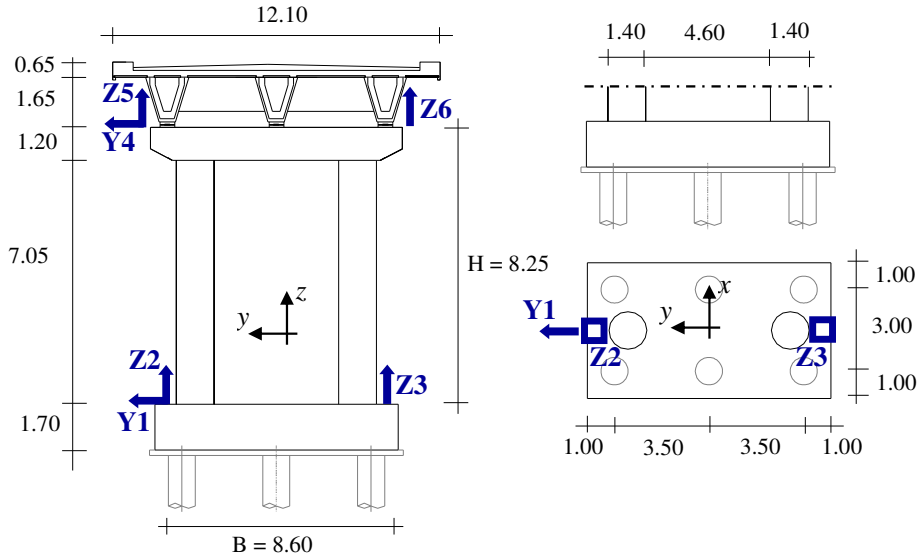

Figure 4.15 P3 Configuration

In this section, some results of experimental tests performed to evaluate the overall dynamic behaviour of the viaduct are reported. Figure 4.4 and Figure 4.5 show the plan view of the first six transverse mode shapes relevant to KC1, to which the pier suitably instrumented to evaluate effects of soil-foundation compliance belongs.

Concerning results of tests performed on pier P3, aimed at evaluating the contributions SSI on modal displacements, Table 9 reports the experimental fundamental frequencies and modal displacements identified by means of SSI-Cov method. These frequencies correspond to those of the 4th, 5th and 6th transverse modes of the deck, respectively (Figure 4.5). It is worth noting that lower transverse modes, characterized by very small displacements in correspondence of pier P3, cannot be captured with the adopted instrumentation (Figure 4.4); on the other hand, for logistic reasons, it was not possible to perform tests on a different pier.

Modal displacements reported in Table 9 were normalized with respect to the maximum displacement, always occurring at the pier top (sensor Y4).

Figure 4.16 Accelerometers photos placed in P3 Configuration

The overall displacement at the pier head is due to both the rigid motion of the foundation (Figure 4.19a) and the elastic deflection of the structural members constituting the pier (Figure 4.19b). Figure 4.18 shows, with a simple scheme, how to calculate the horizontal and vertical displacements due to the rigid rotation, as a function of the Z3 displacements (scheme valid in the hypothesis of small displacements).

Table 9. Modal parameters of P3

f (Hz)	Y1	Z2	Z3	Y4	Z5	Z6
2.23	-0.05	0.05	-0.05	-1.00	0.18	-0.19
2.48	0.06	-0.05	0.05	1.00	-0.18	0.18
2.75	0.05	-0.06	0.04	1.00	-0.19	0.18

The recorded data are processed with standard signal processing techniques before performing the modal analyses through SSI-COV method, which returns a stabilization diagram in which the average of the signals cpsd. The stabilization diagram it is reported in Figure 4.17.

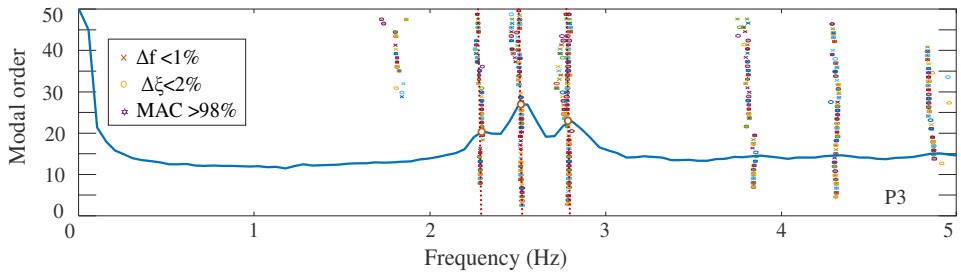

Figure 4.17 Stabilization Diagram of the P3 Configuration

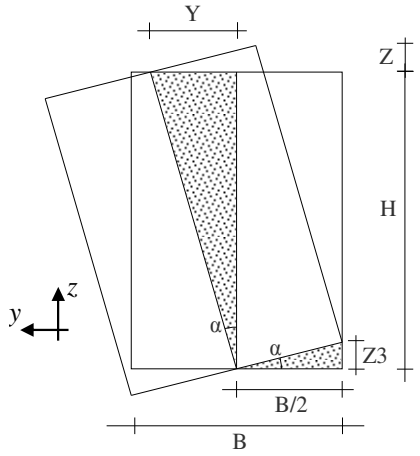

H = vertical distance between the accelerometers
B = horizontal distance between the accelerometers
Z3 = displacement measured by the sensor positioned in Z3
α = rotation angle of the foundation
Y = horizontal displacement due to Z3
Z = vertical displacement due to Z3

$\tan\alpha = Z3/(B/2) = 2 \cdot Z3/B$
Y = $H \cdot \tan\alpha =$ **$(2 \cdot H/B) \cdot Z3$**
Z = Z3

Figure 4.18 Simplified scheme of the rigid displacements due to the rocking for "Chiaravalle viaduct"

In this case H = 8.25 m and B = 8.60 m, so (2·H/B) = 1.9186 and the rigid displacements are reported in Table 10

Table 10. Rigid displacements of P3 due to the rocking

f (Hz)	*Y1*	*Z2*	*Z3*	*Y4*	*Z5*	*Z6*	**Y**	**Y4 – Y – Y1**	**Z5 -Z2**	**Z6 -Z3**
2.23	*-0.05*	*0.05*	*-0.05*	*-1.00*	*0.18*	*-0.19*	**-0.10**	**-0.85**	**0.13**	**-0.14**
2.48	*0.06*	*-0.05*	*0.05*	*1.00*	*-0.18*	*0.18*	**0.10**	**0.84**	**-0.13**	**0.13**
2.75	*0.05*	*-0.06*	*0.04*	*1.00*	*-0.19*	*0.18*	**0.08**	**0.87**	**-0.13**	**0.14**

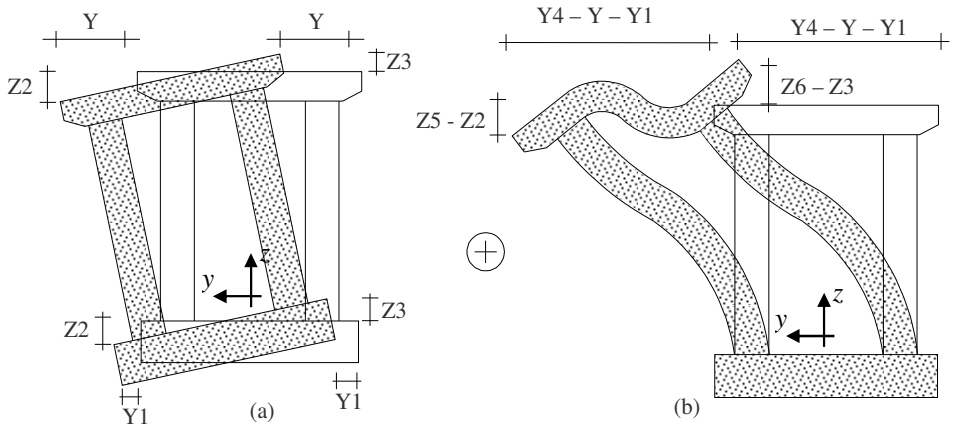

Figure 4.19 Contributions to the modal displacements: (a) foundation rigid translation and rocking and (b) pier deflection

Figure 4.19 clearly shows the contributions to the modal displacements, due to a combination of foundation rigid translation/rocking and pier deflection; in particular, the 6% of the total displacement is due to the foundation translation, the 10% is produced by the foundation rocking while the remaining 84% of the displacement is due to the pier deflection. Finally, it can be observed that normalized modal displacements are the same for all the identified frequencies, i.e. frequencies are not associated to superior modes of the pier.

In conclusion this test highlights that SSI sensibly affects the dynamics of the viaduct, even for low intensity actions, contributing to the 10% of the overall modal displacement of the deck.

For completeness, we compare the results of rocking in the foundation are compared with the corresponding displacements in the deck, to evaluate if it moves rigidly with the pier or there is a deflection of the deck.

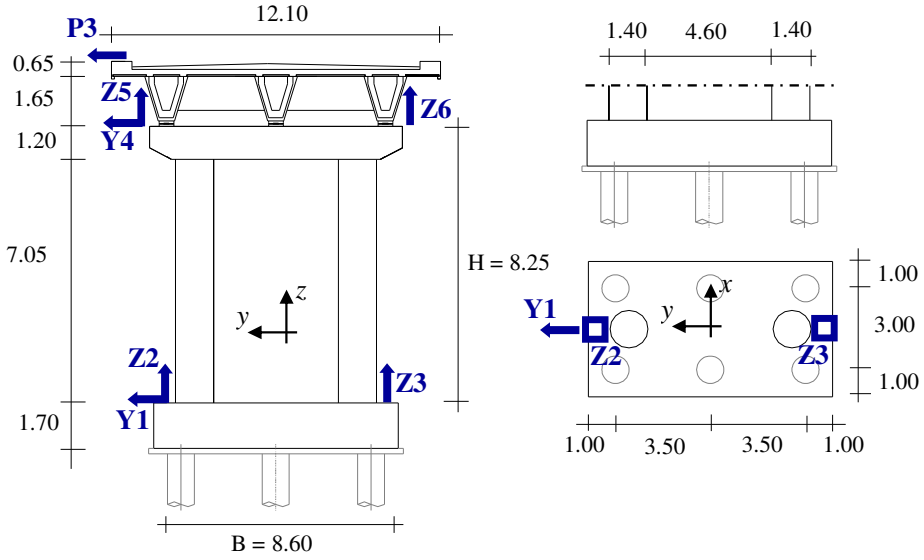

Figure 4.20 Comparison between P3 and foundation rocking

In this case H = 10.55 m and B = 8.60 m, so (2·H/B) = 2.4535 and the rigid displacements are reported in Table 11; the displacements obtained are normalized with respect to the maximum displacement (P3).

Table 11. Rigid displacements of P3 compare with foundation rocking

f (Hz)	*Y1*	*Z2*	*Z3*	*Y4*	*Z5*	*Z6*	**P3**	**Y**	**P3 – Y – Y1**	**Z5 -Z2**	**Z6 -Z3**
2.23	*-0.04*	*0.04*	*-0.04*	*-0.93*	*0.17*	*-0.18*	**-1.00**	**-0.10**	**-0.86**	**0.13**	**-0.14**
2.48	*0.05*	*-0.04*	*0.04*	*0.92*	*-0.17*	*0.17*	**1.00**	**0.10**	**0.85**	**-0.13**	**0.13**
2.75	*0.04*	*-0.05*	*0.03*	*0.94*	*-0.18*	*0.17*	**1.00**	**0.07**	**0.89**	**-0.13**	**0.14**

From the results shown, it is evident that the deck moves rigidly with the underlying piers, so its contribution can be left out for subsequent analyses.

4.1.6. Tests after retrofitting works

Environmental vibration tests of the viaduct were carried out after the seismic retrofit, to evaluate the improvements in terms of modal parameters.

The works involved the foundation system with the introduction of 28 vertical micropiles Φ14 for each pier, the structure in elevation by means of the enlargement of the column bent piers of 0.30 m, so that the new column bent piers have got a diameter of 2.0 m, and the replacement of the support devices with friction pendulum isolators. Figure 4.21 shows an image of the viaduct after the execution of the works.

Figure 4.21 "Chiaravalle viaduct" view after retrofitting works

In Figure 4.22 shows the dimensions and type of works done on all the viaduct piers.

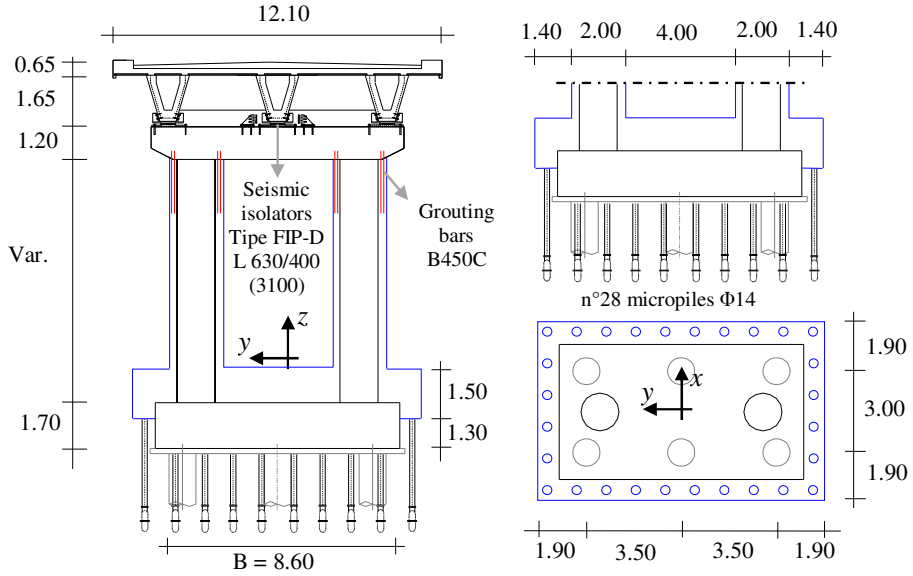

Figure 4.22 Piers after retrofitting works

In this case, unlike ante-operam tests, three configurations were carried out to study the behaviour of the viaduct in its entirety, keeping the reference sensors fixed. “Chiaravalle viaduct” is composed by 30 piers and two abutments, so at least 32 accelerometers are required to cover the entire development of the kinematic chain. But only 13 accelerometers were available, so it was necessary to make three configurations (Conf-1, Conf-2 and Conf-3) (Figure 4.23).

The sensors placed in P11, P19 and P27, called reference sensors, were left in the same place for all the test configurations so that they can be used to scale the data of different tests, acquired by sensors moved in different places (roving sensors).

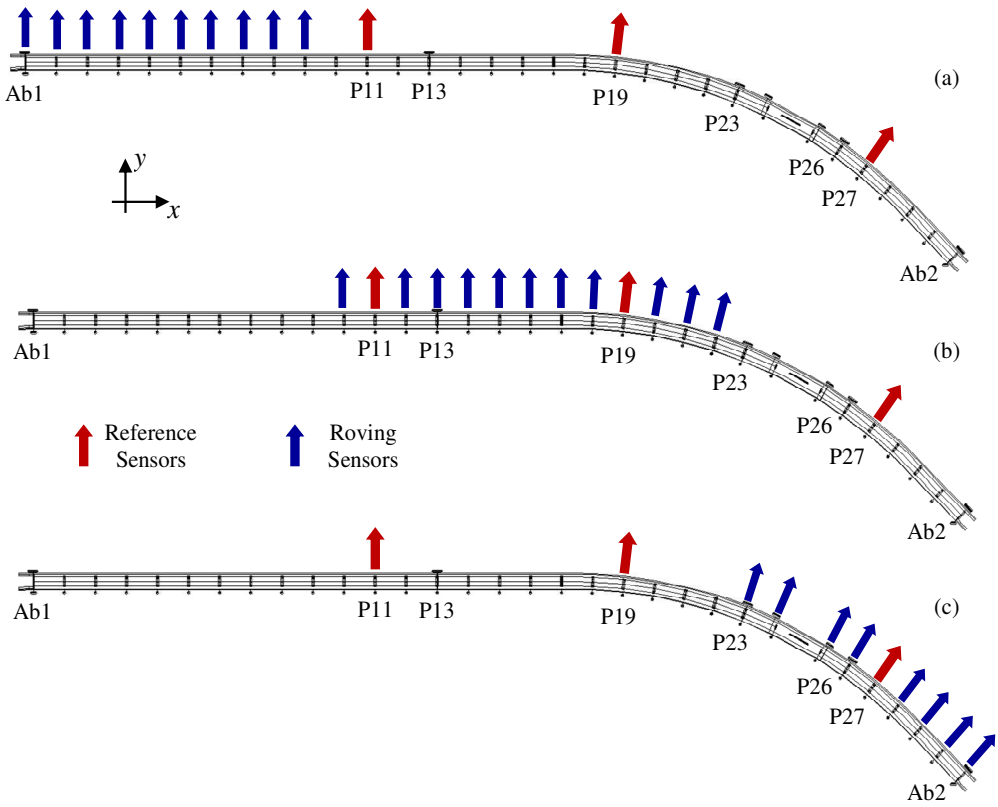

Figure 4.23 “Chiaravalle viaduct” Configurations: (a) Conf-1, (b) Conf-2, (c) Conf-3

All the recorded data, for each configurations, are processed with standard signal processing techniques before performing the modal analyses through SSI-Cov method. This method returns for each configuration, a stabilization diagram in which the average of the cross power spectrum density (cpsd) of the signals, measured by the accelerometers, was represented. Furthermore, the procedure with the increase in the order of the model inserts a symbol if there are negligible variations at the level of frequencies, damping and modal shapes (MAC), as indicated in the legend (Figure 4.24).

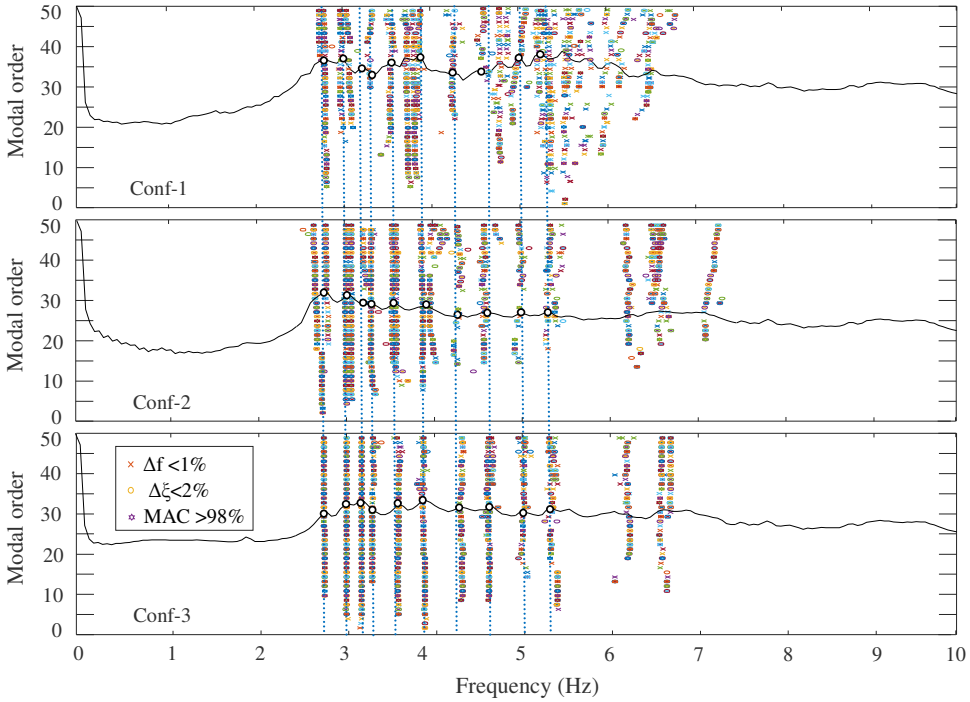

Figure 4.24 Stabilization Diagram of the "Chiaravalle viaduct" (Conf-1, Conf-2 and Conf-3)

Table 12,

Table 13 and Table 14, shows the frequencies, damping and modal displacements related to the first modes of the "Chiaravalle viaduct" after the retrofitting works, for each configuration

Table 12. Modal parameters of Conf-1

f (Hz)	ξ (-)	P11	P27	P19	Ab1	P1	P2	P3	P4	P5	P6	P7	P8	P9
2.77	3.99	-0.01	0.04	1.00	0.00	-0.01	0.00	0.00	0.00	-0.02	-0.01	0.00	-0.03	-0.44
2.96	6.88	1.00	0.10	-0.38	0.00	-0.01	-0.04	0.02	-0.02	0.00	0.02	0.06	0.03	0.27
3.07	6.29	1.00	0.09	-0.48	-0.01	-0.04	0.00	0.00	-0.06	-0.01	0.11	0.12	0.23	0.50
3.27	1.64	0.64	1.00	-0.10	0.00	0.04	-0.03	-0.01	-0.06	-0.01	0.13	0.18	0.16	0.45
3.50	1.92	0.02	-0.63	1.00	0.00	0.01	0.02	-0.02	-0.04	-0.07	-0.06	-0.13	-0.82	-1.00
3.82	2.25	-1.00	0.17	0.06	-0.01	0.00	-0.04	-0.23	-0.53	-0.89	-0.65	0.41	1.00	0.59
4.19	3.67	0.45	0.31	0.00	-0.01	-0.15	-0.44	-1.00	-1.00	-0.55	0.38	0.69	-0.13	-1.00
4.53	1.88	-0.03	-0.04	-0.14	0.01	0.35	0.80	1.00	-0.06	-0.56	-0.31	0.65	-1.00	0.33
4.97	0.85	-0.19	0.31	-0.30	0.00	0.07	0.50	0.31	-0.32	-1.00	-0.01	0.21	0.28	0.57
5.22	2.07	-0.20	-0.69	0.50	0.01	0.48	0.17	-0.70	-0.02	1.00	-0.37	-0.83	-0.57	0.39

Table 13. Modal parameters of Conf-2

f (Hz)	ξ (-)	P11	P27	P19	P10	P12	P13	P14	P15	P16	P17	P18	P20	P21	P22
2.78	1.55	-0.01	-0.01	0.53	0.01	-0.03	-0.07	-0.09	-0.10	-0.06	0.00	0.22	0.87	1.00	0.91
3.06	1.67	-0.17	-0.02	-0.41	-0.04	-0.39	-0.67	-1.00	-0.97	-0.60	-0.15	-0.26	-0.39	-0.08	0.31
3.19	1.22	0.08	-0.45	-1.00	0.14	-0.08	-0.25	-0.26	-0.17	-0.05	-0.18	-0.81	-0.49	0.51	0.91
3.28	2.52	1.00	0.00	0.03	0.89	0.84	0.43	-0.15	-0.47	-0.42	-0.10	0.03	-0.07	-0.12	-0.10
3.56	2.41	0.01	0.45	-0.74	-0.05	0.06	0.05	-0.02	-0.07	-0.13	-0.30	-1.00	0.28	0.94	0.30
3.85	2.37	0.06	-1.00	-0.13	0.01	0.01	-0.05	-0.03	0.02	0.01	-0.08	-0.28	0.19	0.19	-0.13
4.28	3.27	-0.27	-0.38	-0.03	0.04	-0.15	0.24	0.03	-0.16	0.04	0.49	0.94	-1.00	-0.01	0.97
4.54	2.51	-0.31	-0.36	-0.27	-0.04	0.06	0.54	-0.20	-0.32	0.24	0.66	0.96	-1.00	0.41	0.99
4.95	3.22	0.72	-0.41	0.19	-0.29	-0.01	-1.00	0.55	0.44	-0.75	-0.55	0.02	-0.13	-0.10	0.13
5.24	4.43	-0.11	-1.00	0.18	-0.16	0.18	0.08	-0.18	0.06	0.15	-0.21	-0.41	0.24	-0.37	-0.09

Table 14. Modal parameters of Conf-3

f (Hz)	ξ (-)	P11	P27	P19	P23	P24	P25	P26	P28	P29	P30	Ab2
2.77	1.98	0.01	0.03	-0.91	-1.00	-0.33	-0.01	0.05	0.01	0.00	0.00	0.00
3.02	2.13	0.04	0.00	-0.83	1.00	0.57	0.32	0.11	-0.01	0.00	-0.01	0.00
3.19	1.67	-0.02	-0.22	-0.48	0.22	-0.47	-1.00	-0.67	-0.05	0.00	-0.01	0.00
3.33	2.12	1.00	-0.03	0.02	0.13	0.04	-0.09	-0.10	-0.01	0.00	0.03	0.00
3.60	1.88	-0.04	-0.42	0.67	1.00	0.46	-0.48	-0.73	-0.20	-0.05	-0.01	-0.01
3.87	2.22	0.11	-1.00	-0.11	-0.40	0.22	0.19	-0.63	-0.84	-0.41	-0.12	0.00
4.28	2.42	0.33	0.36	-0.05	-0.09	0.59	-0.28	-0.99	1.00	0.70	0.23	-0.02
4.62	1.98	-0.39	-0.37	-0.30	-1.00	-0.45	0.51	-0.43	0.44	0.72	0.15	-0.03
5.00	0.55	0.05	-0.18	0.17	0.74	-0.69	0.42	1.00	-0.06	0.06	0.20	-0.11
5.32	2.87	0.05	0.83	-0.20	-0.51	0.45	-0.48	-0.70	0.23	-1.00	-0.79	-0.10

The three configurations obtained must be scaled with respect to the reference sensor, so that the modal displacements are comparable between the different configurations.

The Post Separate Estimation Re-scaling (PoSER) approach is used to process the data in this case, and the final modal parameters of “Chiaravalle viaduct” are shown in Table 15, Table 16 and Table 17 (the mode shapes are presented in three different table one for each kinematic chains). The main modal shapes of the respective kinematic chain are highlighted in grey background.

Table 15. Modal parameters of KC1 after retrofitting works (PoSER)

f (Hz)	ξ (-)	Ab1	P1	P2	P3	P4	P5	P6	P7	P8	P9	P10	P11	P12	P13
2.76	4.38	0.00	-0.01	0.00	0.00	0.00	-0.02	-0.01	0.00	0.03	0.44	-0.01	0.01	0.03	0.07
3.01	**3.42**	**0.00**	**-0.01**	**-0.04**	**0.02**	**-0.02**	**0.00**	**0.02**	**0.06**	**0.03**	**0.07**	**0.04**	**0.17**	**0.39**	**0.67**
3.16	**3.23**	**0.01**	**0.04**	**0.00**	**0.00**	**0.06**	**0.01**	**-0.11**	**-0.42**	**-0.53**	**-0.50**	**-0.26**	**-0.08**	**0.08**	**0.25**
3.29	**2.63**	**-0.01**	**-0.04**	**0.03**	**0.01**	**0.06**	**0.01**	**-0.13**	**-0.19**	**-0.32**	**-0.61**	**-0.89**	**-1.00**	**-0.84**	**-0.43**
3.55	1.96	0.00	-0.01	-0.02	0.02	0.04	0.07	0.06	0.13	-0.82	-1.00	-0.05	0.01	0.06	0.06
3.84	3.04	-0.01	0.00	-0.04	-0.23	-0.53	-0.89	-0.65	0.41	1.00	0.59	-0.01	-0.06	-0.01	0.05
4.25	2.53	-0.01	-0.15	-0.44	-1.00	-1.00	-0.56	0.38	0.69	-0.13	-1.00	-0.04	0.27	0.15	-0.24
4.55	2.40	0.01	0.35	0.80	1.00	-0.06	-0.56	-0.31	0.65	-0.11	0.04	0.00	-0.03	0.01	0.05
4.97	1.96	0.00	0.07	0.50	0.31	-0.32	-1.00	-0.01	0.21	0.10	0.20	0.08	-0.19	0.00	0.26
5.25	2.76	0.01	0.48	0.17	-0.70	-0.02	1.00	-0.37	-0.83	-0.26	0.18	-0.29	-0.20	0.33	0.15

Table 16. Modal parameters of KC2 after retrofitting works (PoSER)

f (Hz)	ξ (-)	P13	P14	P15	P16	P17	P18	P19	P20	P21	P22	P23
2.76	**4.38**	**0.07**	**0.08**	**0.09**	**0.06**	**0.00**	**-0.20**	**-0.49**	**-0.81**	**-0.94**	**-1.00**	**-1.00**
3.01	**3.42**	**-0.67**	**-1.00**	**-0.97**	**-0.60**	**-0.15**	**0.26**	**0.41**	**0.39**	**0.31**	**0.08**	**-0.04**
3.16	**3.23**	**-0.25**	**-0.26**	**-0.17**	**-0.05**	**-0.18**	**-0.81**	**-1.00**	**-0.49**	**0.51**	**0.91**	**0.22**
3.29	2.63	0.43	-0.15	-0.47	-0.42	-0.10	0.03	0.03	-0.07	-0.12	-0.10	0.13
3.55	1.96	-0.06	0.02	0.07	0.13	0.30	1.00	0.74	-0.28	-0.94	-0.30	1.00
3.84	3.04	0.05	0.03	-0.02	-0.02	0.08	0.28	0.13	-0.19	-0.19	0.13	0.40
4.25	2.53	-0.24	-0.03	0.16	-0.04	-0.49	-0.94	0.03	1.00	0.02	-0.97	-0.10
4.55	2.40	0.54	-0.20	-0.32	0.24	0.66	0.96	-1.00	0.41	0.99	0.00	-0.79
4.97	1.96	0.09	-0.05	-0.04	0.07	0.05	0.00	0.01	0.01	-0.01	0.00	-1.00
5.25	2.76	0.07	-0.16	0.05	0.13	-0.19	-0.37	0.21	-0.33	-0.08	0.00	1.00

Table 17. Modal parameters of KC3 and KC4 after retrofitting works (PoSER)

f (Hz)	ξ (-)	P23	P24	P25	P26	P27	P28	P29	P30	Ab2
2.76	4.38	1.00	0.33	0.01	0.05	0.04	0.02	0.00	0.00	0.00
3.01	3.42	1.00	0.57	0.32	0.14	0.10	-0.01	0.00	-0.01	0.00
3.16	3.23	-0.22	0.47	1.00	0.67	0.09	0.05	0.00	0.01	0.00
3.29	2.63	1.00	0.31	-0.69	-0.10	1.00	-0.01	0.00	0.03	0.01
3.55	**1.96**	**-1.00**	**-0.46**	**0.48**	**0.73**	**0.63**	**0.20**	**0.06**	**0.01**	**0.01**
3.84	3.04	0.63	-0.35	-0.30	0.00	-0.17	-0.84	-0.41	-0.12	0.00
4.25	**2.53**	**-0.09**	**0.60**	**-0.28**	**0.99**	**-0.31**	**-1.00**	**-0.70**	**-0.23**	**0.02**
4.55	2.40	-1.00	-0.45	0.51	-0.60	-0.72	0.61	1.00	0.21	-0.04

4.97	1.96	-0.74	0.69	-0.42	-1.00	0.08	0.06	-0.06	-0.20	0.11
5.25	**2.76**	**0.73**	**-0.64**	**0.69**	**0.70**	**-0.17**	**-0.23**	**1.00**	**0.79**	**0.10**

Figure 4.25 shows the first three mode shapes of KC1

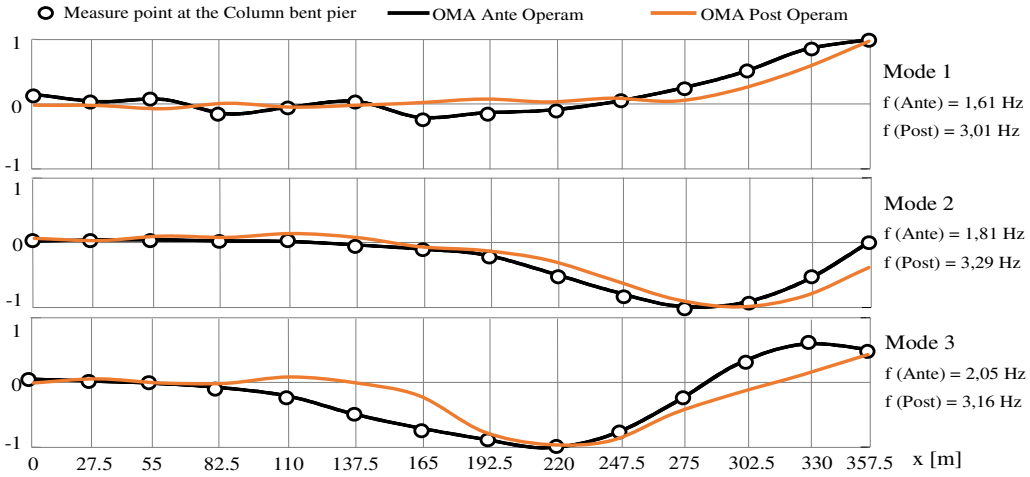

Figure 4.25 First three mode shapes of KC1

Figure 4.26 represents the first three mode shapes of KC2

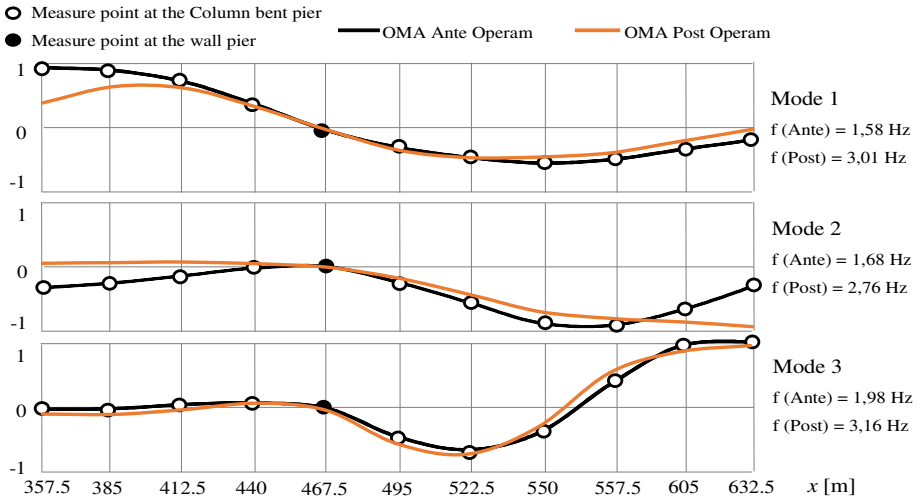

Figure 4.26 First three mode shapes of KC2

Figure 4.27 depicts the first three mode shapes of KC4.

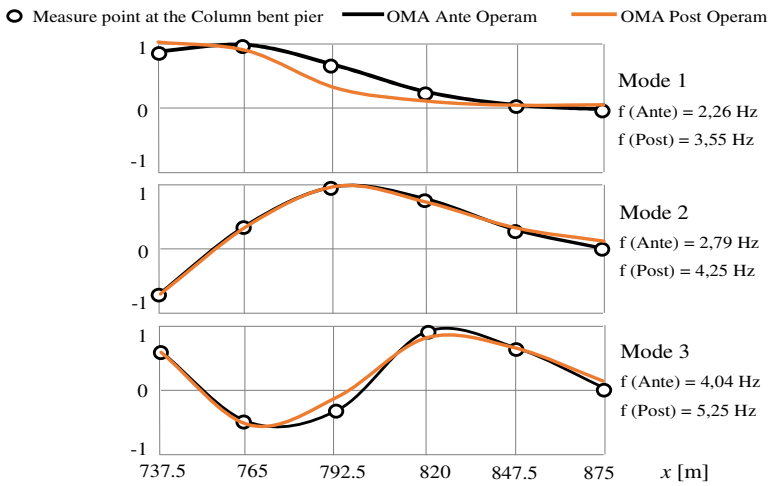

Figure 4.27 First three mode shapes of KC4

Figure 4.28 presents the degree of coupling of the experimental mode shapes through the Modal Assurance Criterion (MAC) for each configuration. According to this criterion, a MAC equal to 1 identifies the perfect matching of the experimental mode shapes while a MAC equal to 0 denotes the orthogonality of the two modes. It is worth noting that the experimental data give good results in terms of mode shapes.

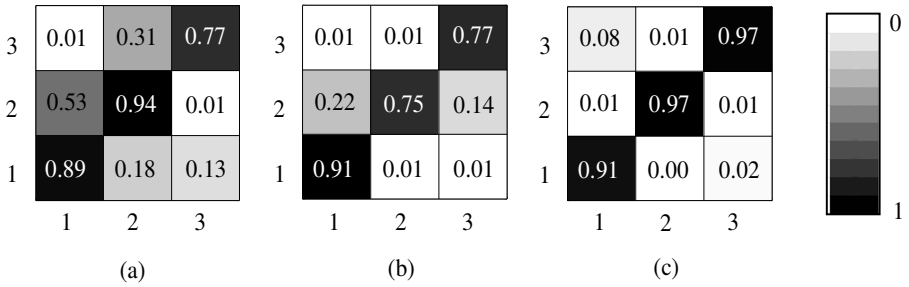

Figure 4.28 MAC of (a) KC1, (b) KC2, (c) KC4

From Figure 4.25, Figure 4.26 and Figure 4.27 , a significant increase in the frequencies of the first three modes of vibration can be detected.

The general increase in frequencies shows a significant stiffening of the structure with respect to transversal displacements; on the other hand, the modal shapes, identified with the post-operam tests, remain very similar to the ante-operam ones. The good agreement of the ante- and post-operam modal shapes shows that the change induced by the retrofitting works, especially in terms of mass and stiffness, are uniformly distributed along the viaduct. It should be noted that the sequence of the corresponding modes does not remain unchanged. For the first kinematic chain, in fact, the 2nd mode ante-operam becomes the third post-

operam (and the other way around); for the second kinematic chain the 1st mode before the operation becomes the second post-operam (and the other way around). Finally, for the fourth kinematic chain there are no displacements as regards the succession of the first three modes.

The insulation system introduced with the seismic retrofitting works does not produce any modification of the modal forms, since the environmental vibrations does not cause any relative movement between the deck and the piers.

Regard the dynamic behaviour of the piers and their soil interaction, the ambient vibration results recorded on the pier P3 have been re-elaborated.

The tests were performed both before and after the seismic retrofitting works, instrumenting the pier with accelerometers placed on the foundation, at the head of the column bent piers cap and on the slab of the deck. The data were reprocessed according to the same procedure used for the deck.

The natural frequencies correspond to those of the deck and they are more evident than those for which the transverse modal shape of the deck shows a maximum at the piers. In order to estimate the soil interaction of the pile, modal displacements were assessed both at the foundation and on the column bent pier. In particular, the instrumentation layout was considered to capture translational and rotational accelerations of the foundation cap and the pier bent.

In this case, the rigid displacements are reported in Table 18 and represented in Figure 4.29

Table 18. Rigid displacements of P3 due to the rocking

f (Hz)	*Y1*	*Z2*	*Z3*	*Y4*	*Z5*	*Z6*	**Y**	**Y4 – Y – Y1**	**Z5 -Z2**	**Z6 -Z3**
3.84	*-0.06*	*0.08*	*-0.08*	*-1.00*	*0.16*	*-0.17*	**-0.16**	**-0.77**	**0.07**	**-0.08**
4.25	*0.06*	*-0.07*	*0.07*	*1.00*	*-0.15*	*0.15*	**0.15**	**0.79**	**-0.08**	**0.07**
4.55	*0.05*	*-0.06*	*0.06*	*1.00*	*-0.16*	*0.17*	**0.12**	**0.83**	**-0.10**	**0.11**

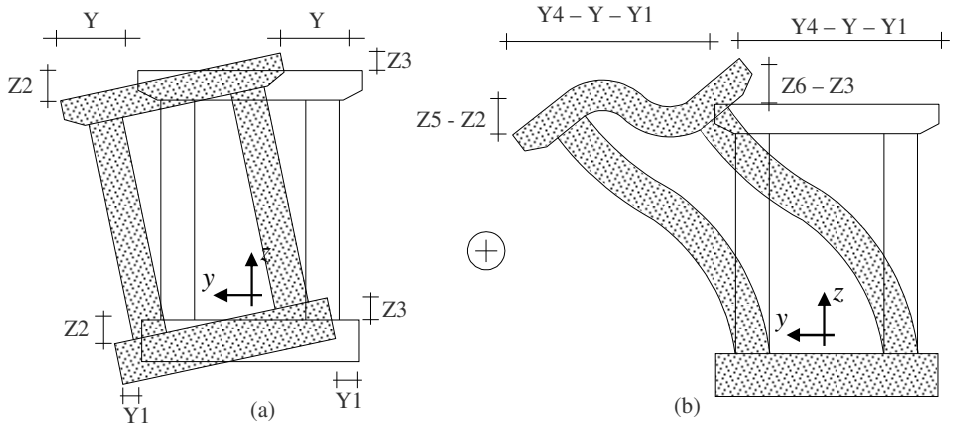

Figure 4.29 Contributions to the modal displacements: (a) foundation rigid translation and rocking and (b) pier deflection

Table 18 clearly shows the post-operam modal displacements as a combination of foundation rigid translation/rocking and pier deflection. In particular, 6% of the total displacement is due to the foundation translation, the 16% is produced by the foundation rocking while the remaining 77% of the displacement is due to the pier deflection. Finally, it can be observed that normalized modal displacements are the same for all the identified frequencies, i.e. frequencies are not associated to superior modes of the pier.

This test was important because highlights that SSI sensibly affects the dynamics of the viaduct, even for low intensity actions, contributing to the 16% of the overall modal displacement of the deck.

In this case, it is interesting to compare the results ante-operam (Table 10) and post-operam (Table 18); it is clear that the contribution offered by the pier deflection has been reduced more than the contribution due to the foundation rocking. In other words, with respect to the transverse modal components of the deck, the stiffening of the piers is greater than that of the foundation.

Finally, the component of the pier deflection is approximately reduced of 10% as a result of the retrofitting works, this is clearly caused by the increase in the resistant section of the piers.

4.2. “Paglia bridge” – Orvieto (TR), Italy

4.2.1. Introduction

The viaduct consists of a single carriageway with two gear lanes, one in each direction. In order to better investigate the dynamic behaviour of the deck taking the global spatial behaviour it was possible to adopt test configurations that involved both lanes. In particular, the environmental vibration measurements were performed according to 2 configurations:

- Conf-1 configuration has been designed to mainly evaluate the transversal behaviour of the viaduct, and therefore provides for the positioning of almost all accelerometers on the upstream lane, with transversal measurement direction (Figure 4.30a) the arrow indicates the measurement direction of the sensors while the square with the dot in the middle indicates the vertical measurement direction upwards;

- Conf-2 configuration was instead designed to capture the bending-torsional behaviour of the deck, and therefore provides for the positioning of the accelerometers on both sides of the carriageway, with vertical measurement direction (Figure 4.30b).

The two accelerometers positioned at measurement point 19, with a progression equal to 90m, one with a transverse measurement direction and the other vertical, were always left in the same position and used as reference sensors, on the basis of which it is possible to join the recordings of the two configurations as if they were acquired synchronously (the two sensors are shown in dark red in Figure 4.30 and in Table 19).
The sensors used in the two configurations, their denomination and position (progressive distance from the left abutment) are shown in Table 19.

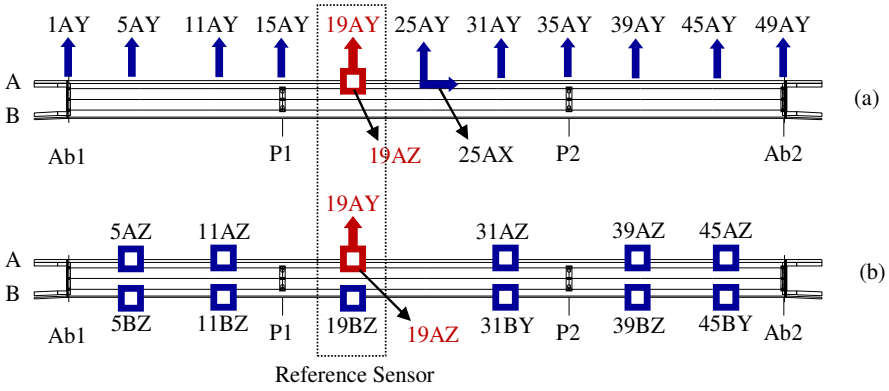

Figure 4.30 “Paglia bridge” configurations: (a) Configuration Conf-1, (b) Configuration Conf-2

In addition to the sensors placed on the deck and shown in Figure 4.30, some accelerometers were positioned at pier P1, at different heights (just above the level of the

ground, at the top of the pier near the support device, on the beam immediately above the support). The sensors were arranged with transversal measuring direction in order to evaluate the contribution of the pier to the measured transverse displacement at the level of the deck.

Table 19. Progressive distances of the accelerometers from Ab1

Position	1#	5#	11#	15#	19#	25#	31#	35#	39#	45#	49#
Distance (m)	0	20	50	70	90	120	150	170	190	220	240

4.2.2. Configurations Conf-1 and Conf-2

All the recorded data are processed with standard signal processing techniques before performing the modal analyses through SSI-Cov method, which returns for each configuration, a stabilization diagram in which the average of the cross power spectrum density (cpsd) of the signals measured by the 13 accelerometers (blue line) is represented; furthermore, the procedure with the increase in the order of the model inserts a symbol if there are negligible variations at the level of frequencies, damping and modal forms (MAC), as indicated in the legend (Figure 4.31).

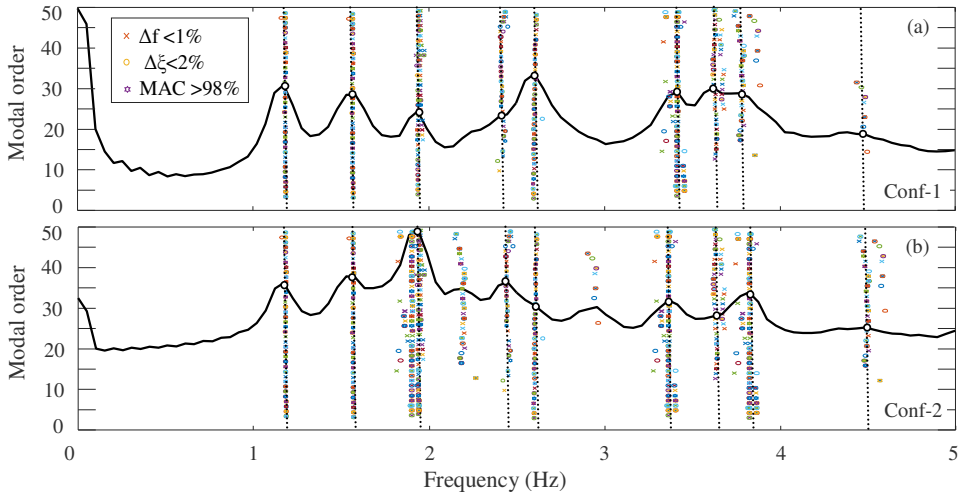

Figure 4.31 Stabilization Diagram of the bridge configurations: (a) Conf-1, (b) Conf-2

The first nine mode shapes of the “Paglia bridge”, are selected in the diagram (dash lines in Figure 4.31).

Table 20 and Table 21 shows the frequencies, damping and modal displacements related to the first nine modes of the Conf-1 and Conf-2

Table 20. Modal parameters of Conf-1

Mode	1	2	3	4	5	6	7	8	9
f (Hz)	**1.14**	**1.53**	**1.89**	**2.39**	**2.54**	**3.33**	**3.54**	**3.73**	**4.35**
ξ (-)	**1.10**	**1.97**	**1.10**	**-1.58**	**0.99**	**1.01**	**1.20**	**1.75**	**4.08**
19AZ	1.00	-1.00	1.00	-0.22	-0.16	-1.00	-0.38	0.43	-1.00
19AY	0.00	-0.07	0.00	0.63	0.67	-0.03	0.38	0.20	0.02
1AY	0.00	0.00	0.01	-0.14	-0.05	0.00	0.36	0.36	-0.01
5AY	0.02	0.03	0.10	-0.09	-0.05	-0.01	0.91	0.96	0.05
11AY	0.00	0.05	0.02	-0.01	0.06	-0.05	1.00	1.00	0.07
15AY	0.00	-0.01	0.01	0.21	0.28	-0.05	0.61	0.52	0.03
25AY	0.03	-0.15	-0.01	0.70	1.00	-0.03	0.03	-0.11	-0.01
31AY	0.04	-0.12	-0.04	0.35	0.67	0.04	-0.31	0.06	-0.01
35AY	0.00	-0.02	0.00	0.19	0.30	0.03	-0.55	0.24	0.00
39AY	0.01	0.04	-0.01	0.05	0.08	0.05	-0.90	0.25	-0.01
45AY	-0.03	0.06	0.11	-0.07	-0.02	0.08	-0.77	0.15	0.01
49AY	-0.01	0.00	0.02	1.00	-0.04	0.03	-0.31	-0.10	0.00
25AX	0.01	-0.02	0.31	0.01	-0.01	0.35	0.05	0.08	-0.84

Table 21. Modal parameters of Conf-2

Mode	1	2	3	4	5	6	7	8	9
f (Hz)	**1.14**	**1.51**	**1.88**	**2.38**	**2.52**	**3.31**	**3.53**	**3.74**	**4.36**
ξ (-)	**1.46**	**2.21**	**0.62**	**0.95**	**1.56**	**1.27**	**2.13**	**0.81**	**4.38**
19AZ	-0.49	-0.45	0.33	0.17	0.24	0.91	-0.84	1.00	-0.87
19AY	0.00	-0.03	0.00	0.04	-1.00	0.02	0.51	0.05	-0.01
19BZ	-0.48	0.44	0.38	0.93	-0.17	1.00	0.69	-0.42	-0.18
5BZ	0.32	-0.21	-0.98	0.79	0.34	0.57	0.70	0.42	-0.18
5AZ	0.34	0.22	-1.00	0.43	-0.29	0.62	-0.83	-0.08	-0.48
11AZ	0.34	0.23	-0.69	0.20	-0.09	-0.29	-0.35	-1.00	-0.99
11BZ	0.35	-0.24	-0.71	0.14	0.12	-0.31	0.22	-0.95	0.94
31AZ	-0.47	-0.43	-0.38	0.21	0.22	-0.90	0.77	0.97	1.00
31BZ	-0.50	0.48	-0.35	0.48	-0.22	-0.93	-0.63	0.11	0.33
39AZ	0.36	0.27	0.68	0.85	-0.04	0.29	0.41	-0.38	0.32
39BZ	0.36	-0.29	0.67	1.00	0.01	0.34	-0.26	0.36	0.32
45AZ	0.36	0.25	0.93	0.55	-0.24	-0.57	1.00	0.10	-0.50
45BZ	0.34	-0.26	0.91	0.19	0.19	-0.55	-0.73	-0.02	0.03

Two configurations obtained must be scaled with respect to the reference sensor, so as to have modal displacements comparable between the different configurations.

The Post Separate Estimation Re-scaling (PoSER) approach is used to process the data in this case, and the final modal parameters of "Paglia bridge" are shown in Table 22.

Table 22. Modal parameters of "Paglia Bridge" (PoSER)

Mode	1	2	3	4	5	6	7	8	9
f (Hz)	**1.14**	**1.52**	**1.89**	**2.39**	**2.53**	**3.32**	**3.54**	**3.74**	**4.36**
ξ (-)	**1.28**	**2.09**	**0.86**	**0.32**	**1.28**	**1.14**	**1.67**	**1.28**	**4.23**
1AY	0.00	0.00	0.01	-0.14	-0.05	0.00	0.36	0.36	-0.01
5AY	0.02	0.03	0.10	-0.09	-0.05	-0.01	0.91	0.96	0.05
5AZ	-0.69	0.49	-3.03	-0.32	0.19	-0.68	-0.44	0.18	-0.21
5BZ	-0.65	-0.47	-2.97	-0.37	-0.23	-0.63	0.37	-0.18	-0.21
11AY	0.00	0.05	0.02	-0.01	0.06	-0.05	1.00	1.00	0.07
11AZ	-0.69	0.51	-2.09	-0.17	0.06	0.32	-0.19	-0.04	-0.55
11BZ	-0.71	-0.53	-2.15	-0.22	-0.08	0.34	0.12	0.04	-0.57
15AY	0.00	-0.01	0.01	0.21	0.28	-0.05	0.61	-0.10	0.03
25AY	0.03	-0.15	-0.01	1.00	1.00	-0.03	0.03	-0.01	0.00
31AY	0.04	-0.12	-0.04	0.70	0.67	0.04	-0.31	-0.11	-0.01
31AZ	0.96	-0.96	-1.15	-0.06	-0.15	0.99	0.41	-0.42	1.08
31BZ	1.02	1.07	-1.06	-0.08	0.15	1.02	-0.33	0.43	1.15
35AY	0.00	-0.02	0.00	0.35	0.30	0.03	-0.55	0.06	-0.01
39AY	0.01	0.04	-0.01	0.19	0.08	0.05	-0.90	0.24	0.00
39AZ	-0.73	0.60	2.06	-0.19	0.03	-0.32	0.22	0.05	0.38
39BZ	-0.73	-0.64	2.03	-0.24	-0.01	-0.37	-0.14	-0.06	0.57
45AY	-0.03	0.06	0.11	0.05	-0.02	0.08	-0.77	0.25	-0.01
45AZ	-0.73	0.56	2.82	-0.34	0.16	0.63	0.53	-0.17	0.37
45BZ	-0.69	-0.58	2.76	-0.40	-0.13	0.60	-0.39	0.16	0.37
49AY	-0.01	0.00	0.02	-0.07	-0.04	0.03	-0.31	0.15	0.01

For the representation of the modal shapes, hypotheses were also made according to the constraints offered to the bridge by the supports; in particular, for the Conf-1 configuration used to describe the transversal behaviour of the bridge, the transversal displacements of the same section were assumed to be identical, while for the Conf-2 configuration, designed to capture the bending-torsional behaviour of the deck, the vertical displacements at the abutments and piers were considered null. These hypotheses can be considered true, for environmental vibration measurements, also for the points in which the support provided a degree of transversal freedom, since the friction forces, even if low, are not exceeded.

Figure 4.32 to Figure 4.39 represents the first eight mode shapes of "Paglia bridge".

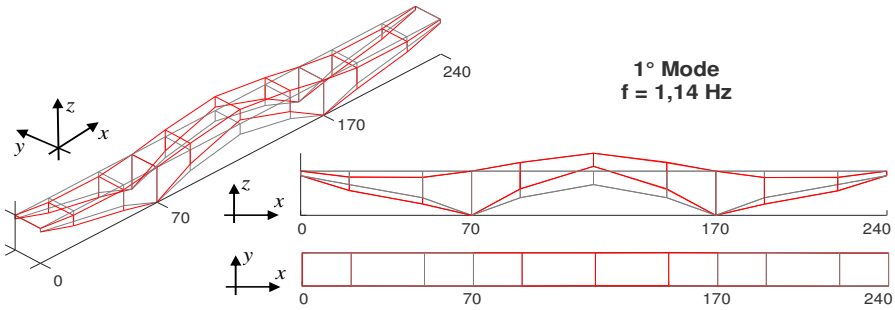

Figure 4.32 Views of the 1°Mode shape

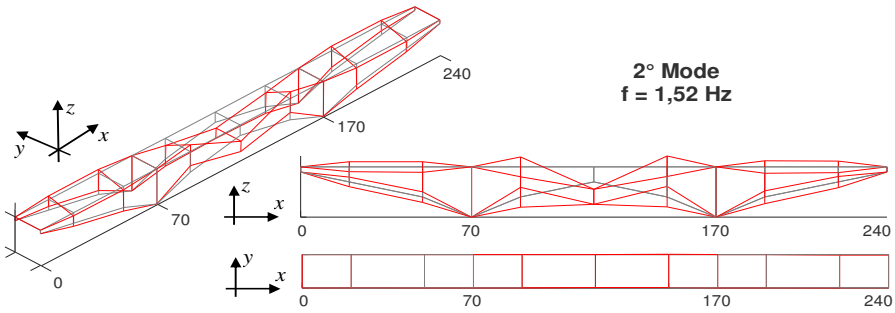

Figure 4.33 Views of the 2°Mode shape

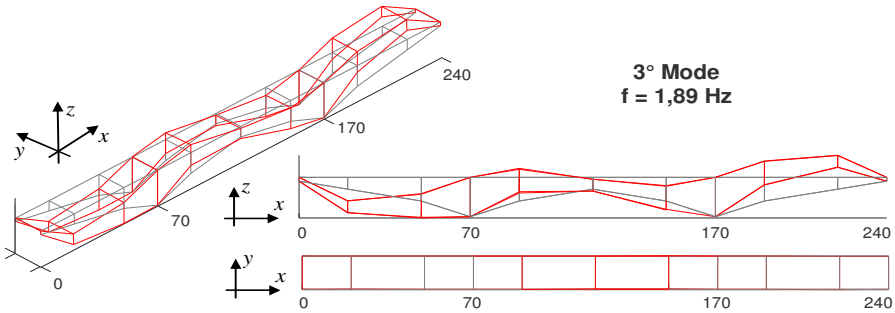

Figure 4.34 Views of the 3°Mode shape

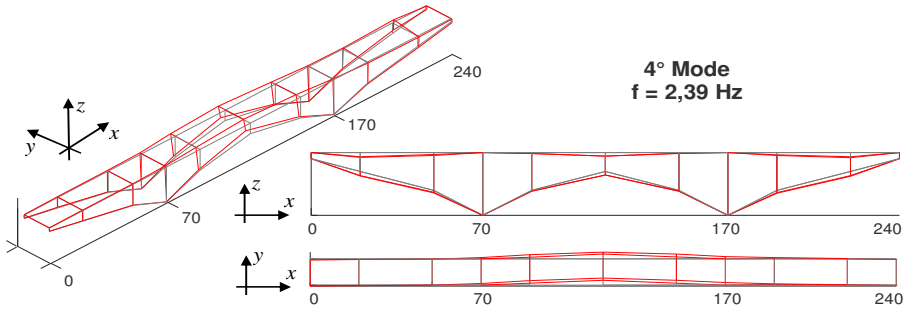

Figure 4.35 Views of the 4°Mode shape

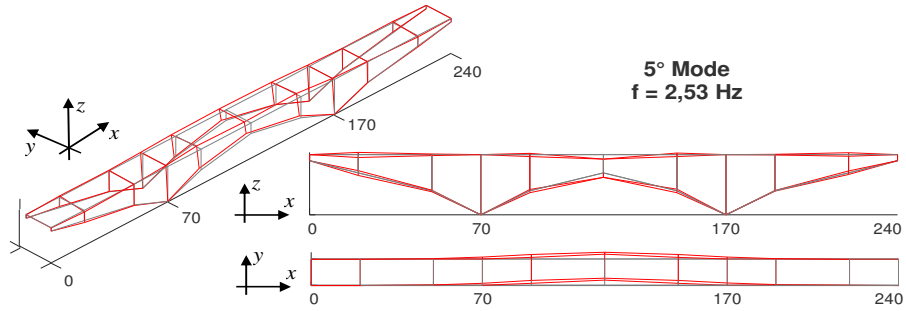

Figure 4.36 Views of the 5°Mode shape

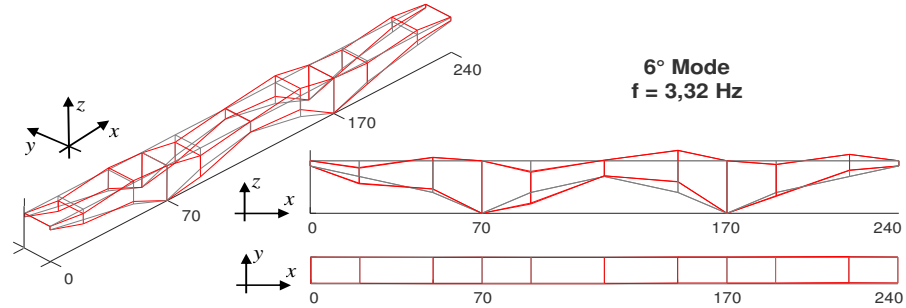

Figure 4.37 Views of the 6°Mode shape

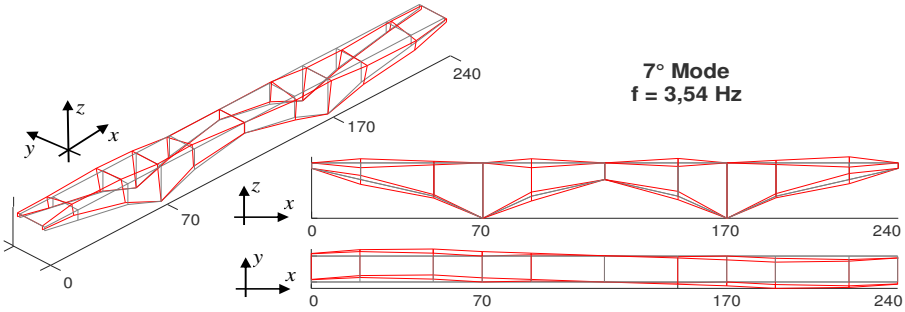

Figure 4.38 Views of the 7°Mode shape

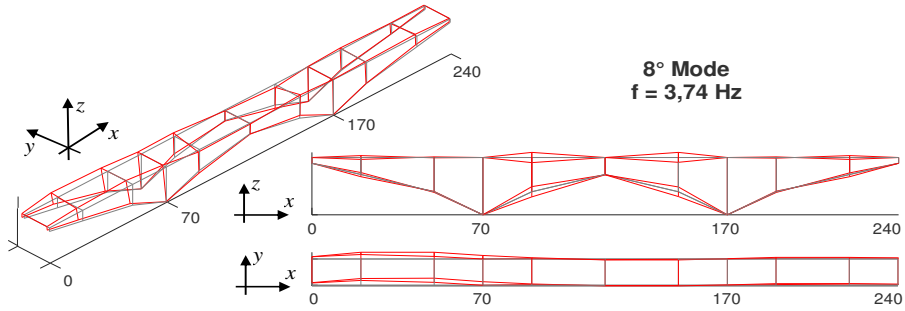

Figure 4.39 Views of the 8°Mode shape

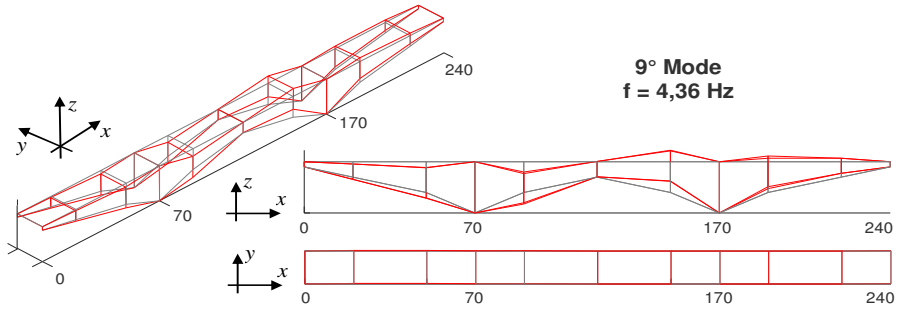

Figure 4.40 Views of the 9°Mode shape

The degree of coupling of the experimental mode shapes is presented through the Modal Assurance Criterion (MAC) in Figure 4.41. According to this criterion, a MAC equal to 1 identifies the perfect matching of the experimental mode shapes while a MAC equal to 0 denotes the orthogonality of the two modes. It is worth noting that the experimental data give good results in terms of mode shapes.

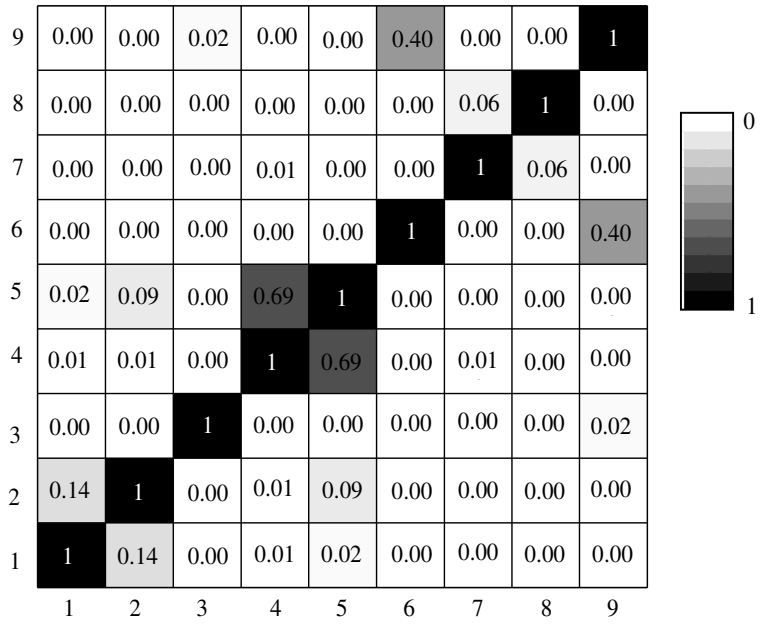

Figure 4.41 Auto MAC of "Paglia bridge"

4.2.3. Configurations P1

In addition to tests carried out for the overall identification of the structure, experimental investigations are performed to evaluate possible contributions of the soil-foundation compliance on the dynamic response of the bridge. For this purpose, pier P1 is selected, and some tests are performed with the aim of identifying the foundation translation and rocking. In particular, the instrumentation layout reported in Figure 4.42 is considered to capture translational and rotational accelerations of the foundation cap and the pier bent. In details, accelerometer 1Y catch the transverse displacement of the foundation cap while accelerometers 2Y, 3Z and 4Z are positioned to capture the rocking of the foundation.

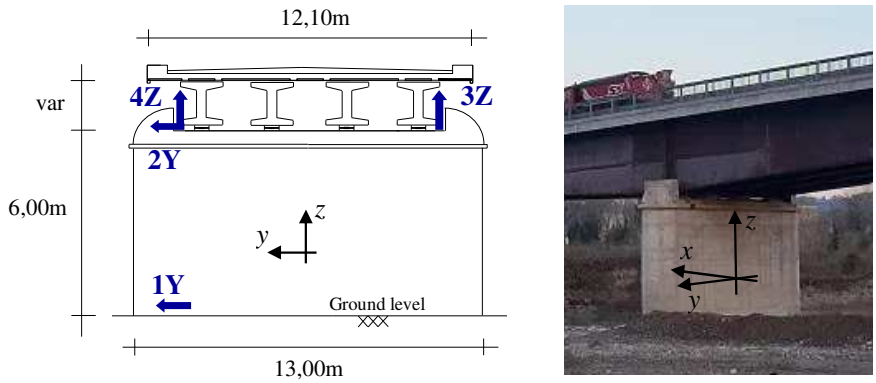

Figure 4.42 P1 Configuration

Concerning results of tests performed on pier P1, aimed at evaluating the contributions SSI on modal displacements, Table 23 reports the experimental fundamental frequencies and modal displacements identified by means of SSI-COV method. These frequencies correspond to those of the 1st, 2nd, 3th, 5th, 7th and 9th transverse modes of the deck, respectively (Figure 4.32 - Figure 4.39). Modal displacements reported in Table 23 are normalized with respect to the maximum displacement, always occurring at the pier top (sensor 2Y).

The overall displacement at the pier head is due to both the rigid motion of the foundation (Figure 4.45a) and the elastic deflection of the structural members constituting the pier (Figure 4.45b); in particular, Figure 4.44 shows, with a simple scheme how to calculate the horizontal and vertical displacements due to the rigid rotation, as a function of the Z3 displacements (scheme valid in the hypothesis of small displacements).

In this case we observe that of the seven selected modes, three modes (highlighted in the table) measure above all the vertical displacements with respect to the horizontal ones, probably deriving from flexional ways of the deck which cause an inflection in the plane of the pier, so we consider only three mode shapes that catch the transverse foundations rocking.

Table 23. Modal parameters of P1

f (Hz)	ξ (-)	1Y	2Y	3Z	4Z
1,14	1,11	-0,01	-0,03	-0,88	-1,00
1,51	1,61	0,47	1,00	0,54	-0,58
1,88	1,19	-0,07	-0,02	-0,68	-1,00
2,53	1,25	-0,46	-1,00	-0,49	0,48
3,56	2,55	0,45	1,00	0,37	-0,33
4,38	2,90	-0,08	-0,10	-0,88	-1,00

Stabilization diagram of the P1 Configuration is reported in Figure 4.43.

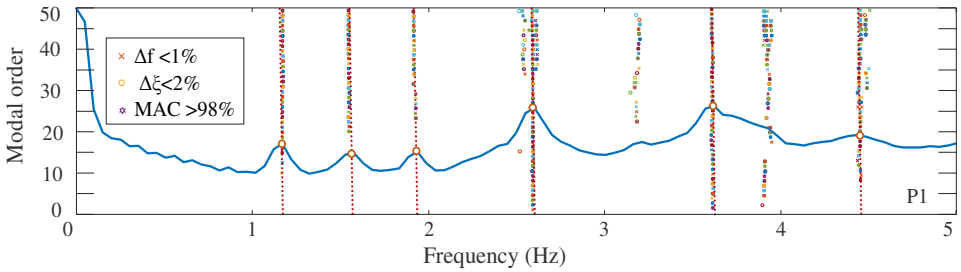

Figure 4.43 Stabilization Diagram of the P1 Configuration

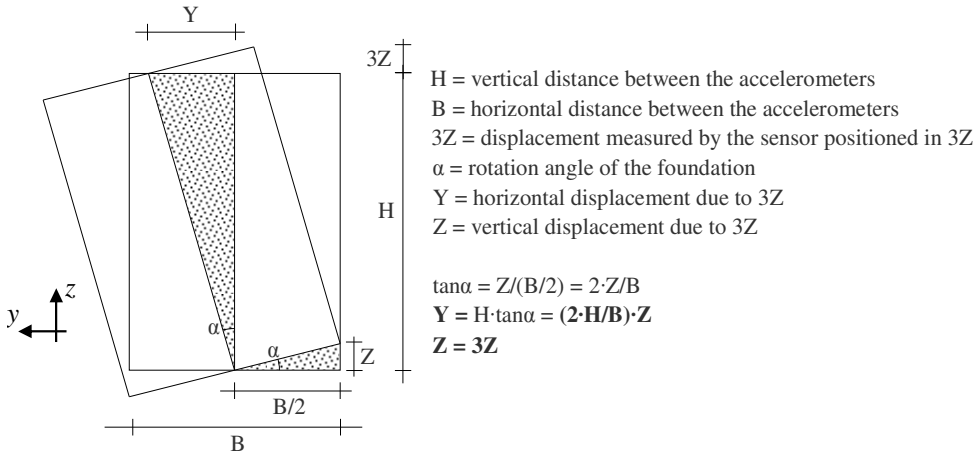

Figure 4.44 Simplified scheme of the rigid displacements due to the rocking for "Paglia bridge"

In this case H = 6.00 m and B = 13.00 m, so (2·H/B) = 0.9231 and the rigid displacements are reported in Table 24.

Table 24. Rigid displacements of P1 due to the rocking

f (Hz)	*1Y*	*2Y*	*3Z*	*4Z*	**Y**	**2Y – Y – 1Y**
1.51	*0.47*	*1.00*	*0.54*	*-0.58*	**0.50**	**0.03**
2.53	*-0.46*	*-1.00*	*-0.49*	*0.48*	**-0.45**	**-0.09**
3.56	*0.45*	*1.00*	*0.37*	*-0.33*	**0.34**	**0.21**

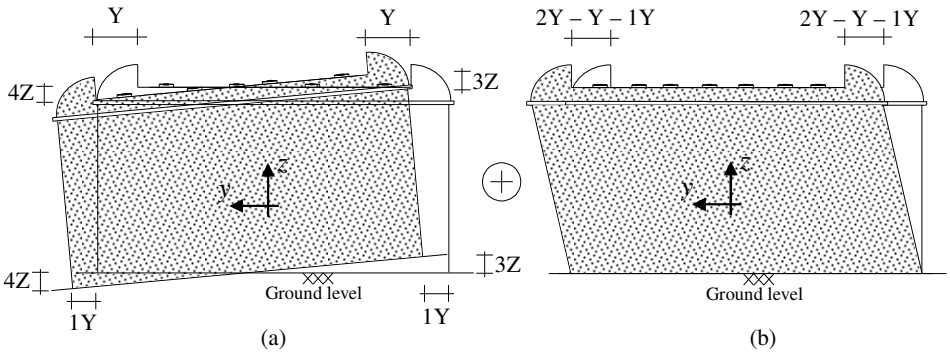

Figure 4.45 Contributions to the modal displacements: (a) foundation rigid translation and rocking and (b) pier deflection

Figure 4.45 clearly show the contributions to the modal displacements, due to a combination of foundation rigid translation/rocking and pier deflection; in particular, the 47% of the total displacement is due to the foundation translation, the 50% is produced by the foundation rocking while the remaining 3% of the displacement is due to the pier deflection. Finally, it can be observed that normalized modal displacements are almost the same for all the identified frequencies, i.e. frequencies are not associated to superior modes of the pier.

In this case, it is important compare the results of foundation rocking with the corresponding displacements in the deck, to evaluate if it moves rigidly with the pier or there is a deflection of the deck.

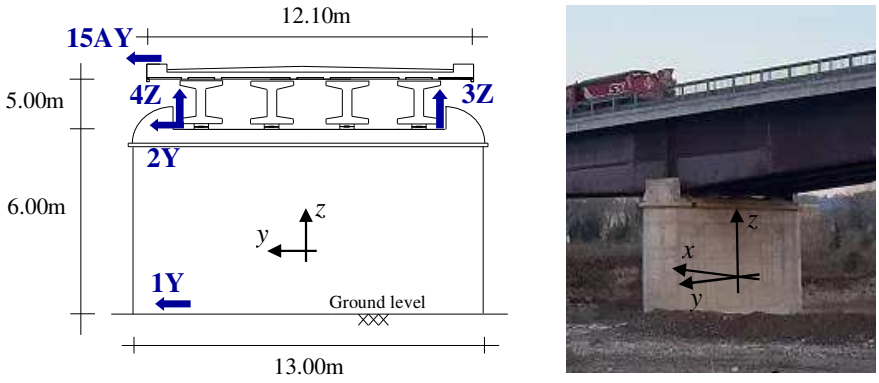

Figure 4.46 Comparison between 15AY and foundation rocking

In the case of the deck, H = 5.00 m and B = 13.00 m, so (2·H/B) = 0.7692 and the rigid displacements are reported in Table 25; the displacements obtained are normalized with respect to the maximum displacement (15AY);

Table 25. Rigid displacements of P3 compare with foundation rocking

f (Hz)	*1Y*	*2Y*	*3Z*	*4Z*	*15AY*	**15AY-2Y**	**Y**	**15AY – 2Y – Y – 1Y**
1.51	*0.17*	*0.33*	*0.17*	*-0.17*	1.00	**0.67**	**0.13**	**0.47**
2.53	*-0.11*	*-0.25*	*-0.14*	*0.11*	-1.00	**-0.75**	**-0.11**	**-0.53**
3.56	*0.15*	*0.31*	*0.11*	*-0.10*	1.00	**0.69**	**0.08**	**0.46**

This test is important because highlights that deck deflections affects the dynamics of the viaduct, even for low intensity actions, contributing to the 50% of the overall modal displacement of the deck.

Moreover, the grey column in the table highlight that about 70% of the deck displacements is caused by deck deflection, so the contribution of the pier is the remain 30%.

So, Table 24 can be scaled considering the value of Table 25, normalized respect the displacement on the deck; in this case H = 6.00 m and B = 13.00 m, so (2·H/B) = 0.9231 and the rigid displacements are reported in Table 26

Table 26. Rigid displacements of P1 due to the rocking without deck deflection

f (Hz)	*1Y*	*2Y*	*3Z*	*4Z*	**Y**	**2Y – Y – 1Y**
1.51	*0.17*	*0.33*	*0.17*	*-0.17*	**0.15**	**0.01**
2.53	*-0.11*	*-0.25*	*-0.14*	*0.11*	**-0.13**	**-0.01**
3.56	*0.15*	*0.31*	*0.11*	*-0.10*	**0.10**	**0.05**

4.3. “Cesano” bridge - Corinaldo (AN), Italy

4.3.1. Introduction

The viaduct consists of a single carriageway with two gear lanes, one in each direction. In order to better investigate the global dynamic behaviour of the deck it was possible to adopt test configurations that involved both lanes. In particular, the environmental vibration measurements were performed according to 2 configurations:

- Conf-1 configuration has been designed to mainly evaluate the transversal behaviour of the viaduct, and therefore provides for the positioning of almost all accelerometers on the upstream lane, with transversal measurement direction (in Figure 4.47a) the arrow indicates the measurement direction of the sensors while the square with the dot in the middle indicates the vertical measurement direction upwards);

- Conf-2 configuration was instead designed to capture the bending-torsional behaviour of the deck, and therefore provides for the positioning of the accelerometers on both sides of the carriageway, with vertical measurement direction (Figure 4.47b).

The two accelerometers positioned at measurement point 44, with a progression equal to about 44 m, one with a transverse measurement direction (44AY) and the other two with vertical measurement direction (44AZ, 44BZ), were always left in the same position and used as reference sensors, on the basis of which it has been possible to join the recordings of the two configurations as if they were acquired synchronously (the two sensors are shown in dark red in Figure 4.47 and in Table 27).
The sensors used in the two configurations, their denomination and position (progressive distance from the left abutment) are shown in Table 27.

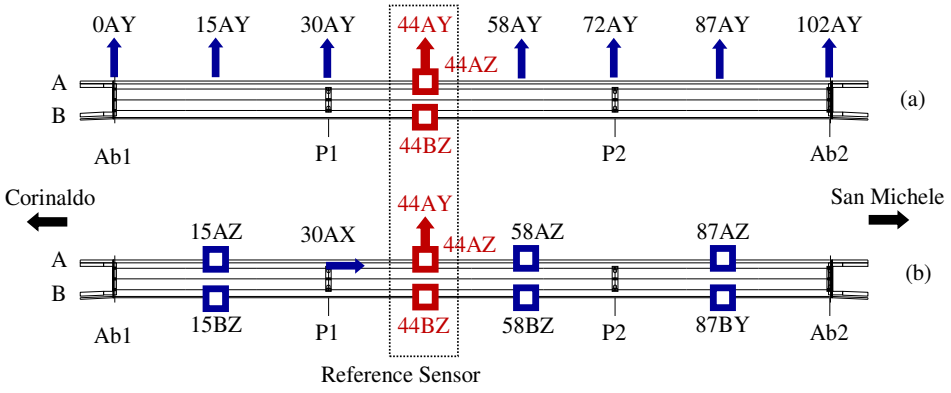

Figure 4.47 “Cesano bridge” configurations: (a) Configuration Conf-1, (b) Configuration Conf-2

In the same test to the sensors placed on the deck and shown in Figure 4.47, some accelerometers were positioned at pier P1 and P2, just above the level of the ground (Figure 4.48). The sensors were arranged with transversal measuring direction in order to evaluate the contribution of the pier to the measured transverse displacement at the level of the deck.

Table 27. Progressive distances of the accelerometers from Ab1

Position	0#	15#	30#	44#	58#	72#	87#	102#
Distance (m)	0	14.73	29.45	43.45	57.45	71.45	86.18	100.90

AVTs are carried out with low noise unidirectional piezoelectric accelerometers connected to a 24-bit data acquisition system by means of coaxial cables and a portable PC for data storage (Figure 4.49). In ambient vibration tests, the input is not controlled and is assumed to have a flat spectrum such as a white noise. This assumption is not really true, and the input magnitude can be of a certain importance when, because of the limited number of available sensors and/or the insufficient number of channels of the acquisition system, the structural response cannot be measured in just one test. In these cases, tests must be repeated in different times, considering different configurations (i.e. varying the position of sensors) and finally a merging operation of the recorded data is necessary. This method requires that a group of sensors, called reference sensors, are left in the same place for all the test configurations so that they can be used to scale the data of different tests, acquired by sensors moved in different places (roving sensors).

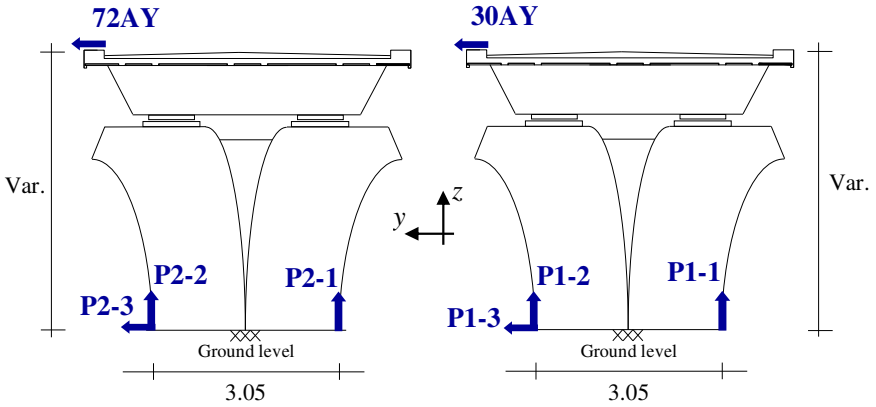

Figure 4.48 P1 and P2 Configurations (Step1)

In order to catch the transverse dynamic behaviour of the bridge, for each configuration unidirectional accelerometers are placed at each span support and oriented in the transverse direction. Bees wax is used to fix accelerometers preventing any relative movements between the deck and the sensor.

For each configuration, 1800 seconds long records sampled at a rate of 2048 Hz (the minimum rate for the used equipment) are acquired; this time length provides enough frequency resolution to guarantee a good accuracy of identified modal parameters.

Figure 4.49 Photos of the instrumentation setup

All the recorded data are processed with standard signal processing techniques before performing the modal analyses. Initially, data are carefully inspected in order to cut those parts characterized by anomalous behaviours (signal clipping, intermittent noise, spikes and so on) due to sensor or measurement chain malfunctioning or due to signal saturation. Then, the contribution of spurious trends is eliminated through a baseline correction (adopting a second order polynomial) and the high frequency content is eliminated by filtering with a Butterworth low pass filter characterized by order 4 and a cut-off frequency of 20 Hz. Finally, signals are down-sampled at 51.2 Hz to decrease the number of data and make the successive analyses faster.
In this case, the Covariance Stochastic Subspace Identification (SSI-Cov) technique was used to identify the dynamic properties of the viaduct from the recordings. For KC1 tests were made at different times, according to different sensors configurations; in operational modal analysis of large structures this often occurs, making necessary to process data from multiple non-simultaneously recorded measurement setups. The Post Separate Estimation Re-scaling (PoSER) approach is used to process the data in this case.
The modal parameter identification (i.e. natural frequencies, damping ratios and the relevant mode shapes) is performed through the SSI-Cov method working in the frequency domain, implemented in Matlab environment. Modal parameters obtained from the AVTs will be presented in a dedicated section in which numerical and experimental results are compared.

The tests covered the viaduct and the piers P1 and P2 at different step. In Figure 4.47 the positioning of the accelerometers for the kinematic chains is reported, specifically they were recorded the transverse accelerations contained in the horizontal plane with direction orthogonal to the axis of the deck, which are the most significant from the point of view of seismic behaviour. In addition to tests carried out for the overall identification of the structure, experimental investigations are performed to evaluate possible contributions of the soil-foundation compliance on the dynamic response of the bridge. For this purpose, pier P1 and P2 of the viaduct is selected, and some tests are performed with the aim of identifying the foundation translation and rocking. In particular, the instrumentation layout reported in Figure 4.48 is considered to capture translational and rotational accelerations of the foundation cap and the pier bent.

Tests carried out will be illustrated in detail below.

4.3.2. Configurations Conf-1 and Conf-2 (global behaviour)

All the recorded data are processed with standard signal processing techniques before performing the modal analyses through SSI-Cov method, which returns for each configuration, a stabilization diagram in which the average of the cross power spectrum density (cpsd) of the signals measured by the 13 accelerometers (black line) is represented; furthermore, the procedure with the increase in the order of the model inserts a symbol if there are negligible variations at the level of frequencies, damping and modal forms (MAC), as indicated in the legend (Figure 4.50).

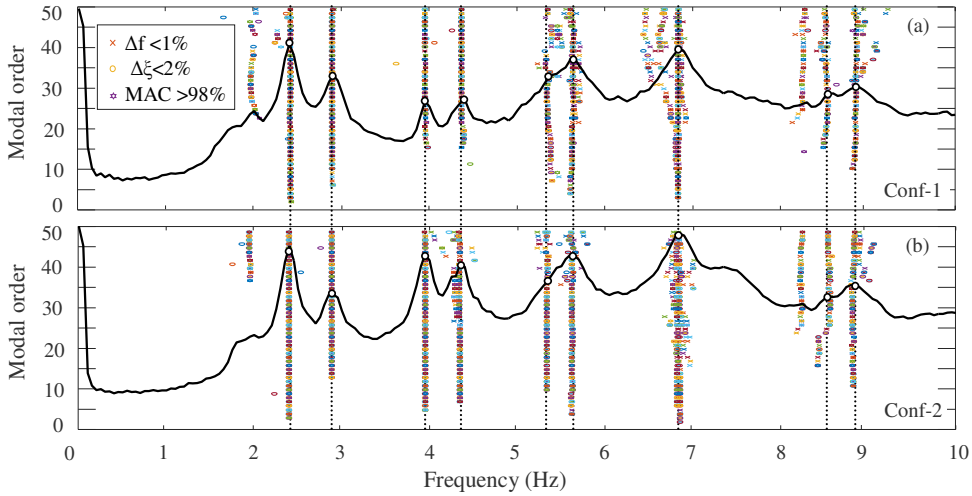

Figure 4.50 Stabilization diagram of "Cesano bridge" configurations (Step 1): (a) Conf-1, (b) Conf-2

The first mode shapes of the "Cesano bridge", are selected in the diagram (dash lines in Figure 4.50).

Table 28 and Table 29 shows the frequencies, damping and modal displacements related to the first mode shapes of the Conf-1 and Conf-2

Table 28. Modal parameters of Conf-1

Mode	1	2	3	4	5	6	7	8	9
***f* (Hz)**	**2.40**	**2.91**	**3.95**	**4.37**	**5.43**	**5.65**	**6.85**	**8.56**	**8.88**
ξ (-)	**1.12**	**1.93**	**0.80**	**1.20**	**2.65**	**1.49**	**1.49**	**1.60**	**1.19**
44AY	0.01	-0.99	-0.01	0.00	0.38	0.11	0.01	-0.12	-0.13
44BZ	-0.97	-0.83	-1.00	-0.99	0.62	-0.99	1.00	1.00	-0.78
44AZ	-1.00	0.85	-0.95	-1.00	-0.72	1.00	0.72	0.71	1.00
0AY	0.00	-0.06	-0.03	0.04	0.40	0.01	-0.01	-0.01	0.11
15AY	0.00	-0.44	-0.11	0.08	1.00	0.08	-0.07	-0.03	0.18
30AY	0.00	-0.75	-0.02	0.00	0.95	0.14	-0.02	-0.03	0.00

58AY	0.01	-1.00	-0.03	0.00	-0.46	0.11	0.11	-0.12	0.07
72AY	0.00	-0.77	0.00	0.01	-0.99	0.14	0.03	-0.02	-0.03
87AY	0.01	-0.43	-0.01	0.01	-0.91	0.08	-0.04	0.00	-0.15
102AY	0.00	-0.06	0.02	0.02	-0.28	0.00	-0.02	0.00	-0.06

Table 29. Modal parameters of Conf-2

Mode	1	2	3	4	5	6	7	8	9
***f* (Hz)**	**2.40**	**2.89**	**3.95**	**4.34**	**5.46**	**5.63**	**6.85**	**8.56**	**8.83**
ξ (-)	**0.90**	**2.27**	**0.96**	**1.43**	**2.78**	**1.66**	**1.21**	**1.37**	**2.05**
44AY	0.01	1.00	0.00	0.01	0.25	0.12	-0.09	0.11	-0.10
44BZ	-0.98	0.87	-0.24	-0.45	0.40	-0.92	0.82	-1.00	-0.92
44AZ	-1.00	-0.83	-0.23	-0.44	-0.40	0.91	1.00	-0.30	0.91
15BZ	0.39	0.42	0.95	-0.98	0.95	-0.07	0.50	0.02	0.22
15AZ	0.40	-0.44	0.98	-1.00	-0.94	0.09	-0.07	-0.15	-0.21
44AX	0.00	-0.10	-0.02	-0.02	0.14	0.03	0.07	0.01	0.08
58AZ	-0.99	-0.80	0.22	-0.43	0.34	0.97	-0.81	-0.75	-0.87
58BZ	-0.99	0.88	0.20	-0.43	-0.34	-1.00	-0.99	-0.24	1.00
87AZ	0.40	-0.46	-0.99	-0.98	1.00	0.28	-0.52	0.01	0.16
87BZ	0.41	0.42	-1.00	-0.98	-1.00	-0.30	0.05	-0.16	-0.26

Two obtained configurations must be scaled with respect to the reference sensor, so as to have modal displacements comparable between the different configurations;

The Post Separate Estimation Re-scaling (PoSER) approach is used to process the data in this case, and the final modal parameters of “Paglia bridge” are shown in Table 30.

Table 30. Modal parameters of “Cesano Bridge” (PoSER)

Mode	1	2	3	4	5	6	7	8	9
***f* (Hz)**	**2.40**	**2.90**	**3.95**	**4.36**	**5.45**	**5.64**	**6.85**	**8.56**	**8.86**
ξ (-)	**1.01**	**2.10**	**0.88**	**1.32**	**2.72**	**1.58**	**1.35**	**1.49**	**1.62**
0AY	0.00	-0.06	-0.03	0.04	0.40	0.02	-0.01	-0.01	0.11
15AY	0.00	-0.44	-0.11	0.08	1.00	0.08	-0.07	-0.03	0.18
15AZ	0.40	-0.44	0.98	-1.00	-0.94	0.09	-0.07	-0.15	-0.21
15BZ	0.39	0.42	0.95	-0.98	0.95	-0.07	0.50	0.02	0.22
30AY	0.00	-0.75	-0.02	0.00	0.95	0.14	-0.02	-0.03	0.00
44AY	0.01	1.00	0.00	0.01	0.25	0.12	-0.09	0.11	-0.10
44AZ	-1.00	-0.83	-0.23	-0.44	-0.40	0.91	1.00	-0.30	0.91
44BZ	-0.98	0.87	-0.24	-0.45	0.40	-0.92	0.82	-1.00	-0.92
58AY	0.01	-1.00	-0.03	0.00	-0.46	0.11	0.11	-0.12	0.07
58AZ	-0.99	-0.80	0.22	-0.43	0.34	0.97	-0.81	-0.75	-0.87

58BZ	-0.99	0.88	0.20	-0.43	-0.34	-1.00	-0.99	-0.24	1.00
72AY	0.00	-0.77	0.00	0.01	-0.99	0.14	0.03	-0.02	-0.03
87AY	0.01	-0.43	-0.01	0.01	-0.91	0.08	-0.04	0.00	-0.15
87AZ	0.40	-0.46	-0.99	-0.98	1.00	0.28	-0.52	0.01	0.16
87BZ	0.41	0.42	-1.00	-0.98	-1.00	-0.30	0.05	-0.16	-0.26
102AY	0.00	-0.06	0.02	0.02	-0.28	0.00	-0.02	0.00	-0.06

For the representation of the modal shapes, hypotheses were also made according to the constraints offered to the bridge by the supports; in particular, for the Conf-1 configuration used to describe the transversal behaviour of the bridge, the transversal displacements of the same section were assumed to be identical, while for the Conf-2 configuration, designed to capture the bending-torsional behaviour of the deck, the vertical displacements at the abutments and piers were considered null. These hypotheses can be considered true, for environmental vibration measurements, also for the points in which the support provided a degree of transversal freedom, since the friction forces, even if low, are not exceeded.

Figure 4.51 to Figure 4.59 represents the first mode shapes of “Cesano bridge”.

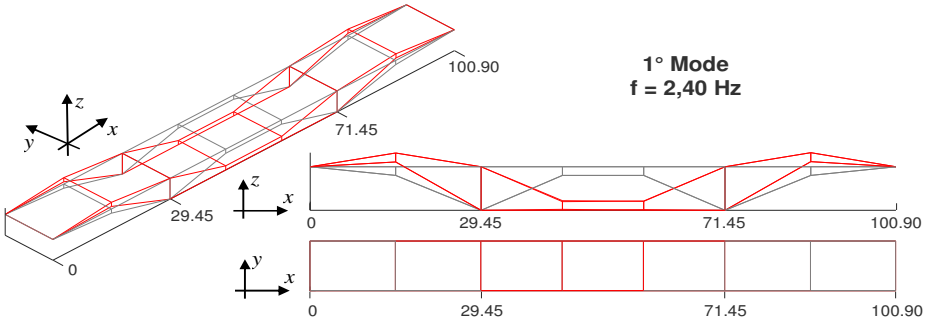

Figure 4.51 Views of the 1°Mode shape

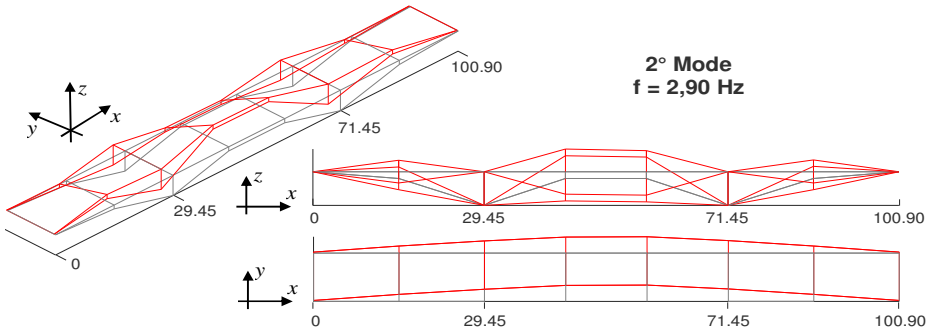

Figure 4.52 Views of the 2°Mode shape

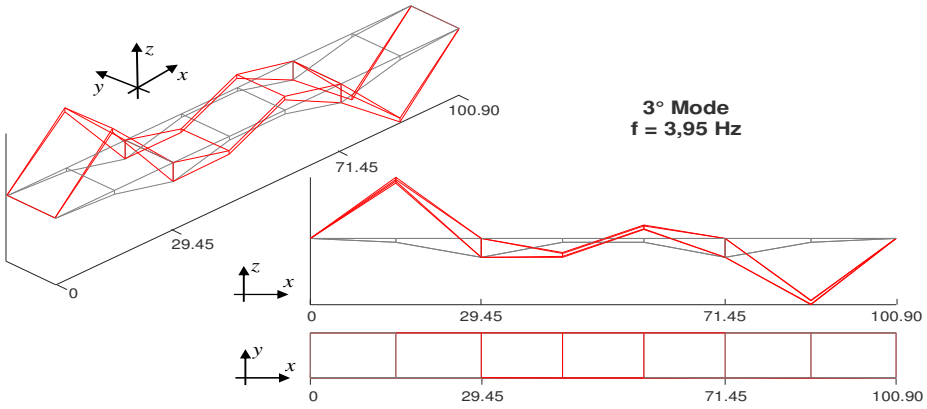

Figure 4.53 Views of the 3°Mode shape

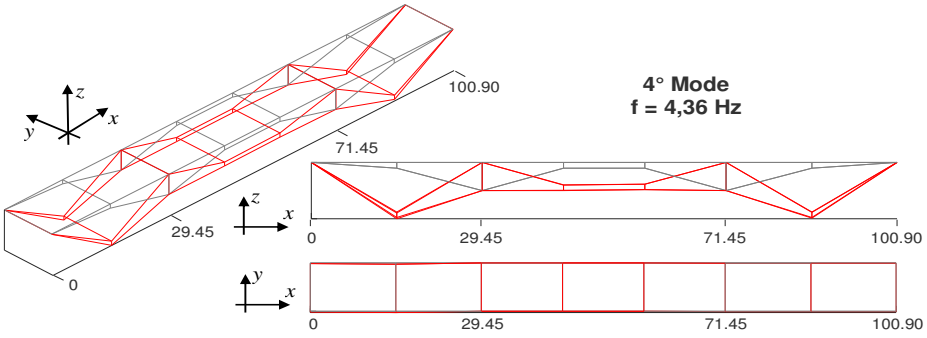

Figure 4.54 Views of the 4°Mode shape

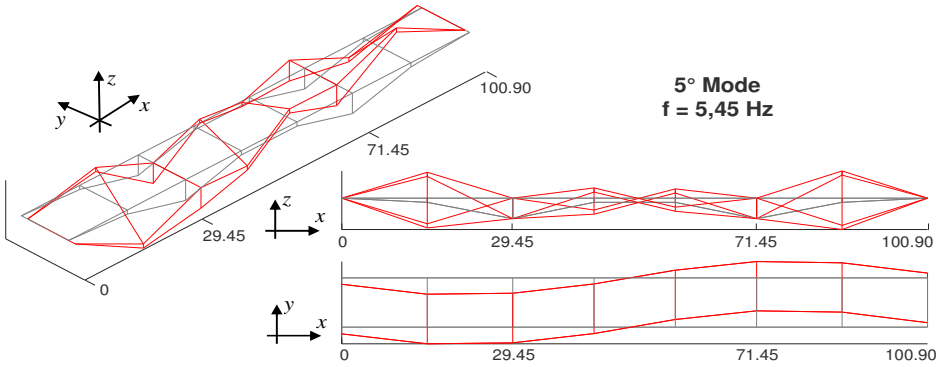

Figure 4.55 Views of the 5°Mode shape

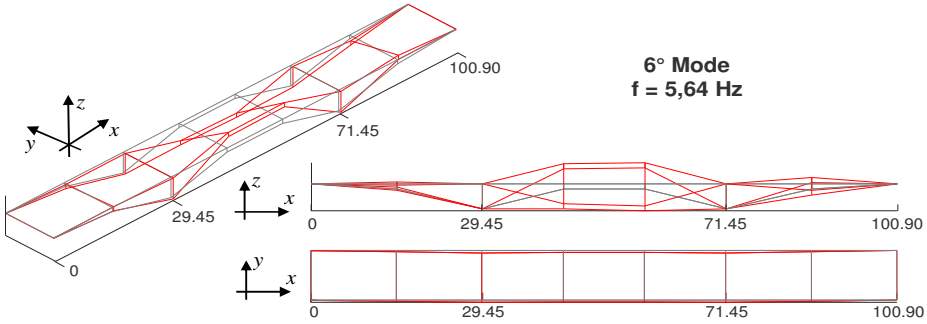

Figure 4.56 Views of the 6°Mode shape

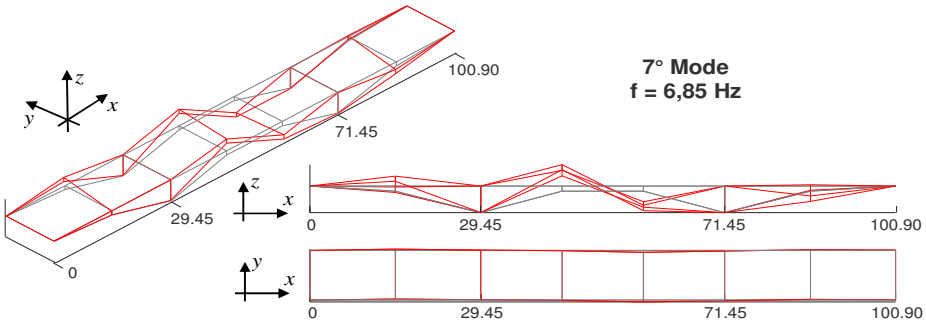

Figure 4.57 Views of the 7°Mode shape

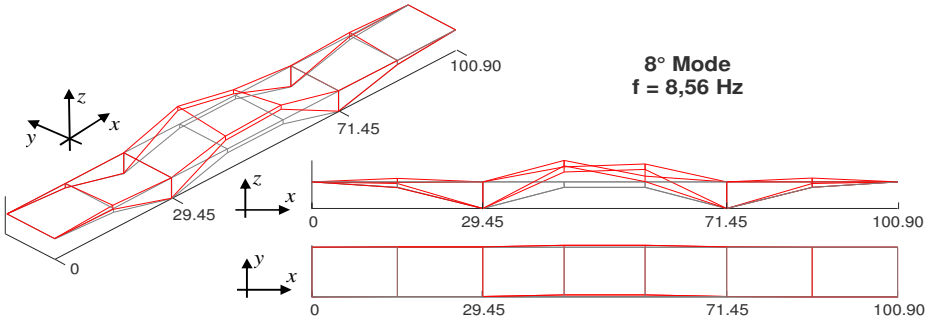

Figure 4.58 Views of the 8°Mode shape

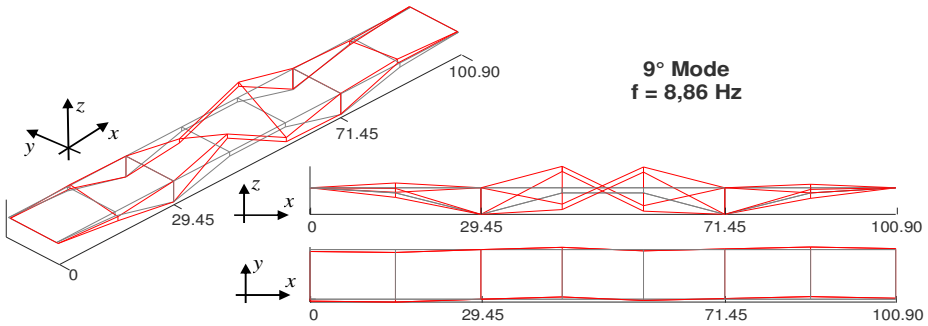

Figure 4.59 Views of the 9°Mode shape

The degree of coupling of the experimental mode shapes is presented through the Modal Assurance Criterion (MAC) in Figure 4.60. According to this criterion, a MAC equal to 1 identifies the perfect matching of the experimental mode shapes while a MAC equal to 0 denotes the orthogonality of the two modes. It is worth noting that the experimental data give good results in terms of mode shapes.

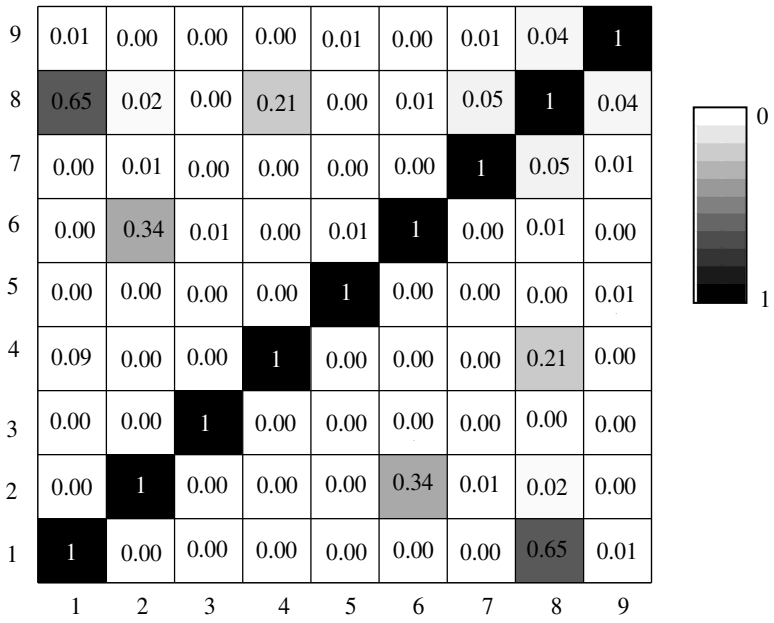

Figure 4.60 Auto MAC of "Cesano bridge"

Tests on the deck were also carried out for the other steps, but from the results it can be seen that the modal shapes are negligibly variable as the pier height varies, so that the stabilization diagrams and modal shapes of the four steps do not reported, but in Table 31 are reported only the final results.

Table 31. Frequency variable at different Step

	Step1	*Step2*	*Step3*	*Step4*
Mode	f (Hz)	f (Hz)	f (Hz)	f (Hz)
1	2.40	2.31	2.30	2.29
2	2.90	2.68	2.42	2.78
3	3.95	3.81	3.81	3.56
4	4.36	4.18	4.19	4.23
5	5.45	4.93	4.84	5.02
6	5.64	5.29	5.14	5.29
7	6.85	6.55	6.50	6.68
8	8.56	7.95	7.98	7.00
9	8.86	8.13	8.13	8.75

Instead, it is important to consider the different steps to evaluate the foundation rocking, so the displacements of the piers are analysed at each step.

4.3.3. Piers P1 and P2 (Step1)

In the same tests carried out for the overall identification of the structure, experimental investigations are performed to evaluate possible contributions of the soil-foundation compliance on the dynamic response of the bridge. For this purpose, pier P1 and P2 some tests are performed with the aim of identifying the foundation translation and rocking. In particular, the instrumentation layout reported in Figure 4.61 is considered to capture translational and rotational accelerations of the foundation cap and the pier bent. In details, accelerometer P#-3 catch the transverse displacement of the foundation cap while accelerometers P#-1 and P#-2 are positioned to capture the rocking of the foundation.

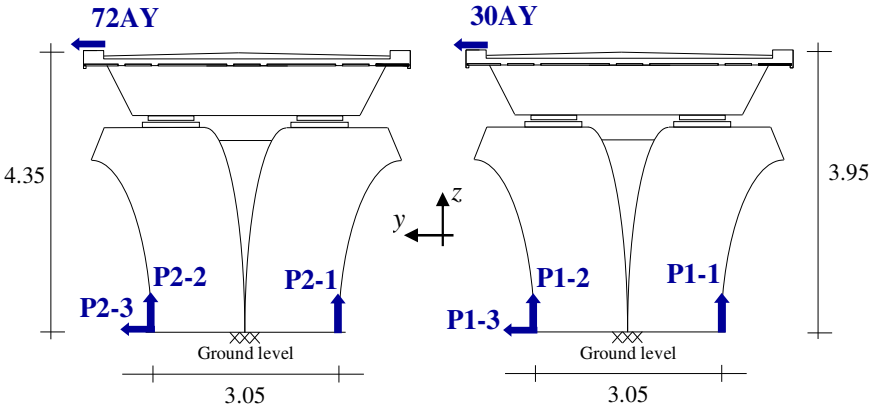

Figure 4.61 P1 and P2 Configurations (Step1)

Concerning results of tests performed on pier P1 and P2, aimed at evaluating the contributions SSI on modal displacements, Table 32 and Table 33 reports the experimental fundamental frequencies and modal displacements identified by means of SSI-Cov method, taking into account separately the sensors on the P1 and those on P2 and normalizing them with respect to the maximum displacement. The overall displacement at the pier head is due to both the rigid motion of the foundation (Figure 4.64a) and the elastic deflection of the structural members constituting the pier (Figure 4.64b).

Table 32. Modal parameters of Configuration P1

f (Hz)	ξ (-)	P1-1	P1-2	P1-3	30AY
1.98	4.62	-1.00	-0.50	-0.36	-0.77
2.40	1.01	-0.73	-1.00	0.32	0.67
2.90	2.10	-0.09	0.09	-0.28	-1.00
3.95	0.88	1.00	0.98	-0.22	-0.60
4.36	1.32	-1.00	-0.95	-0.03	0.03
5.45	2.72	0.07	-0.10	0.20	1.00
5.64	1.58	-0.10	-0.23	0.82	1.00
6.85	1.35	1.00	0.70	0.71	-0.59
8.56	1.49	-0.21	-0.32	-0.43	-1.00
8.86	1.62	0.41	0.20	1.00	-0.03

Table 33. Modal parameters of Configuration P2

f (Hz)	ξ (-)	P2-1	P2-2	P2-3	72AY
1.98	4.62	0.86	1.00	-0.38	-0.99
2.40	1.01	-0.71	-1.00	0.13	0.51
2.90	2.10	-0.09	0.10	-0.25	-1.00
3.95	0.88	-1.00	-0.87	0.09	0.08
4.36	1.32	-1.00	-0.94	-0.02	0.12
5.45	2.72	-0.08	0.10	-0.18	-1.00
5.64	1.58	-0.27	-0.14	0.80	1.00
6.85	1.35	-0.72	-1.00	0.23	0.80
8.56	1.49	-0.41	-0.71	-0.04	-1.00
8.86	1.62	-0.19	0.64	-1.00	-0.52

Stabilization diagram of the only piers configuration is reported in Figure 4.62, and from the comparison with stabilization diagram of the global configuration, we can note that the first two and the last two mode shapes are not typical of the piers, but of the deck (these mode shapes are shown in blue in the tables Table 32 and Table 33).

Furthermore, among the mode shapes listed in tables, there are some modal shapes which do not show a transverse rotation of the foundation, but on the contrary seem to indicate a rotation in the longitudinal direction of the viaduct, probably due to a longitudinal bending of the bridge (these mode shapes are highlighted in grey in the tables Table 32 and Table 33).

Practically, we consider only the two clearly transversal mode shapes.

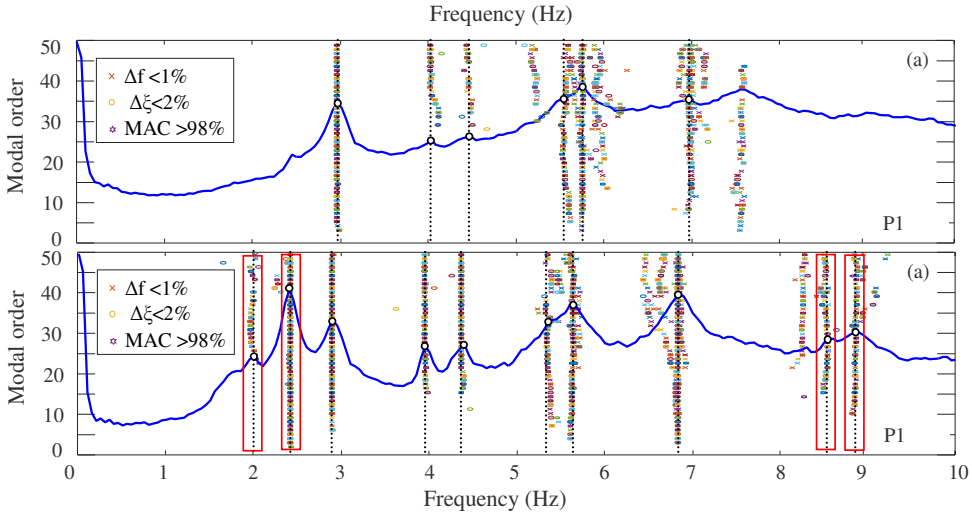

Figure 4.62 Stabilization Diagram: (a) piers configuration, (b) global configuration

Figure 4.63 shows, with a simple scheme how to calculate the horizontal and vertical displacements due to the rigid rotation, as a function of the P2-1 or P1-1 displacements (scheme valid in the hypothesis of small displacements).

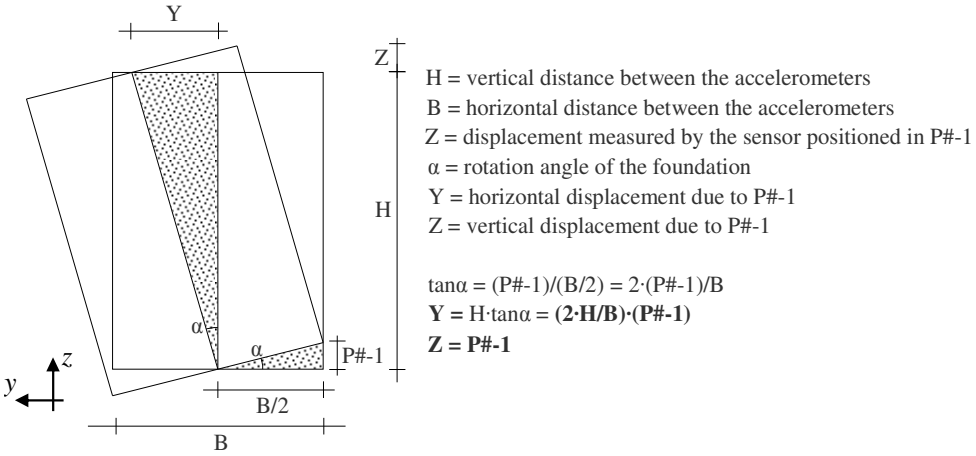

Figure 4.63 Simplified scheme of the rigid displacements due to the rocking for "Cesano bridge"

In the case of P1, H = 3.95 m and B = 3.05 m, so (2·H/B) = 2.5902 and the rigid displacements of the transverse foundation rocking are reported in Table 34

Table 34. Rigid displacements of P1 due to the rocking (Step1)

f (Hz)	ξ (-)	P1-1	P1-2	P1-3	30AY	Y	30AY - Y - (P1-3)
2.90	2.10	-0.09	0.09	-0.28	-1.00	-0.23	-0.49
5.45	2.72	0.07	-0.10	0.20	1.00	0.18	0.62

In the case of P2, H = 4.35 m and B = 3.05 m, so (2·H/B) = 2.8525 and the rigid displacements of the transverse foundation rocking are reported in Table 35

Table 35. Rigid displacements of P2 due to the rocking (Step1)

f (Hz)	ξ (-)	P2-1	P2-2	P2-3	72AY	Y	72AY - Y - (P2-3)
2.90	2.10	-0.09	0.10	-0.25	-1.00	-0.26	-0.49
5.45	2.72	-0.08	0.10	-0.18	-1.00	-0.23	-0.59

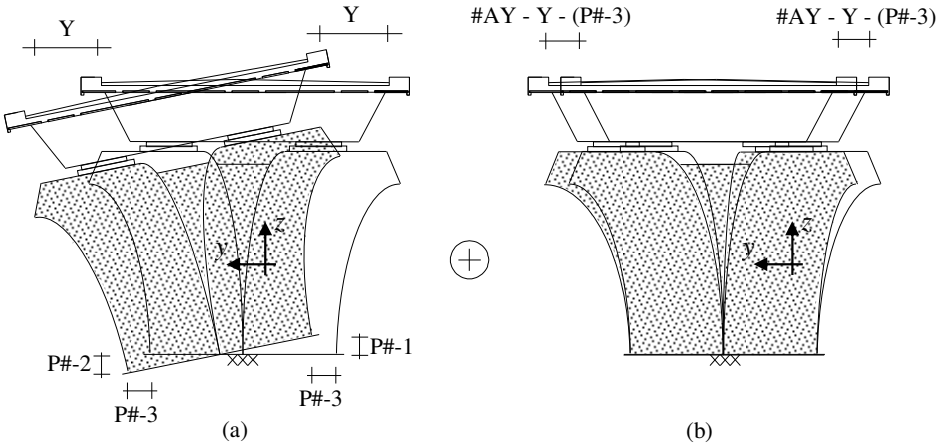

Figure 4.64 Contributions to the modal displacements "Cesano bridge" (Step1): (a) foundation rigid translation and rocking and (b) pier deflection

Figure 4.64 clearly show the contributions to the modal displacements, due to a combination of foundation rigid translation/rocking and pier deflection; in particular, the 18÷28% of the total displacement is due to the foundation translation, the 18÷26% is produced by the foundation rocking while the remaining 49÷62% of the displacement is due to the pier deflection. Finally, it can be observed that normalized modal displacements are almost the same for all the identified frequencies, i.e. frequencies are not associated to superior modes of the pier.

This test is important because highlights that SSI affects the dynamics of the viaduct, even for low intensity actions, contributing to the 18÷26% of the overall modal displacement of the deck.

4.3.4. Piers P1 and P2 (Step 2)

In the same tests carried out for the overall identification of the structure, experimental investigations are performed to evaluate possible contributions of the soil-foundation compliance on the dynamic response of the bridge. For this purpose, pier P1 and P2 some tests are performed with the aim of identifying the foundation translation and rocking. In particular, the instrumentation layout reported in Figure 4.65 is considered to capture translational and rotational accelerations of the foundation cap and the pier bent. In details, accelerometer P#-3 catch the transverse displacement of the foundation cap while accelerometers P#-1 and P#-2 are positioned to capture the rocking of the foundation.

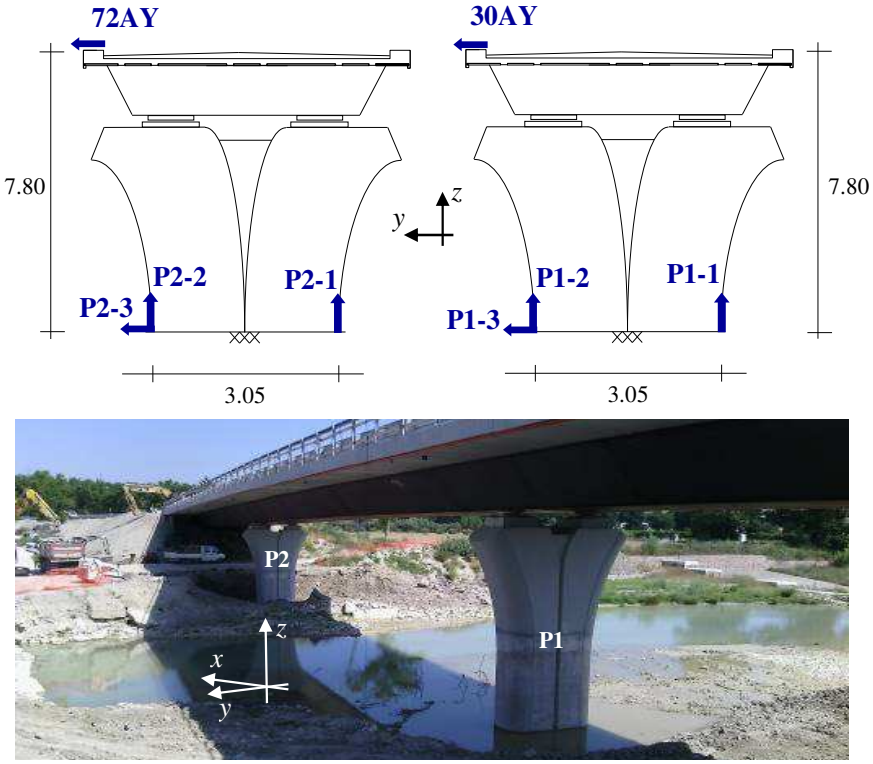

Figure 4.65 P1 and P2 Configurations (Step2)

Concerning results of tests performed on pier P1 and P2, aimed at evaluating the contributions SSI on modal displacements, Table 36 and Table 37 reports the experimental fundamental frequencies and modal displacements identified by means of SSI-Cov method, taking into account separately the sensors on the P1 and those on P2 and normalizing them with respect to the maximum displacement. The overall displacement at the pier head is due to both the rigid motion of the foundation (Figure 4.66a) and the elastic deflection of the structural members constituting the pier (Figure 4.66b).

As demonstrated in the case of Step1, only the transversal modes are significant for the rigid rotation of the foundation, so in this case the demonstrations are left out and only the two transversal modes are considered (2°Mode and 5°Mode).

Table 36. Modal parameters of Configuration P1 (Step2)

f (Hz)	ξ (-)	P1-1	P1-2	P1-3	30AY
2.68	1.86	-0.07	0.07	-0.10	-1.00
4.93	2.41	0.05	-0.07	0.07	1.00

Table 37. Modal parameters of Configuration P2 (Step2)

f (Hz)	ξ (-)	P2-1	P2-2	P2-3	72AY
2.68	1.86	-0.08	0.06	-0.12	-1.00
4.93	2.41	-0.05	0.07	-0.12	-1.00

Figure 4.66 shows, with a simple scheme how to calculate the horizontal and vertical displacements due to the rigid rotation, as a function of the P2-1 or P1-1 displacements (scheme valid in the hypothesis of small displacements).

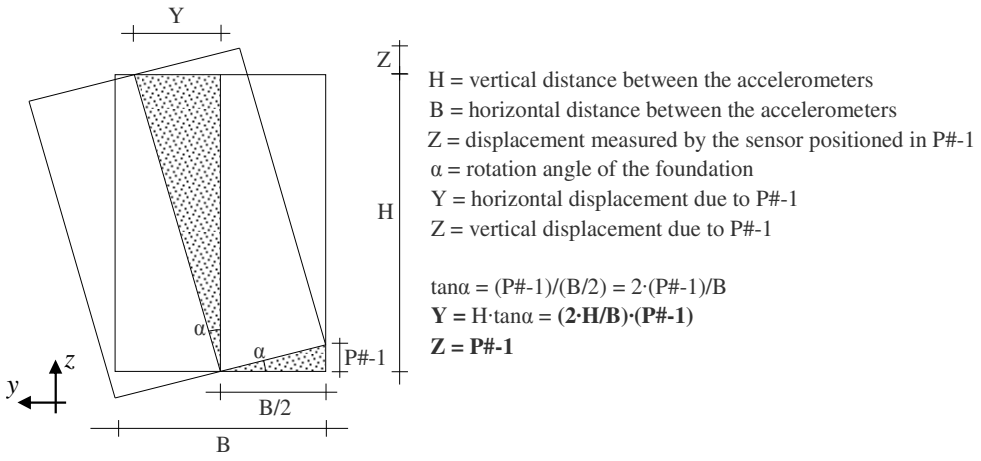

Figure 4.66 Simplified scheme of the rigid displacements due to the rocking for "Cesano bridge"

In the case of P1, H = 7.80 m and B = 3.05 m, so (2·H/B) = 5.1148 and the rigid displacements of the transverse foundation rocking are reported in Table 38

Table 38. Rigid displacements of P1 due to the rocking (Step2)

f (Hz)	ξ (-)	P1-1	P1-2	P1-3	30AY	Y	30AY - Y - (P1-3)
2.68	1.86	0.07	-0.07	0.10	1.00	0.36	0.54
4.93	2.41	0.06	-0.07	0.07	1.00	0.31	0.62

In the case of P2, H = 7.80 m and B = 3.05 m, so (2·H/B) = 5.1148 and the rigid displacements of the transverse foundation rocking are reported in Table 39.

Table 39. Rigid displacements of P2 due to the rocking (Step2)

f (Hz)	ξ (-)	P2-1	P2-2	P2-3	72AY	Y	72AY - Y - (P2-3)
2.68	1.86	-0.08	0.06	-0.12	-1.00	-0.41	-0.47
4.93	2.41	-0.06	0.07	-0.12	-1.00	-0.31	-0.57

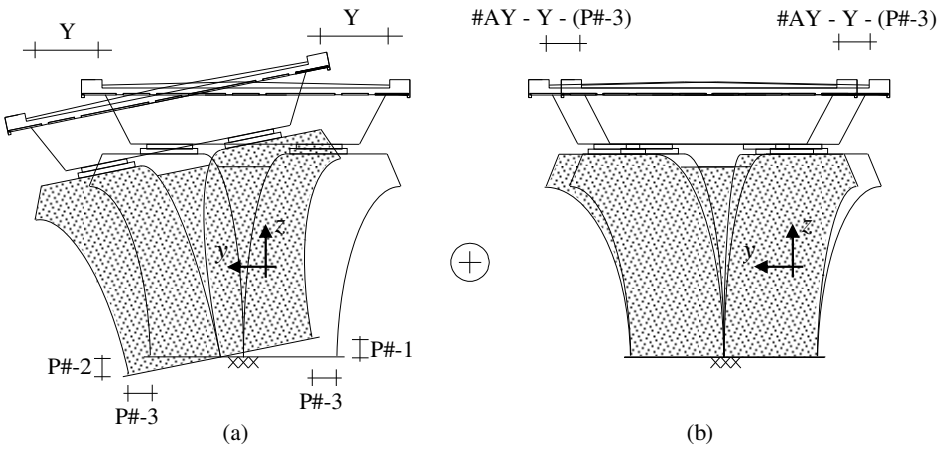

Figure 4.67 Contributions to the modal displacements "Cesano bridge": (a) foundation rigid translation and rocking and (b) pier deflection

Figure 4.67 clearly shows the contributions to the modal displacements, due to a combination of foundation rigid translation/rocking and pier deflection; in particular, the 7÷12% of the total displacement is due to the foundation translation, the 31÷41% is produced by the foundation rocking while the remaining 47÷62% of the displacement is due to the pier deflection. Finally, it can be observed that normalized modal displacements are almost the same for all the identified frequencies, i.e. frequencies are not associated to superior modes of the pier.

This test is important because highlights that SSI affects the dynamics of the viaduct, even for low intensity actions, contributing to the 31÷41% of the overall modal displacement of the deck.

4.3.5. Piers P1 and P2 (Step 3)

In the same tests carried out for the overall identification of the structure, experimental investigations are performed to evaluate possible contributions of the soil-foundation compliance on the dynamic response of the bridge. For this purpose, pier P1 and P2 some tests are performed with the aim of identifying the foundation translation and rocking. In particular, the instrumentation layout reported in Figure 4.65 is considered to capture translational and rotational accelerations of the foundation cap and the pier bent. In details, accelerometer P#-3 catch the transverse displacement of the foundation cap while accelerometers P#-1 and P#-2 are positioned to capture the rocking of the foundation.

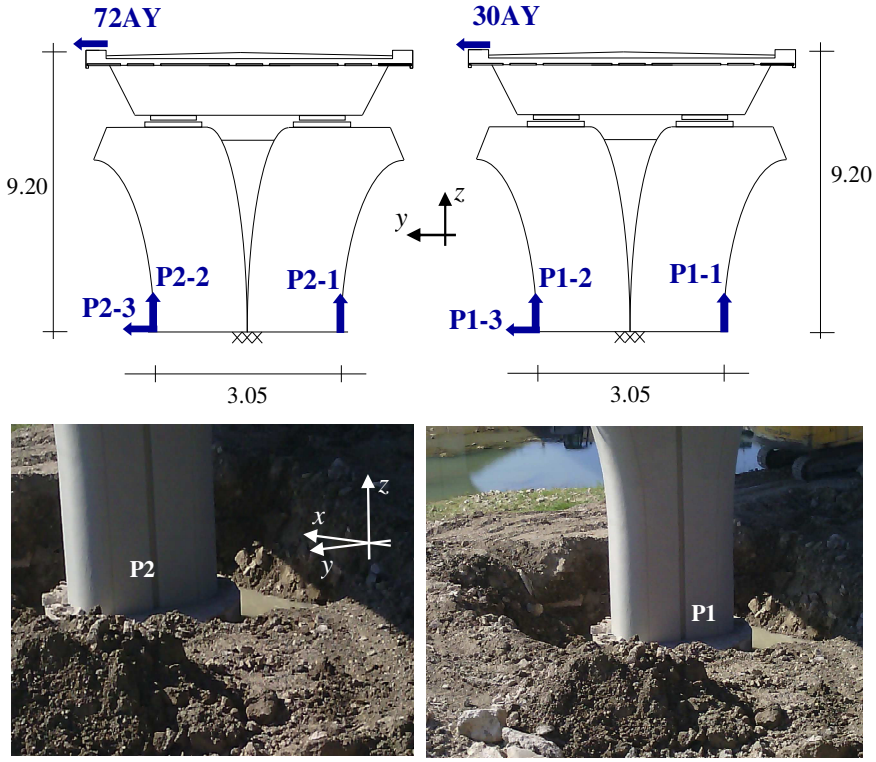

Figure 4.68 P1 and P2 Configurations (Step3)

Concerning results of tests performed on pier P1 and P2, aimed at evaluating the contributions SSI on modal displacements, Table 36 and Table 37 reports the experimental fundamental frequencies and modal displacements identified by means of SSI-Cov method, taking into account separately the sensors on the P1 and those on P2 and normalizing them with respect to the maximum displacement. The overall displacement at the pier head is due to both the rigid motion of the foundation (Figure 4.66a) and the elastic deflection of the structural members constituting the pier (Figure 4.66b).

As demonstrated in the case of Step1, only the transversal modes are significant for the rigid rotation of the foundation, so in this case the demonstrations are left out and only the two transversal modes are considered (2°Mode and 5°Mode).

Table 40. Modal parameters of Configuration P1 (Step3)

f (Hz)	ξ (-)	P1-1	P1-2	P1-3	30AY
2.42	2.75	-0.07	0.09	-0.16	-1.00
4.84	2.69	0.08	-0.07	0.14	1.00

Table 41. Modal parameters of Configuration P2 (Step3)

f (Hz)	ξ (-)	P2-1	P2-2	P2-3	72AY
2.42	2.75	-0.08	0.08	-0.16	-1.00
4.84	2.69	-0.07	0.08	-0.16	-1.00

Figure 4.66 shows, with a simple scheme how to calculate the horizontal and vertical displacements due to the rigid rotation, as a function of the P2-1 or P1-1 displacements (scheme valid in the hypothesis of small displacements).

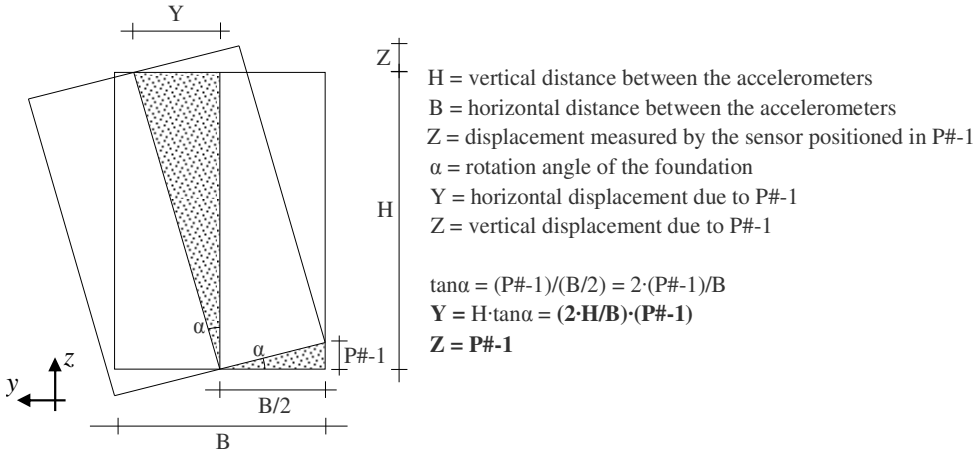

Figure 4.69 Simplified scheme of the rigid displacements due to the rocking for "Cesano bridge"

In the case of P1, H = 9.20 m and B = 3.05 m, so (2·H/B) = 6.0328 and the rigid displacements of the transverse foundation rocking are reported in Table 38.

Table 42. Rigid displacements of P1 due to the rocking (Step3)

f (Hz)	ξ (-)	P1-1	P1-2	P1-3	30AY	Y	30AY - Y - (P2-3)
2.42	2.75	-0.07	0.09	-0.16	-1.00	-0.42	-0.42
4.84	2.69	0.08	-0.07	0.14	1.00	0.48	0.38

In the case of P2, H = 9.20 m and B = 3.05 m, so (2·H/B) = 6.0328 and the rigid displacements of the transverse foundation rocking are reported in Table 39.

Table 43. Rigid displacements of P2 due to the rocking (Step3)

f (Hz)	ξ (-)	P2-1	P2-2	P2-3	72AY	Y	72AY - Y - (P2-3)
2.42	2.75	-0.08	0.08	-0.16	-1.00	-0.48	-0.36
4.84	2.69	-0.07	0.08	-0.16	-1.00	-0.42	-0.42

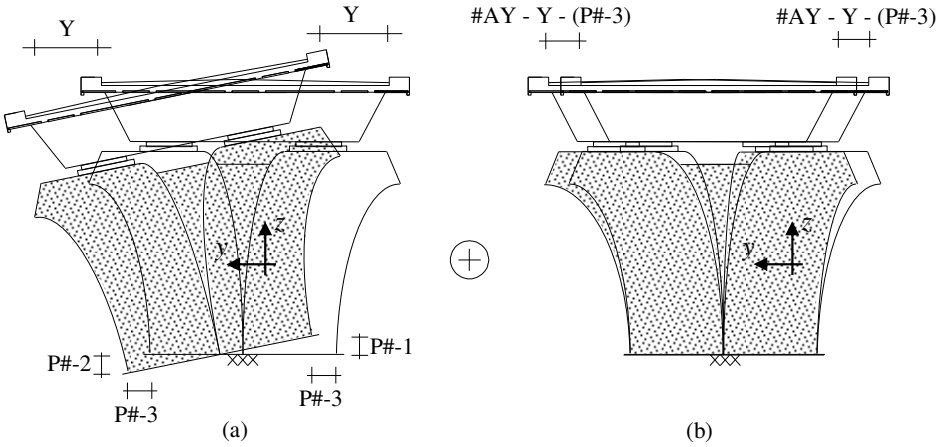

Figure 4.70 Contributions to the modal displacements "Cesano bridge": (a) foundation rigid translation and rocking and (b) pier deflection

Figure 4.67 clearly show the contributions to the modal displacements, due to a combination of foundation rigid translation/rocking and pier deflection; in particular, the 16% of the total displacement is due to the foundation translation, the 42÷48% is produced by the foundation rocking while the remaining 36÷42% of the displacement is due to the pier deflection. Finally, it can be observed that normalized modal displacements are almost the same for all the identified frequencies, i.e. frequencies are not associated to superior modes of the pier. This test is important because highlights that SSI affects the dynamics of the viaduct, even for low intensity actions, contributing to the 42÷48% of the overall modal displacement of the deck.

In step 4, the works were completed and the means to place the instruments on the piers were no longer available, so the piers tests in this step were not performed.\

Chapter 5.
Numerical modelling

5.1. “Chiaravalle viaduct” Finite Element Model

5.1.1. General

A refined 3D finite element model of the Chiaravalle viaduct is developed to interpret results of AVTs and for the subsequent design of the seismic bridge upgrading. As for the superstructure, both the deck and the column bent piers are modelled with elastic frame elements taking into account the real position of the elements centroids through the use of rigid links. Mechanical properties of the concrete are based on experimental results presented in Table 2. At the abutments and piers positions, bridge supports are modelled through elastic links reproducing stiffnesses of elastomeric bearings.

A Fixed Base model (FB) as well as Compliant Base models (CB) of the viaduct, accounting for the soil-foundation dynamic stiffnesses with different level of accuracy, are developed. In Figure 5.1 some pictorial views of the FB model are reported. CB models, addressing the SSI problem, are developed in the framework of the substructure approach, which allows analysing separately the soil-foundation and the superstructure systems, exploiting potentials of dedicated software for the modelling of the two subdomains. The analysis of the soil-foundation subdomain furnishes the frequency-dependent complex dynamic impedance matrix of the system that represents the behaviour of the superstructure restraints. Since software dedicated to structural modelling generally performs time domain analyses, also in the case of linear problems, the frequency dependent behaviour of the soil-foundation system is generally included through the use of LPMs constituted by assemblages of frequency independent springs, dashpots and masses. Parameters of the lumped system are calibrated (in the least square sense) in order to assure the best match between its dynamic stiffness matrix and that of the actual soil-foundation system in a selected frequency range.

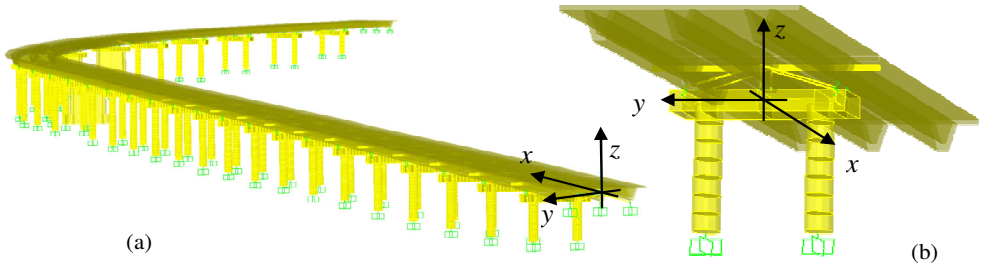

Figure 5.1 Fixed Base model (FB): (a) global view, (b) detail of one pier

5.1.2. *Lamped Parameter Models (LPMs)*

In this thesis the LPM presented by Carbonari et al. is adopted to simulate the soil-foundation dynamic behaviour of each pier in the CB models (Figure 5.2). Each LPM is characterized by 24 parameters, namely the translational (m_x, m_y and m_z) and rotational masses (I_x, I_y and I_z), lumped at the external node of the LPM, the elastic (k_x, k_y, k_{rx}, k_{ry}, k_z and k_{rz}) and viscous (c_x, c_y, c_{rx}, c_{ry}, c_z and c_{rz}) constants that define the relevant spring-dashpot elements and two additional eccentric masses (m_{xh}, m_{yh}) connected to the external node by stiff links (of lengths h_x and h_y) and to the ground by spring-dashpot elements (k_{xh}, k_{yh}, c_{xh}, c_{yh}). The adopted LPM is capable to reproduce the frequency dependent dynamic impedance matrix of pile foundations characterised by a double symmetric layout, assuming the external node (i.e. the node representing the interface between the soil-foundation system and the superstructure) located at the intersection of the two symmetry axes (Figure 5.2). By defining by U_x, U_y, U_z, Φ_x, Φ_y and Φ_z the displacement and rotations of the external node along and around axes of the reference system frame (Figure 5.2), the dynamic equilibrium equations of the LPM in the frequency domain can be formulated as follows:

$$\begin{bmatrix} F_x \\ F_y \\ F_z \\ M_x \\ M_y \\ M_z \end{bmatrix} = \begin{bmatrix} \Im_x & 0 & 0 & 0 & \Im_{x-ry} & 0 \\ & \Im_y & 0 & \Im_{y-rx} & 0 & 0 \\ & & \Im_z & 0 & 0 & 0 \\ & & & \Im_{rx} & 0 & 0 \\ & sym & & & \Im_{ry} & 0 \\ & & & & & \Im_{rz} \end{bmatrix} \begin{bmatrix} U_x \\ U_y \\ U_z \\ \Phi_x \\ \Phi_y \\ \Phi_z \end{bmatrix} \tag{29}$$

where ω is the circular frequency and F_x, F_y, F_z, M_x, M_y and M_z are the external generalised forces applied at the external node. Components of the impedance matrix in equation (29) assume the form

$$\Im_x = \left(k_x + k_{xh}\right) - \omega^2 \left(m_x + m_{xh}\right) + i\omega\left(c_x + c_{xh}\right) \tag{30}$$

$$\Im_y = \left(k_y + k_{yh}\right) - \omega^2 \left(m_y + m_{yh}\right) + i\omega\left(c_y + c_{yh}\right) \tag{31}$$

$$\Im_z = k_z - \omega^2 m_z + i\omega c_z \tag{32}$$

$$\Im_{rx} = \left(k_{rx} + k_{xh}h_{kx}^2\right) - \omega^2 \left(I_x + m_{xh}h_{mx}^2\right) + i\omega\left(c_{rx} + c_{xh}h_{cx}^2\right) \tag{33}$$

$$\Im_{ry} = \left(k_{ry} + k_{yh}h_{ky}^2\right) - \omega^2 \left(I_y + m_{yh}h_{my}^2\right) + i\omega\left(c_{ry} + c_{yh}h_{cy}^2\right) \tag{34}$$

$$\Im_{rz} = k_{rz} - \omega^2 I_z + i\omega c_{rz} \tag{35}$$

$$\Im_{x-ry} = k_{xh}h_{kx} - \omega^2 m_{xh}h_{mx} + i\omega c_{xh}h_{cx} \tag{36}$$

$$\Im_{y-rx} = -\left(k_{yh}h_{ky} - \omega^2 m_{yh}h_{my} + i\omega c_{yh}h_{cy}\right) \tag{37}$$

It is worth noting that the lumped system can account for the translational, rotational and coupled roto-translational behaviour of deep foundations, as well as the vertical and torsional behaviour. According to the LPM assemblage, real part of the impedance matrix components are characterised by second-order parabolas while imaginary parts vary linearly with ω. Further details about the LPM can be found in Carbonari et al.

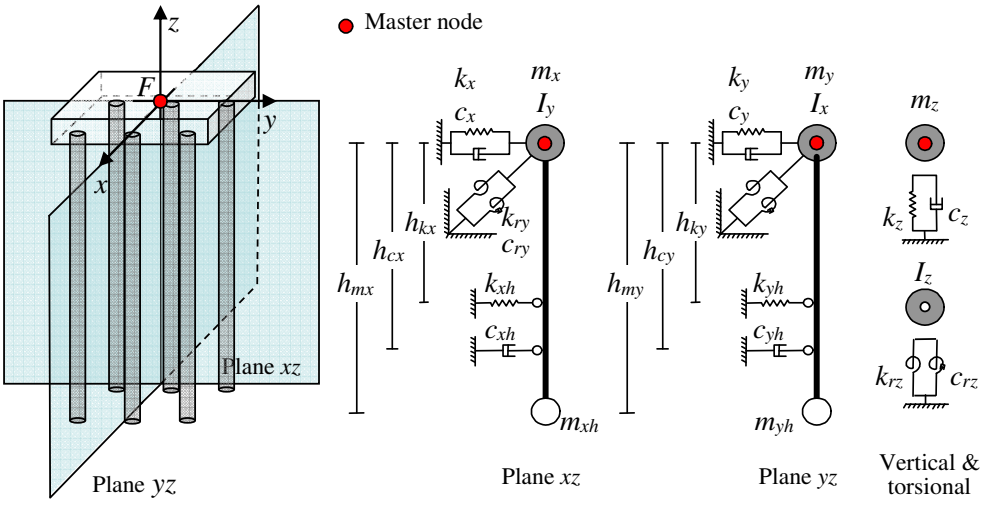

Figure 5.2 Scheme of the adopted LPM

5.1.3. Soil-Foundation modelling

The analysis of the soil-foundation system necessary to determine the relevant frequency-dependent impedance matrix is performed adopting models characterised by different level of accuracy in addressing the pile-soil-pile interaction and the effects of the pile cap embedment, as well as the spatial variability of the soil stratigraphic conditions in correspondence of each pier.

5.1.4. SSI model accounting for spatial variability of stratigraphy and pile-soil-pile interaction

In order to account for the local soil stratigraphy at each pier in the evaluation of the soil-foundation impedance matrix, considering the significant number of bridge piers (30 piers), a refined 3D finite element solid model of the soil-foundation system was not attempted firstly, because of the high computational effort associated to this type of models. Instead, the numerical model proposed by Dezi et al. is used to get impedances for the soil-foundation systems of each pier. The model allows to perform the kinematic interaction analysis of soil-foundation systems characterised by a generic layout in horizontally layered soil profiles; piles are modelled with beam finite elements while the soil is schematised with independent infinite horizontal layers. The pile-soil-pile interaction is introduced through the use of Green's functions and attenuation laws for the waves propagation available in the literature, accounting for the soil hysteretic and radiation damping and capable to include the cut-off effects through empirical adjustments. The model neglects the soil-piles cap interaction. Although the numerical tool has been validated by the Authors, results obtained with the model are herein compared with those achieved through a refined 3D solid model for one of the soil-foundation system of the bridge piers (pier 3 of KC1 is considered to this purpose). The refined 3D solid model is developed within the computer software ANSYS. 8-node linear brick elements are used to model a cylindrical soil portion with diameter D and height T satisfying condition D/d = 50 and T/d = 45 (Figure 5.3) where d is the pile diameter. A viscoelastic material model is adopted for the soil and infinite elements are provided at the boundaries to absorb the outgoing waves and satisfy the radiation condition. Piles are modelled with 2-node cubic beam elements and their physical dimensions are taken into account by removing the relevant cylinders of soils. The beam-solid coupling is assured exploiting potentials of the adopted software; furthermore, piles are connected at the head by a rigid constraint (Figure 5.3). Meshing criteria aim at obtaining an as much as possible structured mesh and assuring a sufficient number of nodes per wavelength. Some validation studies are preliminarily performed to define the mesh dimension in order to balance results reliability with computational efforts; in particular, the mesh dimension is selected so as the propagation of waves with frequency up to 10 Hz are well captured. While the model proposed by Dezi et al. directly provides the foundation impedance matrix of the soil-foundation system, for the 3D solid model, components of the matrix are obtained by imposing unit steady harmonic displacements at the fully restrained master node and evaluating the relevant reaction forces. This implies that the analysis time needed to assemble the impedance matrix for a soil-foundation system within the frequency range 0-10 Hz is of the order of hours while the Dezi et al. model runs in minutes.

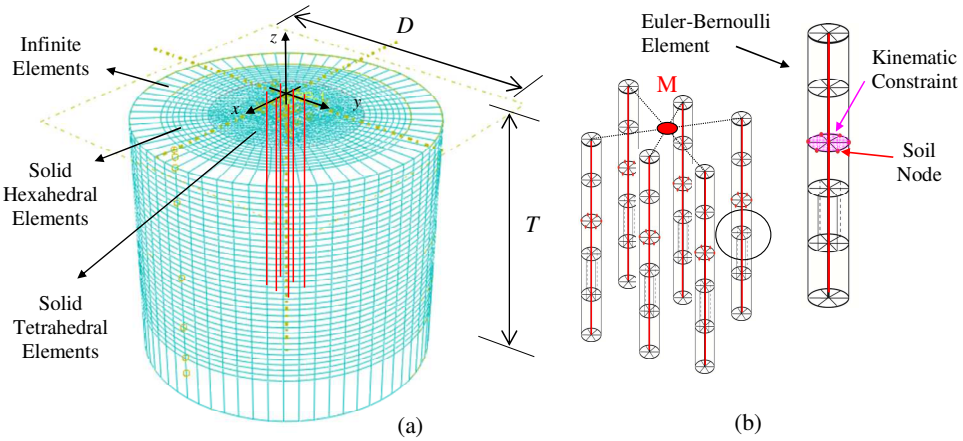

Figure 5.3 3D finite element model without not including the pile-cap interaction

Figure 5.4 compares the non-null components of the impedance matrix of the soil foundation system relevant to pier 3 of KC1 obtained with the 3D solid model (symbols) and the numerical procedure by Dezi et al. (continuous lines). It can be observed that the translational and rotational impedances (both real and imaginary parts) are very well captured within the investigated frequency range while vertical and torsional stiffnesses present some inaccuracies. Anyway, from an engineering point of view the numerical procedure by Dezi et al. is able to reproduce the dynamic behaviour of the soil foundation system of the specific case study.

It is worth noting the change of the impedance functions slopes in correspondence of 9.2 Hz, corresponding to the cut-off frequency of the deposit associated to the first vibration mode of the first soil layer (lithotype AD1) which is characterised by a very low shear modulus with respect to the underlying lithotypes; as well known in the literature, radiation damping occurs for frequencies higher than the cut-off one, overall increasing the soil-system energy dissipation capabilities. However, results of experimental tests (AVTs) revealed that the first three structural fundamental frequencies, which are expected to dominate the transverse dynamic response of the bridge, fall below 5 Hz. For this reason, parameters of LPMs are calibrated to reproduce the soil-foundation impedances in correspondence of each pier in the frequency range 0-8 Hz. For pier 3 of KC1, impedances of the LPM are reported in Figure 5.4 with dashed lines. It can be observed that the adopted lumped system reproduces very well the actual behaviour of the soil-foundation system in the desired frequency range. LPMs are calibrated for the soil-foundation systems of each pier and implemented in the finite element model of the superstructure (Figure 5.5); in details the external node of the lumped system is located in the pile cap extrados in correspondence of its centroid. Furthermore, the pile cap mass is added to the external node.

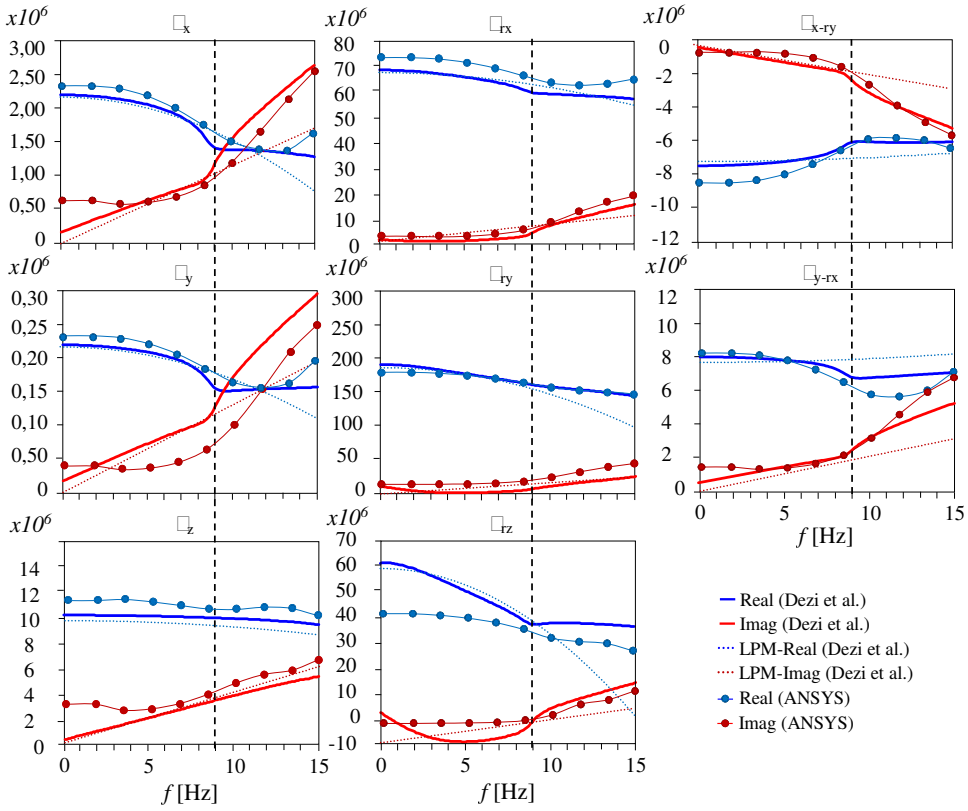

Figure 5.4 Comparison between impedances from different models

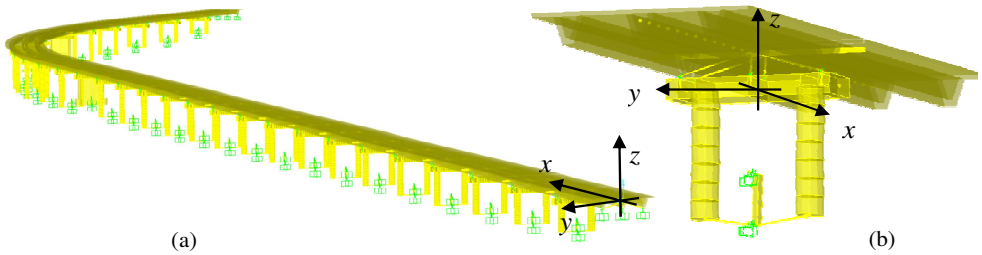

Figure 5.5 Compliant base models (CB-P and CB-P&C): (a) global view, (b) detail of one pier

Parameters of the LPMs relevant to some piers located near the available BHs are reported in Table 44. It is worth noting that parameters are overall very similar. This observation suggests that also impedances of soil-foundations system of piers along the longitudinal direction of the bridge are quite similar too. Figure 5.6 shows the non-null components of the impedance matrixes relevant to piers P3, P6, P12, P16 and P29, whose relevant LPMs parameters are reported in Table 44. As expected the dynamic behaviour of all the soil-

foundation systems within the whole viaduct length are comparable; this is mainly due to the contribution of the upper soil layer which presents an almost constant depth along the viaduct (Figure 3.7a) and is characterised by a low shear modulus, compared to the underlying lithotypes. This implies that the surface layer, located within the active pile length, strongly affects the dynamics of the all the soil-foundation systems.

Table 44. Parameters of LPMs for piers in proximity of BHs

	Pier P3	Pier P6	Pier P12	Pier P16	Pier P29
m_x [tons]	4.34E+01	3.94E+01	4.81E+01	4.13E+01	4.08E+01
m_y [tons]	4.44E+01	4.03E+01	4.86E+01	4.43E+01	4.23E+01
m_z [tons]	7.80E+01	6.77E+01	8.02E+01	7.52E+01	7.38E+01
I_x [tons m²]	1.33E+03	1.32E+03	1.30E+03	1.38E+03	1.35E+03
I_y [tons m²]	5.96E+03	5.36E+03	5.25E+03	5.60E+03	5.46E+03
I_z [tons m²]	6.01E+03	6.20E+03	6.19E+03	6.21E+03	6.20E+03
k_x [kN/m]	7.82E+04	7.79E+04	7.78E+04	7.86E+04	7.79E+04
c_x [kN s/m]	1.30E+04	1.33E+04	1.41E+04	1.34E+04	1.33E+04
k_y [kN/m]	7.97E+04	7.97E+04	7.97E+04	8.05E+04	7.97E+04
c_y [kN s/m]	1.04E+04	1.06E+04	1.06E+04	1.06E+04	1.06E+04
k_z [kN/m]	1.46E+07	1.41E+07	1.44E+07	1.47E+07	1.49E+07
c_z [kN s/m]	5.20E+04	5.20E+04	5.19E+04	5.26E+04	5.24E+04
k_{rx} [kN/m]	5.70E+07	5.79E+07	5.61E+07	5.87E+07	5.99E+07
c_{rx} [kN s/m]	0.00E+00	0.00E+00	0.00E+00	0.00E+00	0.00E+00
k_{ry} [kN/m]	1.76E+08	1.76E+08	1.78E+08	1.79E+08	1.73E+08
c_{ry} [kN s/m]	0.00E+00	0.00E+00	0.00E+00	0.00E+00	0.00E+00
k_{rz} [kN/m]	5.76E+07	5.35E+07	5.35E+07	5.47E+07	5.56E+07
c_{rz} [kN s/m]	1.42E+04	1.30E+04	1.49E+04	1.38E+04	1.43E+04
m_x [tons]	1.55E+02	1.54E+02	1.58E+02	1.51E+02	1.51E+02
m_y [tons]	1.38E+02	1.40E+02	1.39E+02	1.44E+02	1.42E+02
k_{xh} [kN/m]	2.40E+06	2.85E+06	2.85E+06	2.85E+06	2.85E+06
c_{xh} [kN s/m]	9.36E+03	9.88E+03	1.02E+04	9.82E+03	9.83E+03
k_{yh} [kN/m]	2.40E+06	2.85E+06	2.85E+06	2.85E+06	2.85E+06
c_{yh} [kN s/m]	1.54E+04	1.48E+04	1.39E+04	1.38E+04	1.48E+04

Figure 5.6 includes impedances of the LPM calibrated to reproduce the behaviour of the soil-foundation system of pier P3. From a practical point of view, this can substitute those tailored to represent the specific soil-foundation systems of each pier.

In order to evaluate effects of the above simplification (i.e. the use of a unique LPM overall addressing the dynamics of all the foundations) on the superstructure response, numerical applications considering tailored LPMs in correspondence of each piers and the above mentioned LPM (of P3) are performed.

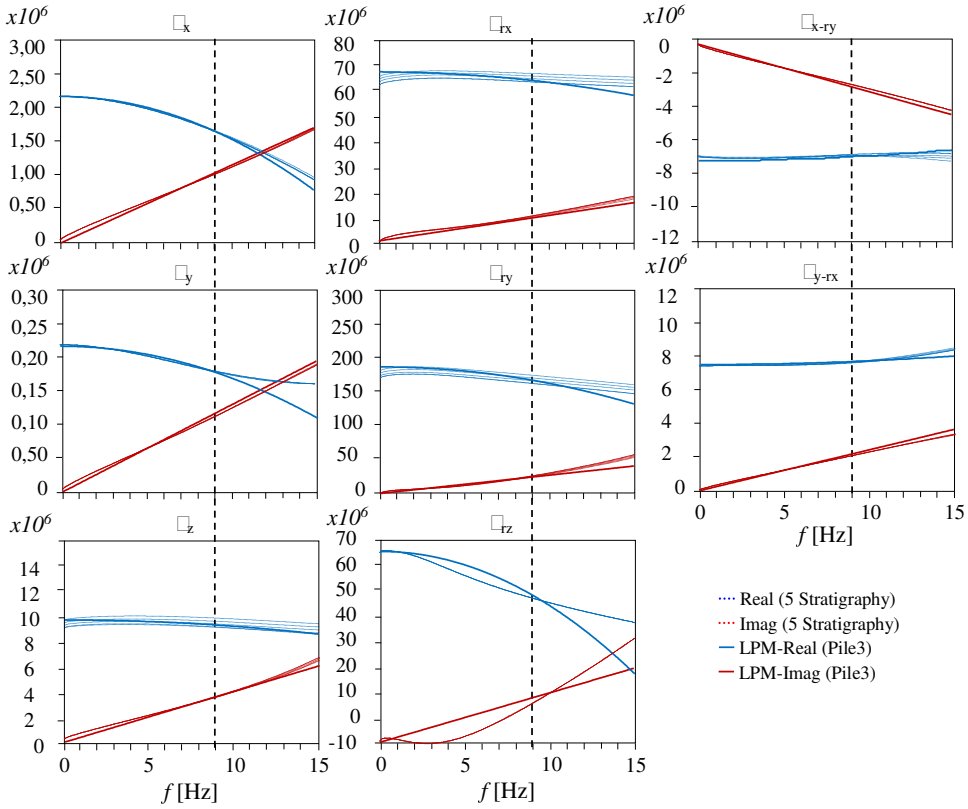

Figure 5.6 Comparison of foundation impedances obtained from Dezi et al. at different piers and impedances of LPM of P3

In order to account for the non-classical damping of the structural system, due to the introduction of LPMs, modal parameters are determined through a steady state analysis instead of using a classical modal one. Thus, harmonic horizontal and vertical forces of unit amplitudes are applied at the external nodes of the LPMs at each pier location, with frequencies ranging between 0-15 Hz.

Figure 5.7 shows amplitude of displacements along the x, y, and z directions (obtained from the application of forces acting in the relevant directions) for the deck nodes located above P3, P12 and P29 obtained from models implementing the tailored LPMs and the LPM of P3 for all piers. It can be observed that fundamental frequencies of the superstructure, clearly identified in correspondence of the response pecks, are practically unaffected by the proposed simplification with variations of the first three frequencies overall below 0.1%.

In the sequel, the model implementing LPM of P3 for all the substructures will be considered and labelled with CB-P (where P suggests that Pile-soil-pile interaction is considered in determining the soil-foundation dynamic impedances, disregarding effects of the pile cap embedment). Comparison of modal parameters obtained from the CB-P model with the experimental ones will be shown and discussed in a dedicated section.

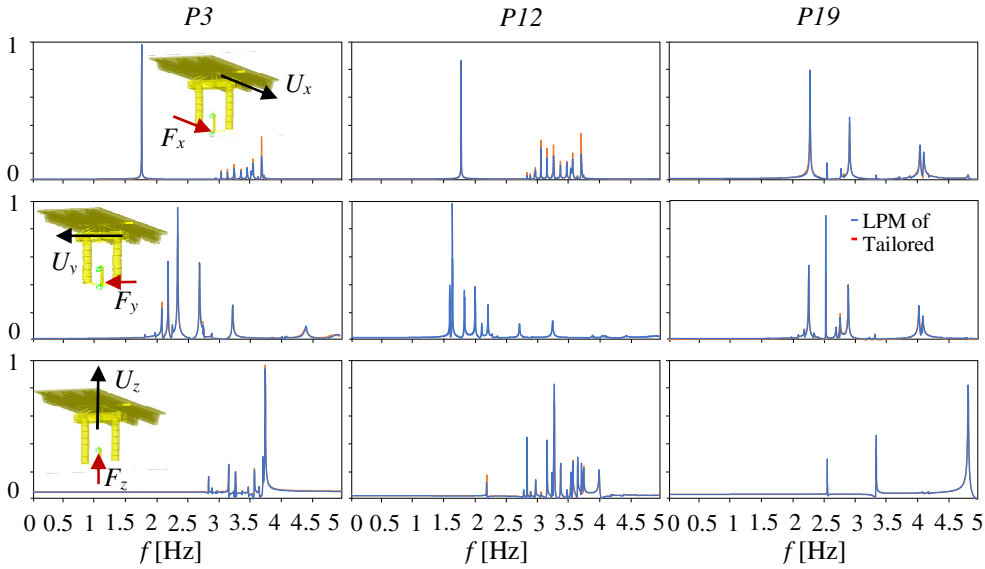

Figure 5.7 Amplitude of displacements at P3, P12 and P19 obtained from tailored LPMs and the LPM of P3

5.1.5. SSI model accounting for pile-soil-pile cap interaction

The CB-P model does not account for the contribution of the soil-pile cap interaction in addressing the SSI problem. In order to include the effect of the pile cap embedment in the superstructure model, a refined 3D finite element solid model of the soil-pile-cap foundation system is developed in ANSYS. Taking into account above considerations concerning the effects of the local soil stratigraphies at each pier on the overall viaduct response, only the soil-foundation system of P3 is analysed. In detail, the modelling of the pile cap, which is assumed to be rigid, is added in the previous 3D solid model by adding the soil excavation and introducing a rigid constraint between soil-cap interfaces and the piles head (i.e. a perfect bonding is assumed between the soil and the cap). Figure 5.8 shows some views of the developed model.

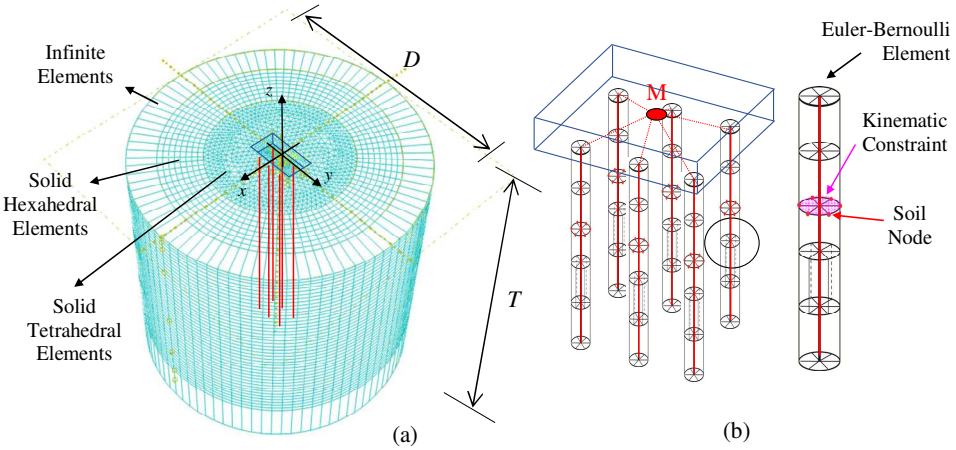

Figure 5.8 3D finite element model including the pile-cap interaction

Figure 5.9 compares impedances of the 3D solid model including the cap effects with the impedances obtained from the previous models (i.e. the ANSYS model disregarding the cap and the model by Dezi et al.). A significant increase of the translational impedances ($\Im_x$ and $\Im_y$) can be observed as a consequence of the soil-pile cap contribution to the lateral response of the soil-foundation system. On the contrary, rotational impedances ($\Im_{rx}$ and $\Im_{ry}$) are less affected by the cap embedment contribution which is limited to the shear tractions at the level of the soil-cap interfaces. Effects on the coupled roto-translational terms ($\Im_{x-ry}$ and $\Im_{y-rx}$) are also negligible for the same reason. Finally, it is worth noting that the torsional and vertical impedances are strongly affected by the pile cap embedment; in particular, the vertical impedance diminishes as a consequence of the soil drag effect which drastically reduces the piles contribution to the foundation vertical stiffness; this results is clearly affected by the assumption of perfect bonding between the soil and the pile cap. Figure 5.9 also shows impedances of the LPM calibrated to reproduce impedances of the soil-pile-cap system in the frequency range 0-8 Hz. The lumped model is able to capture the dynamic behaviour of the comprehensive 3D solid model very well. Finally, Table 45 shows parameters of the calibrated LPM which is implemented in the superstructure model to include the effects of the soil-pile-cap system. In the sequel this model will be labelled with CB-P&C (where P&C suggests that both the Pile-soil-pile interaction and the effects of the Cap embedment are included). Results of the CB-P&C model in terms of fundamental frequencies and mode shapes will be presented later and compared with the experimental ones.

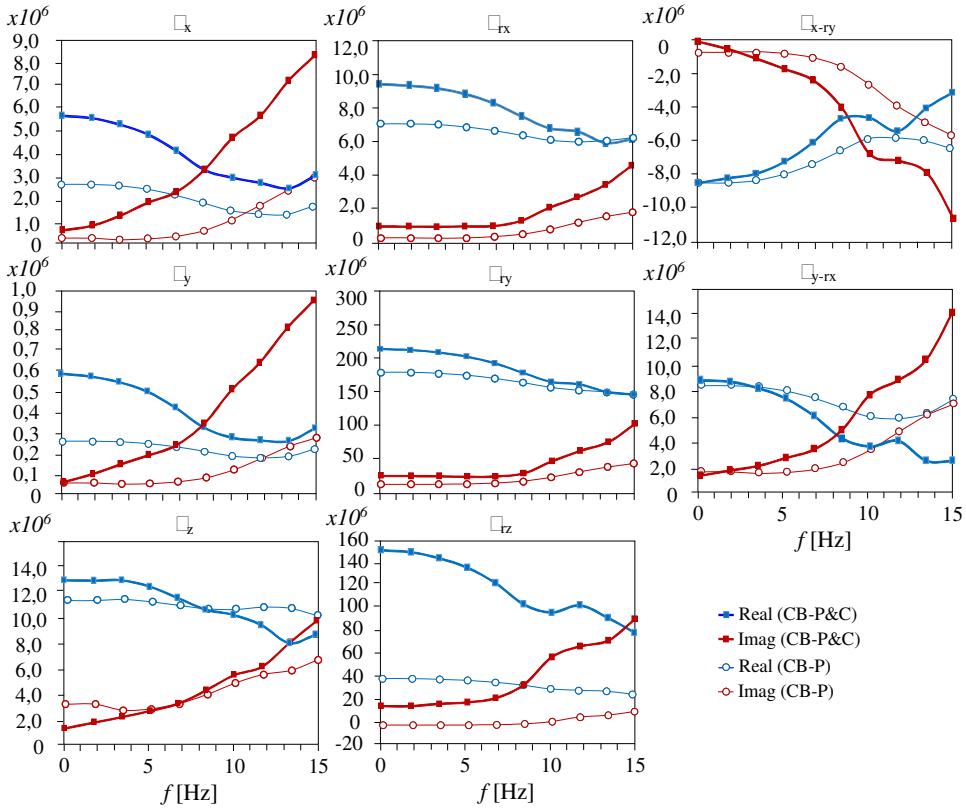

Figure 5.9 Comparison of foundation impedances adopted for the CB-P and CB-P&C models

Table 45. Parameters of LPM for P3 (CB-P&C)

m_x [tons]	1,57E+02	k_x [kN/m]	1,25E+06	k_{rx} [kN/m]	7,85E+07
m_y [tons]	2,19E+02	c_x [kN s/m]	2,15E+04	c_{rx} [kN s/m]	1,18E+05
m_z [tons]	6,57E+02	k_y [kN/m]	1,42E+06	k_{ry} [kN/m]	1,83E+08
I_x [tons m²]	3,27E+03	c_y [kN s/m]	2,39E+04	c_{ry} [kN s/m]	4,04E+05
I_y [tons m²]	1,04E+04	k_z [kN/m]	1,22E+07	k_{rz} [kN/m]	1,44E+08
I_z [tons m²]	1,26E+04	c_z [kN s/m]	8,15E+04	c_{rz} [kN s/m]	7,14E+05
m_{xh} [tons]	5,66E+02	k_{xh} [kN/m]	4,06E+06	k_{yh} [kN/m]	4,29E+06
m_{yh} [tons]	6,32E+02	c_{xh} [kN s/m]	4,10E+04	c_{yh} [kN s/m]	4,54E+04

5.1.6. *Simplified modelling of soil-pile interaction*

Two sophisticated CB models (CB-P and CB-P&C) are developed to include the SSI problem in the finite element model of the superstructure that will be used to interpret results of AVTs. The need of such sophisticated models is herein proven by also presenting results of a more conventional approach, which foresees piles schematised as beams on Winkler foundation directly included in the superstructure model (Figure 5.10). The latter approach can be easily adopted by practical engineers to roughly include the SSI effects in the superstructure response by neglecting the pile-soil-pile interaction (i.e. the group effects) as well as the cap embedment. The model is developed considering vertical k_z and horizontal k_h distributed springs along the piles obtained from

$$k_z = 0.6E_s \tag{38}$$

$$k_h = 1.2E_s \tag{39}$$

where E_s is the soil Young's modulus. Equations (38,39) results from literature, for the static case (i.e. ω=0). provides an overview of the elastic constants of springs calculated for each lithotype. This model will be labelled with CB-CONV (where CONV suggests its CONVentional nature) and the relevant results will be shown in the next section.

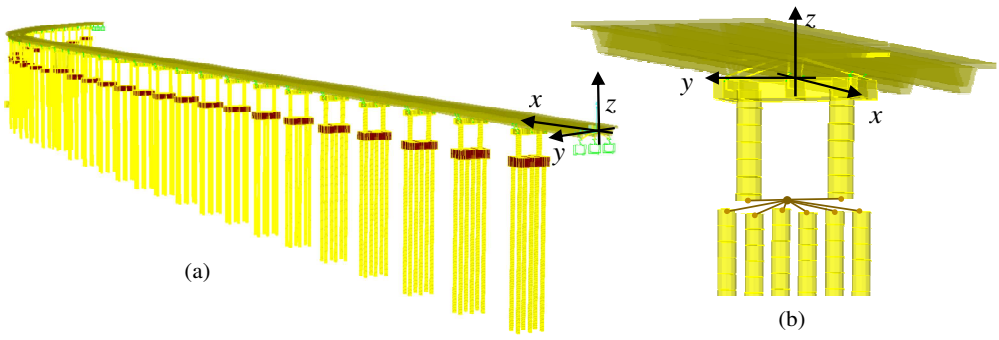

Figure 5.10 Conventional soil-structure interaction model (CB-CONV): (a) global view, (b) detail of one pier

Table 46. Elastic constants of springs calculated for each lithotype.

Depth [m]	*Vs* [m/s]	*Go* [kPa]	*E* [kPa]	*Kz* [kPa]	*Kh* [kPa]
0 ÷ 6	230	92000	257600	154560	309120
6 ÷ 20	540	567000	1587600	952560	1905120
20 ÷ 26	325	218000	610400	366240	732480
26 ÷ 35	600	770000	2156000	1293600	2587200

Kv = vertical elastic constant
Ko = horizontal elastic constant
Vs = shear wave speed
G = dynamic cutting module
E = elastic module

5.1.7. Rocking foundation of pier P3, for different models

In the previous paragraphs, to better represent the Chiaravalle viaduct, four finite element models were developed:

- FB: Fixed Base model;
- CB-P: Pile-soil-pile interaction is considered in determining the soil-foundation dynamic impedances, disregarding effects of the pile cap embedment;
- CB-P & C: both the Pile-soil-pile interaction and the effects of the cap embedment are included;
- CB-CONV: Conventional nature of the model, with springs along the piles.

for each of them the rotation of the pile 3 was also investigated, to evaluate the compliance with the experimental data and to assign the best model also in this respect.

Firstly, consider FB model, and consider the configuration show in Figure 5.11

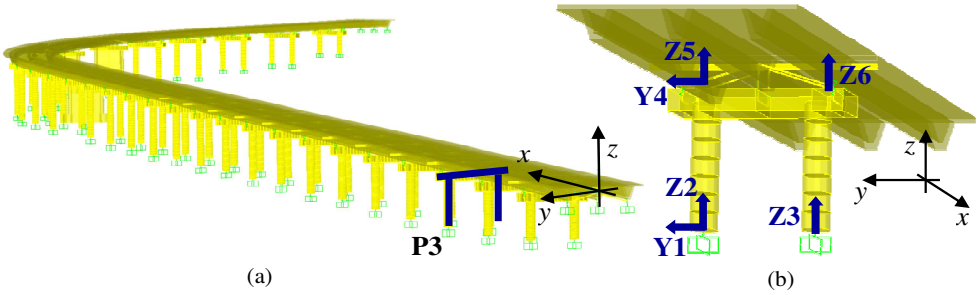

Figure 5.11 P3 Configuration in Fixed base model (FB): (a) P3 position, (b) displacements layout

Displacements, derived from modal analysis, reported in Table 47 are normalized with respect to the maximum displacement, always occurring at the pier top (sensor Y4); moreover, in the columns to the right of the table are reported the values of the displacements caused by the foundation rocking and the component due to piers deflection (as shown in the scheme of Figure 4.18)

In all the models of P3, H = 7.80 m and B = 3.05 m, so (2·H/B) = 5.1148 and the rigid displacements of the transverse foundation rocking is Y = 5.1148·Z3

Table 47. Displacements of P3 in FB model

f (Hz)	Y1	Z2	Z3	Y4	Z5	Z6	**Y**	**Y4 – Y – Y1**	**Z5 -Z2**	**Z6 -Z3**
2.25	0.00	0.00	0.00	1.00	-0.03	0.03	**0.00**	**1.00**	**0.03**	**-0.03**
2.43	0.00	0.00	0.00	1.00	-0.03	0.03	**0.00**	**1.00**	**0.03**	**-0.03**
2.77	0.00	0.00	0.00	1.00	-0.03	0.03	**0.00**	**1.00**	**0.03**	**-0.03**

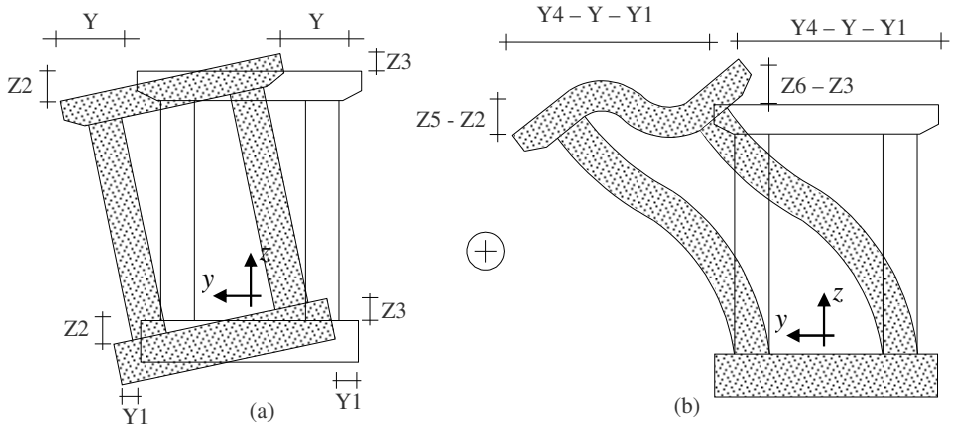

Figure 5.12 Contributions to the modal displacements: (a) foundation rigid translation and rocking and (b) pier deflection

Table 47 and Figure 5.12 clearly shown that in the case of fixed base model, the contribution to the modal displacements due to the foundation rigid translation/rocking of the rotation is zero, and all the horizontal displacement is due to the pier deflection. Finally, it can be observed that normalized modal displacements are the same for all the identified frequencies, i.e. frequencies are not associated to superior modes of the pier.

This test is important because highlights that with FB model, the foundation rocking is not considered in the overall modal displacement of the deck.

Then CB-P and CB-P&C models are considered together because they refer to the same model but with different LPMs values; the configuration show in Figure 5.13

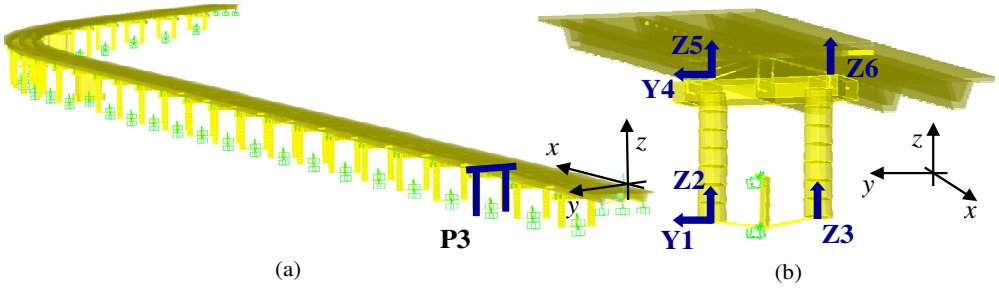

Figure 5.13 P3 Configuration in Compliant base model (CB-P and CB-P&C): (a) P3 position, (b) sensor layout

Displacements, derived from steady-state analysis, reported in Table 48 and Table 49 are normalized with respect to the maximum displacement, always occurring at the pier top (sensor Y4); moreover, in the columns to the right of the table are reported the values of the displacements caused by the foundation rocking and the component due to piers deflection (as shown in the scheme of Figure 4.18)

Table 48. Displacements of P3 in CB-P model

f (Hz)	Y1	Z2	Z3	Y4	Z5	Z6	**Y**	**Y4 – Y – Y1**	**Z5 -Z2**	**Z6 -Z3**
2.20	0.07	-0.03	0.03	1.00	-0.06	0.06	**0.15**	**0.78**	**-0.03**	**0.03**
2.39	0.06	-0.03	0.03	1.00	-0.06	0.06	**0.15**	**0.79**	**-0.03**	**0.03**
2.69	0.02	-0.03	0.03	1.00	-0.06	0.06	**0.15**	**0.83**	**-0.03**	**0.03**

Table 49. Displacements of P3 in CB-P&C model

f (Hz)	Y1	Z2	Z3	Y4	Z5	Z6	**Y**	**Y4 – Y – Y1**	**Z5 -Z2**	**Z6 -Z3**
2.25	0.08	-0.01	0.01	1.00	-0.02	0.02	**0.05**	**0.87**	**-0.01**	**0.01**
2.44	0.05	-0.01	0.01	1.00	-0.02	0.02	**0.05**	**0.90**	**-0.01**	**0.01**
2.72	0.03	-0.02	0.02	1.00	-0.03	0.03	**0.10**	**0.87**	**-0.01**	**0.01**

Figure 5.12 clearly show the contributions to the modal displacements, due to a combination of foundation rigid translation/rocking and pier deflection; in particular, the 7% of the total displacement is due to the foundation translation, the 15% is produced by the foundation rocking while the remaining 78% of the displacement is due to the pier deflection, in the CB-P model, while the 8% of the total displacement is due to the foundation translation, the 5% is produced by the foundation rocking while the remaining 87% of the displacement is due to the pier deflection, in the CB-P&C model. Finally, it can be observed that normalized modal displacements are the same for all the identified frequencies, i.e. frequencies are not associated to superior modes of the pier.

This test is important because highlights that SSI sensibly affects the dynamics of the viaduct, even for low intensity actions, contributing to the 15% of the overall modal displacement of the deck in the CB-P model, while 5% in the CB-P&C model.

Finally, CB-CONV model is considered and the displacements configuration show in Figure 5.14

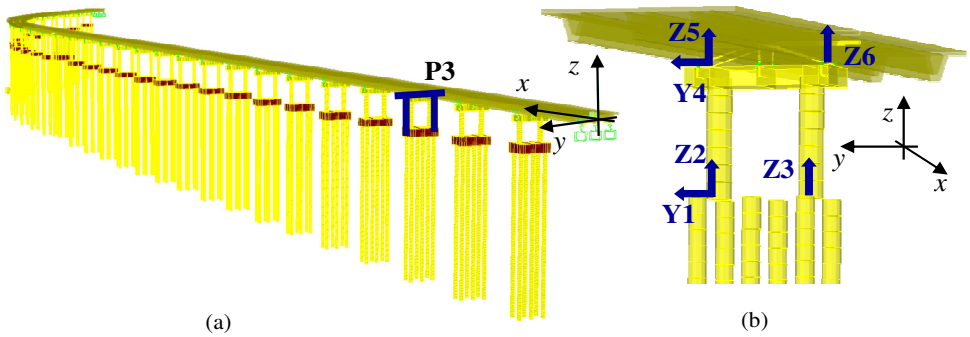

(a) (b)

Figure 5.14 P3 Configuration in Conventional base model (CB-CONV): (a) P3 position, (b) sensor layout

Displacements, derived from modal analysis, reported in Table 50 are normalized with respect to the maximum displacement, always occurring at the pier top (sensor Y4); moreover, in the columns to the right of the table are reported the values of the displacements

caused by the foundation rocking and the component due to piers deflection (as shown in the scheme of Figure 4.18)

Table 50. Displacements of P3 in CB-CONV model

f (Hz)	Y1	Z2	Z3	Y4	Z5	Z6	**Y**	**Y4 – Y – Y1**	**Z5 -Z2**	**Z6 -Z3**
1.88	0.07	-0.04	0.04	1.00	-0.06	0.06	**0.20**	**0.73**	**-0.02**	**0.02**
2.12	0.06	-0.05	0.05	1.00	-0.18	0.18	**0.26**	**0.68**	**-0.13**	**0.13**
2.42	0.05	-0.06	0.04	1.00	-0.19	0.18	**0.20**	**0.77**	**-0.13**	**0.14**

Table 50 and Figure 5.12 clearly show the contributions to the modal displacements, due to a combination of foundation rigid translation/rocking and pier deflection; in particular, the 7% of the total displacement is due to the foundation translation, the 20% is produced by the foundation rocking while the remaining 73% of the displacement is due to the pier deflection. Finally, it can be observed that normalized modal displacements are the same for all the identified frequencies, i.e. frequencies are not associated to superior modes of the pier.

This test is important because highlights that SSI sensibly affects the dynamics of the viaduct, even for low intensity actions, contributing to the 20% of the overall modal displacement of the deck.

5.2. “Paglia bridge” Finite Element Model

5.2.1. General

A 3D finite element model of the “Paglia bridge” is developed to interpret results of AVTs and for the subsequent design of the seismic bridge upgrading; some figures are reported in Figure 5.15.

The design model has been used for the comparison of the modal parameters.

Four metal beams connected by reticular beams are modelled through "beam" finite elements with linear elastic behaviour. The deck is modelled using "shell" type finite elements with linear elastic behaviour. The abutments and the piers were schematized with fixed supports.

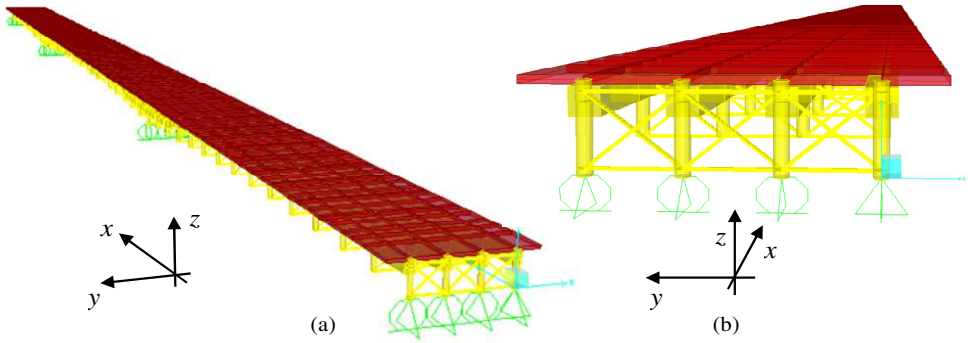

Figure 5.15 Conventional model of “Paglia bridge”: (a) global view, (b) detail of one pier

A static scheme of continuous beam on three spans with lights of 70 m, 100 m and 70 m is considered.

5.2.2. Comparison between experimental and analytical results

Finite Element Model with these characteristics provides modal parameters similar with those deriving from experimental tests both in terms of frequencies and in terms of modal forms, as can be seen from Table 51

Table 51. Comparison between frequencies of “Paglia Bridge”

	Mode	1	2	3	4	5	6	7
OMA	*f* (Hz)	1.14	1.52	1.89	2.39	2.53	3.32	3.54
FEM	*f* (Hz)	1.29	1.37	2.12	2.41	2.57	3.45	3.60
	Error (%)	11.6	-9.9	10.8	0.01	0.02	0.04	0.02

From Table 51, it is clear that fixed model, in this case, with rigid piers, not provides significant errors at level of frequencies respect to the other fixed based case studies, because most of the displacement is caused by the deformation of the deck, and not by the foundation rocking, as we have been observed from ambient vibration tests.

5.3. “Cesano bridge” Finite Element Model

5.3.1. General

A refined 3D finite element model of the “Cesano bridge” is developed to interpret results of AVTs and for the subsequent design of the seismic bridge upgrading Figure 5.16.

The piers, pile foundation cap and foundations pile are modelled through "beam" finite elements with linear elastic behaviour. The deck is modelled using "shell" type finite elements with linear elastic behaviour. The abutments were initially schematized with fixed supports. The structural masses are concentrated at the nodes.

The external constraint represented by the soil around the piles is schematized with the "Winkler" model by applying springs with linear elastic behaviour along the entire length of the foundation piles, with variable stiffness with depth.

The connection between the deck and the substructures (piles and abutments), consisting of sliding pendulum isolators, and it is modelled by means of "link" type finite elements with non-linear behaviour.

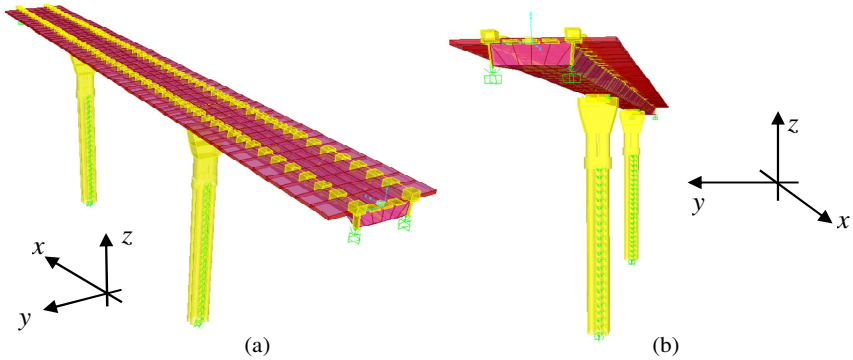

Figure 5.16 Conventional model of “Cesano bridge”: (a) global view, (b) detail of one pier

The properties shown in Table 52 have been assigned to the concrete elements of the model, as prescribed in the "Specialized technical report - structural calculation" of the Executive Project.

Table 52. Mechanical properties of concrete ("Cesano bridge")

Structural element	*Class*	R_{ck} [MPa]
Foundation piles	C25/35	35
Abutments	C32/40	40
Piers	C35/45	45
Concrete slab	C35/45	45
Predalles	C32/40	40

The metal components have the following characteristics:
f_t > 510 MPa
f_y > 355 MPa
E_a > 206000 MPa

From the loads analysis contained in the structural relationship, the following weights are expected, with reference to a static scheme of continuous beam on three spans with lights of 29.45 m, 42.00 m and 29.45 m.

Own weight of the structure (G1)
Metallic carpentry (G1,1)
- Average weight of the caisson = 14.81 kN/m
- Average weight secondary metal components = 5.06 kN/m
Concrete slab (G1,2) = 25 kN/m^3 x 3.84 m^2 = 96.00 kN/m^3

Permanent loads (G2)
- Left sidewalk = 25 kN/m^3 x (0.75 x 0.18 m^2) = 3.38 kN/m
- Right sidewalk = 25 kN/m^3 x (0.75 x 0.18 m^2) = 3.38 kN/m
- Road surface = 23 kN/m^3 x (10.50 x 0.11 m^2) = 26.57 kN/m
- Veil + carter left = 1.50 kN/m
- Veil + carter right = 1.50 kN/m
- Left raceway = 2.00 kN/m
- Right raceway = 2.00 kN/m
- Left guardrails = 1.00 kN/m
- Right guardrails = 1.00 kN/m
Total permanent loads = 42.33 kN/m

In order to compare the model with the results of the dynamic tests, the displacements of the links to the supports, which simulate the behaviour of the seismic isolators, have been fixed in the three directions, knowing that, due to the environmental forcing, their operation does not work.

The concrete of the structural elements as non-cracked was also considered, applying the actual non-reduced flexural stiffnesses.

The elastic modulus of the concrete of the structural elements has been increased by 10%, to take into account that, due to the low stresses to which the structure is subjected during the

environmental vibration tests, the secant module of the stress-strain curve of the concrete will be greater of that adopted for the final state limit checks.

To correctly model the structure's behaviour, it is essential that the stiffness assigned to the springs accurately reflects the lateral stiffness of the soil around the piles. Having available the "Geological-Geotechnical Report" attached to the Preliminary Design of the bridge, the stiffness of the springs has been recalculated starting from direct measurements in situ of the stiffness due to small deformations. Specifically, reference was made to the results of the two Down Hole seismic surveys, inside the boreholes S1 and S4 made at the bottom of the valley, near to the areas of the bridge.

Interpretation of results of geotechnical and geophysical surveys leads to the mechanical and dynamic parameters reported in Table 53 for each lithotype.

Table 53. Mechanical and dynamic parameters ("Cesano bridge") – Borehole B1

depht	z	γ	V_p	V_s	V_p/V_s	E_0	G_0	ν
	[m]	[kN/m³]	[m/s]	[m/s]	[-]	[kPa]	[kPa]	[-]
0.0÷1.5	0.75	1800	300	175	1.71	137000	55100	0.2421
1.5÷3.0	2.25	1900	740	220	3.36	26700	92000	0.4515
3.0÷6.0	4.5	2000	1305	375	3.48	818000	281000	0.4550
6.0÷10.0	8	1900	1060	190	5.58	204000	68600	0.4834
10.0÷12.5	11.25	2000	1340	400	3.35	929000	320000	0.4511
12.5÷30.0	21.25	2000	1680	315	5.33	588000	199000	0.4818
30.0÷35.0	32.5	2000	1975	420	4.70	104000	353000	0.4763

z = Thickness — *V_s = shear wave velocity* — *E_0 = elastic modulus*
γ = unit weight of soil — *G_0 = small strain shear modulus* — *ν = Poisson modulus*

The conventional approach, which foresees piles schematised as beams on Winkler foundation directly included in the superstructure model. The latter approach can be easily adopted by practical engineers to roughly include the SSI effects in the superstructure response by neglecting the pile-soil-pile interaction (i.e. the group effects) as well as the cap embedment. The model is developed considering vertical k_z and horizontal k_h distributed springs along the piles obtained from

$$k_z = 0.6E_s \tag{40}$$

$$k_h = 1.2E_s \tag{41}$$

where E_s is the soil Young's modulus. Equations (40, 41) results from literature, for the static case (i.e. ω=0).

5.3.2. Comparison between experimental and analytical results

Finite Element Model with these characteristics provides modal parameters similar with those deriving from experimental tests both in terms of frequencies and in terms of modal forms, as can be seen from the following tables

In the model of Step1, the soil is in the initially condition, so the springs were left to the ground level, at about 3.95 m for pier P1 and 4.35 m for pier P2.

Table 54. Comparison between modal parameters of "Cesano Bridge" – Step1

	Mode	1	2	3	4	5	6
OMA	f (Hz)	2.40	2.90	3.95	4.36	5.45	5.64
FEM	f (Hz)	2.37	2.92	3.72	4.44	5.44	5.66
	Error (%)	1.3	-0.7	5.8	-1.8	0.2	-0.4

To model the step2, in which the soil is removed around the piles, increasing the height of the excavation at 7.80 m, the model remained the same, simply removed the springs at the top of the pile up to the height of the excavation.

Table 55. Comparison between modal parameters of "Cesano Bridge" – Step2

	Mode	1	2	3	4	5	6
OMA	f (Hz)	2.31	2.68	3.81	4.18	4.93	5.29
FEM	f (Hz)	2.34	2.45	3.60	4.40	5.29	5.55
	Error (%)	-1.3	8.6	5.5	-5.0	-6.8	-4.7

In the model of step3, the soil is removed around the piles, increasing the height of the excavation at 9.20 m.

Table 56. Comparison between modal parameters of "Cesano Bridge" – Step3

	Mode	1	2	3	4	5	6
OMA	f (Hz)	2.30	2.42	3.81	4.19	4.84	5.14
FEM	f (Hz)	2.34	2.30	3.58	4.41	5.27	5.52
	Error (%)	-1.7	5.0	6.0	-5.0	-8.2	-6.9

In the model of step4, the soil is removed around the piles, increasing the height of the excavation at 7.00 m.

Table 57. Comparison between modal parameters of "Cesano Bridge" – Step4

	Mode	1	2	3	4	5	6
OMA	f (Hz)	2.29	2.78	3.56	4.23	5.02	5.29
FEM	f (Hz)	2.34	2.54	3.61	4.40	5.30	5.57
	Error (%)	-2.1	8.6	-1.4	-3.9	-5.3	-5.0

From Table 54, Table 55, Table 56 and Table 57, it is clear that the frequency response in the direction of the transversal one shows the greater sensitivity to the formation of the excavation. Transversally (Mode 2 and Mode 5 in the tables), the analytical model is more sensitive than the real structure, with a percentage variation of approximately 21%. The third frequency, associated with the second flexural mode, decreases in percentage terms almost the same quantity, while all the other analytical frequencies are less affected by the removal of soil around the piers than those measured experimentally.

Finally, a sensitivity analysis is conducted to see how the model frequencies vary with the excavation depth. Simulations are repeated on the Sap2000 software, removing the springs of the soil around the piers every meter of depth. For the first two frequencies the results are shown in Figure 5.17. The graphs also show the three points corresponding to the experimental tests; The depths are taken positive from the extrados of the pile cap downwards.

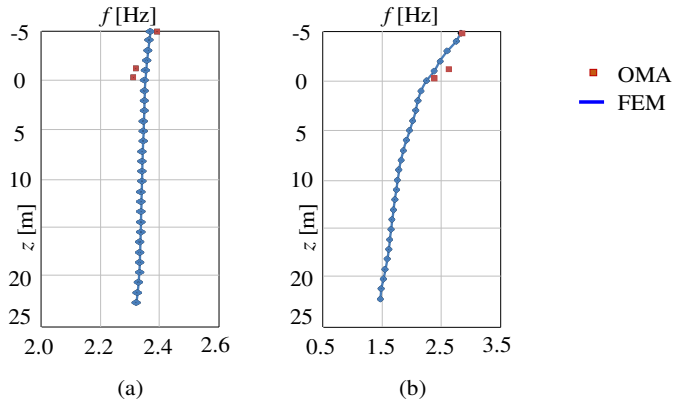

Figure 5.17 Sensitivity study of frequency variance according to the excavation depth (a) First bending mode; (b) First transversal mode

5.3.3. Rocking foundation of piers, for different steps

Displacements of the modelled pier were evaluated in correspondence with those measured in the two steps; for each of them the rotation of the pier was also investigated, to evaluate the compliance with the experimental data.

For the model, the configuration show in Figure 5.18 is considered.

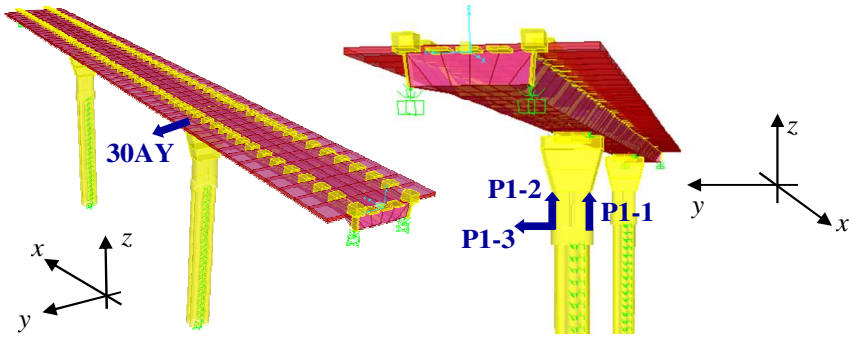

Figure 5.18 Configuration layout of P1 in "Cesano bridge": (a) global view, (b) detail of one pier

Displacements, derived from modal analysis, reported in Table 58, Table 59 and Table 60 are normalized with respect to the maximum displacement, always occurring at the pier top (sensor Y4); moreover, in the columns to the right of the table are reported the values of the displacements caused by the foundation rocking and the component due to piers deflection (as shown in the scheme of Figure 5.19)

In Step1, the piers dimension are H = 3.95 m and B = 3.05 m, so (2·H/B) = 2.5902 and the rigid displacements of the transverse foundation rocking is Y = 2.5902·(P1-1)

Table 58. Analytical displacements of P1 "Cesano bridge" – Step1

f (Hz)	P1-1	P1-2	P1-3	30AY	Y	30AY - Y - (P1-3)
2.92	0.10	-0.11	0.13	1.00	0.26	0.61
5.44	0.09	-0.10	0.14	1.00	0.23	0.63

In Step2, the piers dimension are H = 7.80 m and B = 3.05 m, so (2·H/B) = 5.1148 and the rigid displacements of the transverse foundation rocking is Y = 5.1148·(P1-1)

Table 59. Analytical displacements of P1 "Cesano bridge" – Step2

f (Hz)	P1-1	P1-2	P1-3	30AY	Y	30AY - Y - (P1-3)
2.30	0.07	-0.06	0.08	1.00	0.36	0.56
5.27	0.06	-0.05	0.06	1.00	0.31	0.63

In Step3, the piers dimension are H = 9.20 m and B = 3.05 m, so (2·H/B) = 6.0328 and the rigid displacements of the transverse foundation rocking is Y = 6.0328·(P1-1)

Table 60. Analytical displacements of P1 "Cesano bridge" – Step3

f (Hz)	P1-1	P1-2	P1-3	30AY	Y	30AY - Y - (P1-3)
2.30	0.07	-0.06	0.08	1.00	0.42	0.50
5.27	0.06	-0.05	0.06	1.00	0.36	0.58

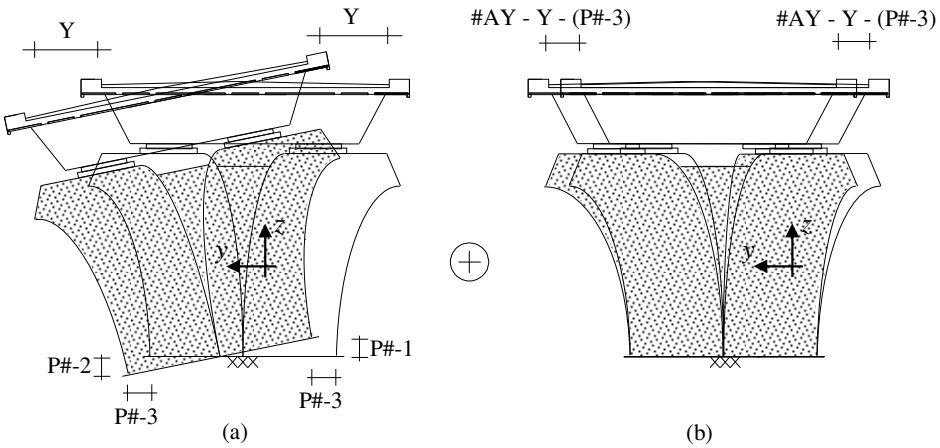

Figure 5.19 Contributions to the modal displacements “Cesano bridge”: (a) foundation rigid translation and rocking and (b) pier deflection

Table 58, Table 59, Table 60 and Figure 5.19 clearly show that in the case of an underground foundation (Step1) the effect of rocking foundation is greater to Step1, the results are consistent with the experimental data.

Chapter 6.
Comparison of experimental and numerical modal parameters

In this section results of AVTs are presented in terms of fundamental structural frequencies, modal damping ratios and mode shapes, providing comparisons with those obtained from the developed numerical model. In particular, modal parameters obtained from the FB, CB-P, CB-P&C and CB-CONV models will be presented and commented. KCs are separated by expansion joints but interact each other through piers to which they are connected; thus, the viaduct presents transverse fundamental mode shapes that involves deflections of all KCs. However, depending on the fundamental frequency, mode shapes are characterised by displacements amplitudes which differ sensibly from one KC to another. Actually, each KC tends to develop its proper fundamental frequencies and mode shapes, which are unavoidably altered by the other chains; consequently, greater modal displacements will be observed for a specific KC in correspondence of its proper frequencies, which in the sequel will be referred to as fundamental frequencies of the chain. Figure 6.1a shows for each KC the normalised mean amplitude of transverse displacements measured above piers at the deck level, obtained from the steady-state analysis of the CB-P&C model. For each KC, the highest amplitude peaks are clearly evident in correspondence of the relevant chain fundamental frequencies. In addition, as expected, the interaction of the *i*-th KC is revealed by the presence of lower response peaks also in the response of the other KCs. Three fundamental frequencies are highlighted in Figure 6.1a for each KC, referred to mode 1, 2 and 3 of the relevant KC for sake of simplicity; these will be used in the sequel to compare experimental and numerical mode shapes. Figure 6.1b shows the stabilization diagrams (where continuous lines are the average of cross power spectrum density of sensors positioned on the KCs) obtained from the OMA, used to identify the viaduct fundamental frequencies. It can be observed that the experimental response is consistent with the numerical one; in particular, peaks in the stabilization diagrams are almost aligned with the numerical ones for each KC, as highlighted by vertical dotted lines (different colours are used for the KCs). Furthermore, also the measured relative amplitude of peaks at different frequencies is almost reproduced by the numerical model for all the KCs, with minor differences for what concern the first peaks of KC1.

The response of the less refined finite element models (FB, CB-CONV and CB-P) are not reported in Figure 6.1a since their response is sensibly different from the measured one in terms of fundamental frequencies. Results from these models will be presented below in terms of frequencies and mode shapes. In details, frequencies and mode shapes are

determined from steady-state analyses for model CB-P and from modal analysis for models FB and CB-CONV since the latter constitutes classically damped.

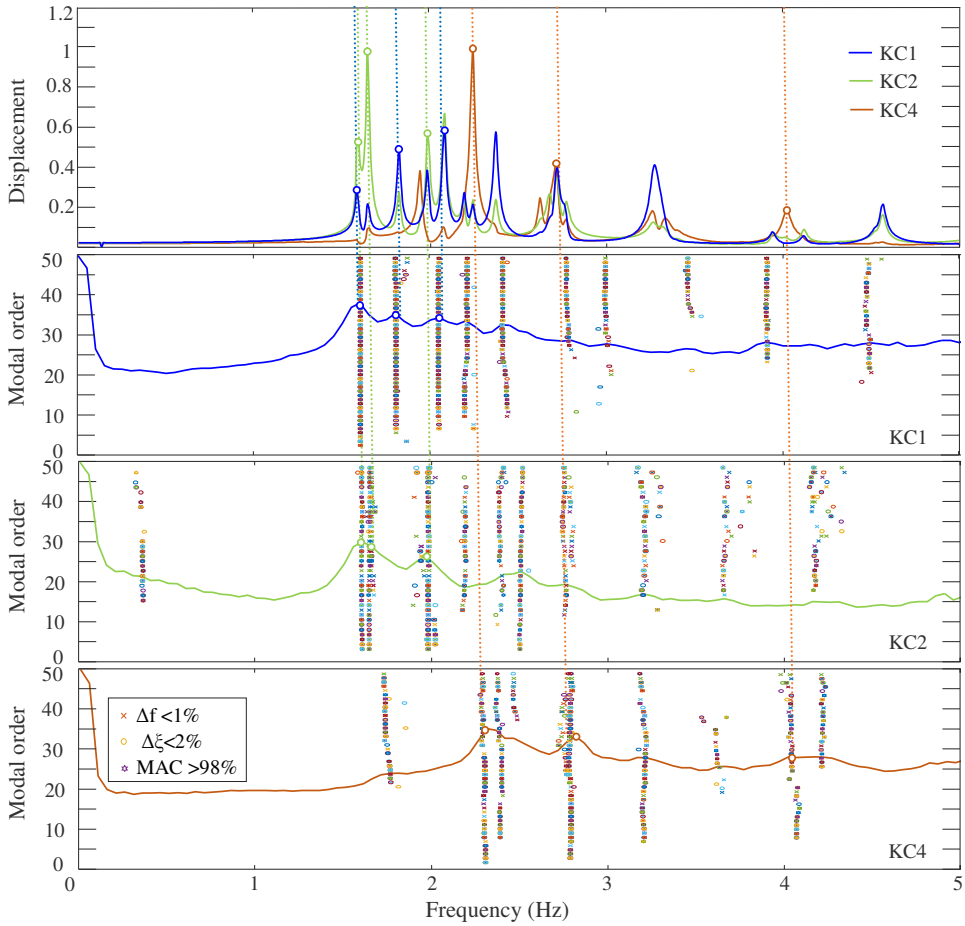

Figure 6.1 (a) Mean displacement amplitudes obtained from the CB-P&C model; (b) stabilization diagrams of KC1, KC2 and KC4

Table 61 compares the selected three fundamental structural frequencies obtained from the AVTs through the OMA and from the developed numerical models, differently accounting the SSI problem. Fundamental frequencies obtained from the FB model are also reported as well as the percentage error of each numerical estimation with respect to the experimental one, which is assumed to be the target. It can be observed that frequencies resulting from the FB model are sensibly higher than the experimental ones; thus, the model appears not able to capture the actual viaduct dynamic behaviour. On the other hand, frequencies obtained from the CB-CONV are always lower than the experimental ones, also suggesting that a conventional simplified analysis of the SSI phenomena is not sufficient to adequately capture the actual bridge dynamics. The CB-P and the CB-P&C models better reproduce the

experimental data; in details, results of the CB-P&C model are the best ones, with relative errors always below 1% (excepting mode 3 of KC2). Finally, trends of frequencies with respect to the different models, reflect the expected degree of restraints exerted by the soil-foundation system (depending on how it is modelled).

Table 61. Comparison of experimental and numerical fundamental frequencies of "Chiaravalle viaduct"

KC#	Mode	OMA		CB-P&C		CB-P		FB		CB-CONV	
		f (Hz)	ξ (-)	f (Hz)	Δf (%)	f (Hz)	Δf (%)	f (Hz)	Δf (%)	f (Hz)	Δf (%)
1	1	**1.61**	0.57	1.60	-0.6	1.57	-2.5	1.71	5.8	1.42	-13.4
	2	**1.81**	1.91	1.83	1.1	1.78	-1.7	1.87	3.2	1.61	-12.4
	3	**2.05**	1.78	2.08	1.4	1.98	-3.5	2.14	4.2	1.76	-16.5
2	1	**1.58**	0.93	1.59	0.6	1.56	-1.3	1.62	2.5	1.42	-11.3
	2	**1.66**	0.43	1.66	0.0	1.61	-3.1	1.71	2.9	1.69	1.8
	3	**1.98**	0.6	2.03	2.5	1.96	-1.0	2.14	7.5	1.88	-5.3
3	1	**2.26**	0.42	2.26	0.0	2.23	-1.3	2.41	6.2	1.76	-28.4
	2	**2.79**	0.27	2.79	0.0	2.66	-4.9	2.84	1.8	2.05	-36.1
	3	**4.04**	0.21	4.04	0.0	4.02	-0.5	4.28	5.6	3.34	-21.0

Figure 6.2 compares the three transverse mode shapes previously selected for KC1, KC2 and KC4, obtained from the experimental tests and the numerical models. Since AVTs are performed separately for each KC, mode shapes of each bridge segment is normalised with respect to its relevant maximum transverse displacement. Experimental data are reported with dots connected with black lines while continuous coloured lines are used for the results of the different numerical models. It can be observed that both the CB-P and the CB-P&C models are able to adequately capture the experimental mode shapes, even if the best results are clearly obtained from the most sophisticated model (CB-P&C) for which numerical and experimental mode shapes are practically superimposed, with slight differences in the case of mode 2 of KC2. On the contrary, the FB and CB-CONV models are not able to interpret all the experimental mode shapes, with particular reference to modes 2 and 3 of KC1 and KC2. It is worth mentioning that the effect on the mode shapes due to the wall pier (P5) of KC2 (reported with a black filled dot in Figure 6.2) induces very low modal transverse displacements.

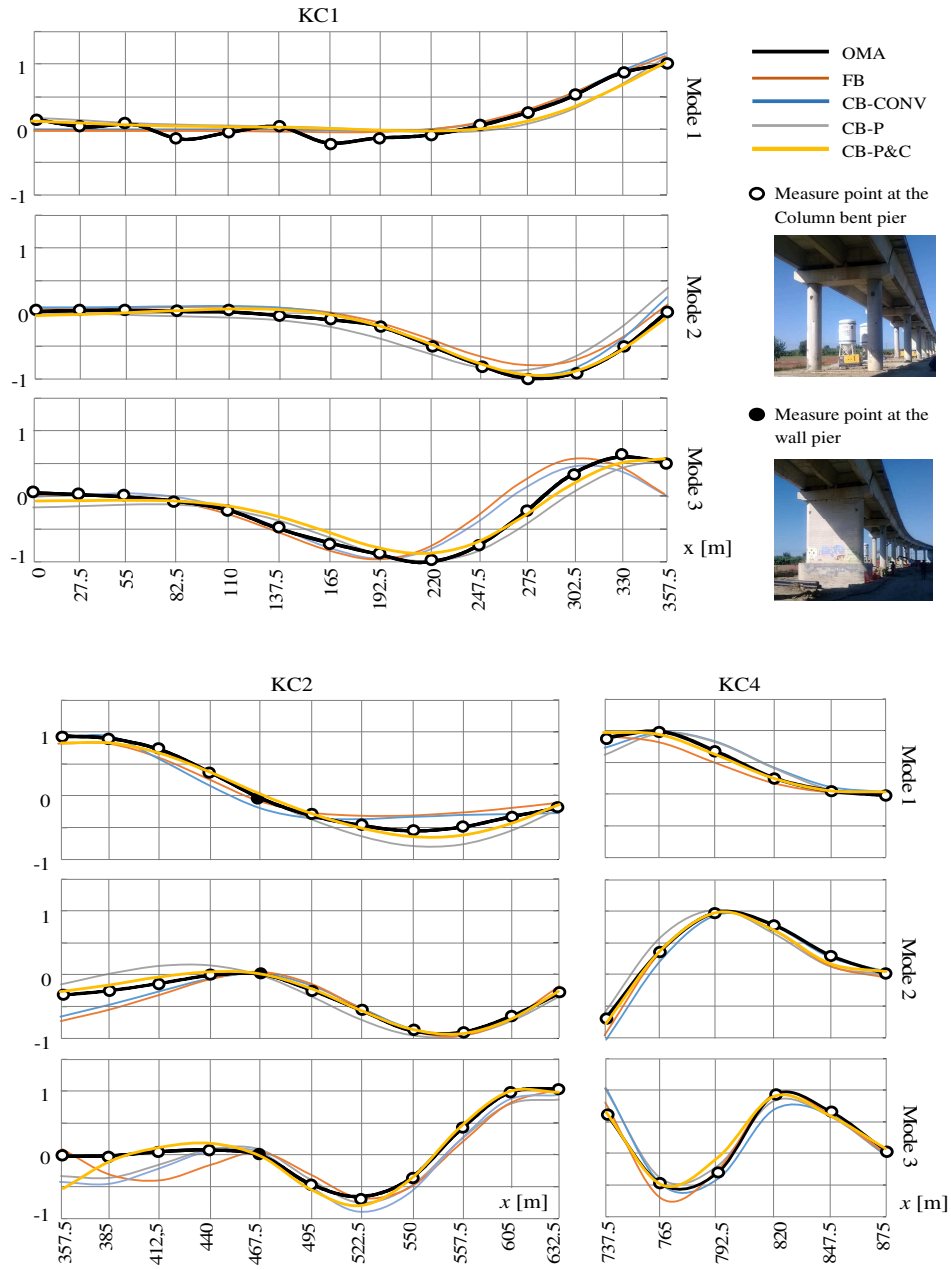

Figure 6.2 Comparison of numerical and experimental mode shapes

With reference to the transverse behaviour, some tests are performed in correspondence of one or more piers, measuring accelerations of the foundation cap (both translational and rotational components) and the pier bent, in order to identify contribution to the transverse modal displacement due to the elastic deflection of the pier and the foundation rocking.

As regards “Chiaravalle viaduct”, the transversal mode of KC1 that involving the pier P3 (for example at frequency of 2.46 Hz) and the displacements at correspondence frequency (2.48 Hz) are represented in Figure 6.3

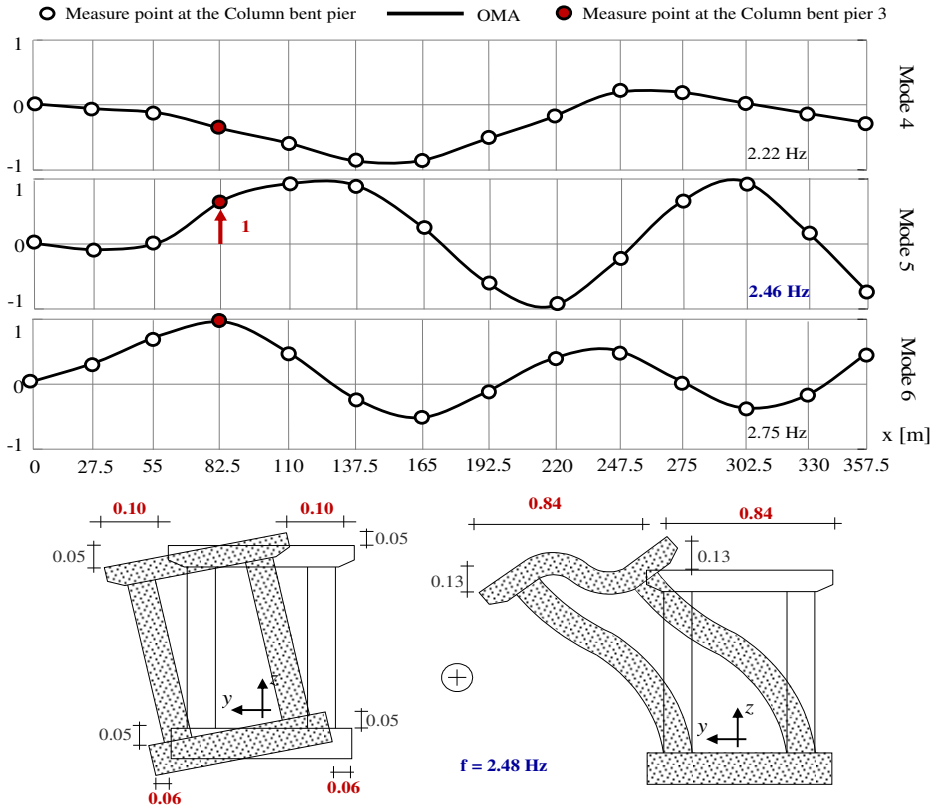

Figure 6.3 Modal displacements of pier P3 in “Chiaravalle viaduct”

About “Paglia bridge” (Orvieto), the comparisons between analytical and experimental results are summarized in Table 62

Table 62. Comparison of experimental and numerical fundamental frequencies of “Orvieto bridge”

	Mode	***1***	***2***	***3***	***4***	***5***	***6***	***7***
OMA	*f* (Hz)	1.14	1.52	1.89	2.39	2.53	3.32	3.54
FEM	*f* (Hz)	1.29	1.37	2.12	2.41	2.57	3.45	3.60
	Error (%)	11.6	9.9	10.8	0.01	0.02	0.04	0.02

As regards the foundation rocking of “Orvieto bridge”, the transversal mode that involving the pier P1 (for example at frequency of 2.53 Hz) and the displacements at correspondence frequency (2.53 Hz) are represented in Figure 6.4.

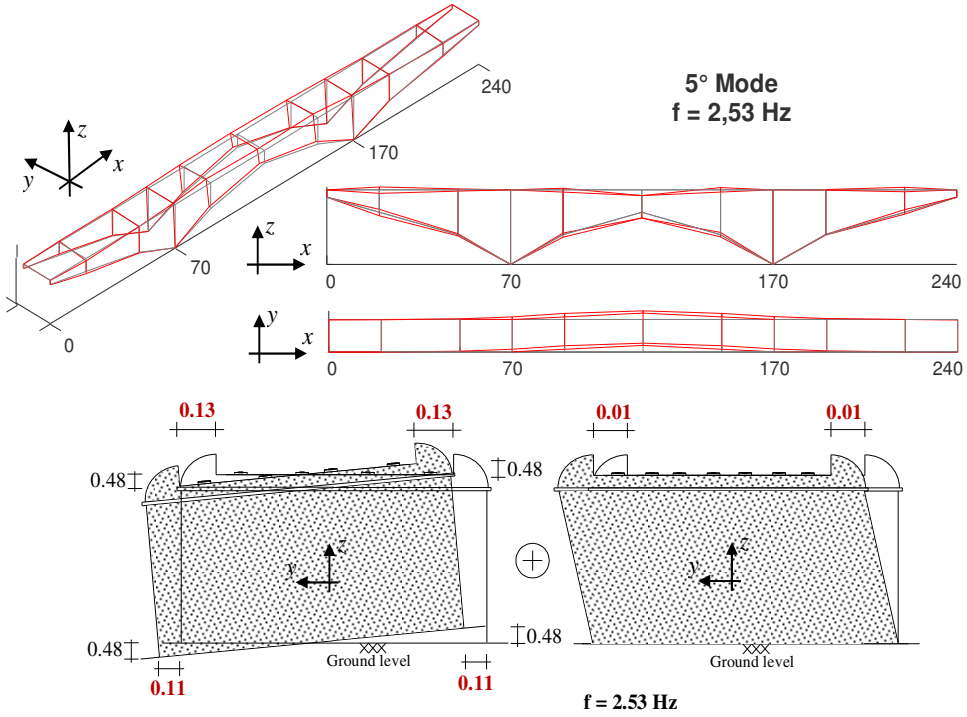

Figure 6.4 Modal displacements of pier P1 in “Orvieto bridge”

The component of the remaining translation is caused by the deflection of the deck as evidenced by the experimental tests.

For “Cesano bridge” (Corinaldo), the comparisons between analytical and experimental results are summarized in Table 63 for each step

Table 63. Comparison of experimental and numerical fundamental frequencies of “Cesano bridge”

		Mode	*1*	*2*	*3*	*4*	*5*	*6*
	OMA	*f* (Hz)	2.40	2.90	3.95	4.36	5.45	5.64
Step1	***FEM***	*f* (Hz)	2.37	2.92	3.72	4.44	5.44	5.66
		Error (%)	1.3	-0.7	5.8	-1.8	0.2	-0.4
	OMA	*f* (Hz)	2.31	2.68	3.81	4.18	4.93	5.29
Step2	***FEM***	*f* (Hz)	2.34	2.45	3.60	4.40	5.29	5.55
		Error (%)	-1.3	8.6	5.5	-5.0	-6.8	-4.7
	OMA	f (Hz)	2.30	2.42	3.81	4.19	4.84	5.14
Step3	***FEM***	f (Hz)	2.34	2.30	3.58	4.41	5.27	5.52
		Error (%)	-1.7	5.0	6.0	-5.0	-8.2	-6.9
	OMA	f (Hz)	2.29	2.78	3.56	4.23	5.02	5.29
Step4	***FEM***	f (Hz)	2.34	2.54	3.61	4.40	5.30	5.57
		Error (%)	-2.1	8.6	-1.4	-3.9	-5.3	-5.0

As regards the foundation rocking of “Cesano bridge”, the transversal mode that involving the pier P1 (for example at frequency of 2.90 Hz) and the displacements at correspondence frequency (2.90 Hz) are represented in Figure 6.5 for step1

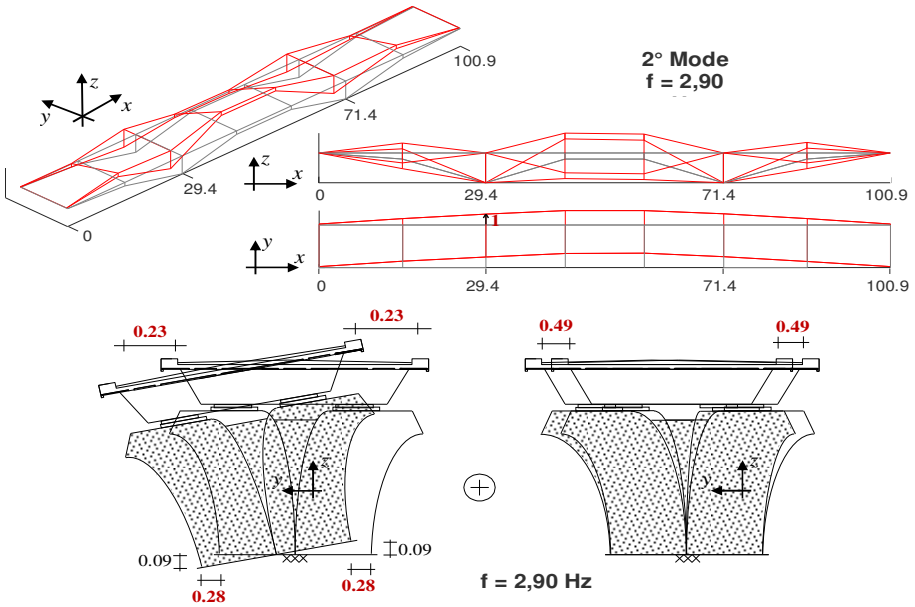

Figure 6.5 Modal displacements of pier P1 in “Cesano bridge”

Conclusions

The significance of soil-structure interaction in the interpretation of vibrational tests performed on bridges has been discussed in this work, with reference to the Chiaravalle viaduct, linking the SS76 with the airport of Ancona (in Central Italy). On this viaduct, detailed experimental campaigns and surveys on both the soil deposit and the superstructure were available for the need of a seismic upgrading of the structure. In detail, a very high level of knowledge about the geometry of structural components and mechanical properties of materials was achieved. A conventional fixed base, as well as numerical models accounting for the soil-foundation compliance with different level of sophistication, are developed to interpret the experimental data. The soil-structure interaction is always included through the sub-structure approach, simulating the frequency-dependent soil-foundation impedances through lumped parameter models. Models accuracy in reproducing the experimental modal parameter are evaluated on the basis of both fundamental frequencies and mode shapes. The following main conclusions can be drawn:

- the numerical models accounting for the soil-structure interaction in a rigorous way, namely including the pile-soil-pile and the soil-pile cap interactions as well as the hysteretic and radiation problems can adequately capture the measured dynamics of the viaduct;
- with respect to the experimental data, only the numerical model addressing the soil-structure interaction problem in a comprehensive way, i.e. also including the soil-pile-cap interaction, provides errors lower than 1% in the estimation of the fundamental frequencies of the viaduct and almost perfectly matching mode shapes;
- the conventional fixed base model or the model implementing the foundation compliance exploiting the beam-on-Winkler foundation approach for piles revealed not able to capture the viaducts frequencies with errors lower than about 15% for KC1 and KC2 and about 35% for KC4. In addition, mode shapes presents important inaccuracies with respect to the experimental ones, especially for higher frequencies.

Overall, the presented case study demonstrates that the common practice of calibrating and updating numerical finite element models to fit experimental results from ambient vibration tests by only changing the mechanical properties of materials (to account for heterogeneity and ageing effects) should be carefully evaluated for the case of bridges. In this case, the soil-structure interaction effects may significantly affects the dynamics of structure, especially in the case of soft or medium soil deposits.

Some notable aspects concerning the contribution of Soil-Structure Interaction (SSI) on the measured dynamic response of the different viaducts subjected to ambient excitations have been shown in this work. Ambient vibration tests are performed on the viaduct in order to evaluate the actual modal properties of the structure to be used for the calibration of a

reliable numerical model for the retrofit design of the bridge. Besides conventional tests aimed to evaluating the overall transverse, torsional and vertical vibration modes of the deck, un-conventional identification tests have been performed on a selected bridge pier in order to assess the contribution of SSI on the modal displacements. It was found that SSI sensibly affects the dynamics of the bridge, even for low intensity actions, contributing to the 10% of the overall modal displacement of the deck in the case of "Chiaravalle viaduct". For the case of "Cesano bridge" the SSI contribute for 23÷42% and finally it provides about 13% for the case of "Paglia bridge" that has two wall piers.

Results of tests, in terms of fundamental frequencies and mode shapes, have been compared with those resulting from a 3D refined finite element model of the bridge. In order to accurately capture the measured response a numerical model incorporating SSI phenomena was necessary; the model, suitably calibrated was able to accurately predict the dynamic behaviour of the bridge subjected to ambient vibrations.

References

Behmanesh, Moaveni B, Papadimitriou C. Probabilistic damage identification of a designed 9-story building using modal data in the presence of modelling errors. Engineering Structures 2016.

Cabboi A, Magalhães F, Gentile C, Cunha A. Automated modal identification and tracking: Application to an iron arch bridge. Struct. Control Health Monit. 2017; 24: e1854.

Cantieni R. Experimental methods used in system identification of civil engineering structures. Proc. 1st Int. Operational Modal Analysis Conf., Copenhagen, Denmark, pp. 249-260, 2005.

Capatti MC, Tropeano G, Morici M, Carbonari S, Dezi F, Leoni G, Silvestri F. Implications of non-synchronous excitation induced by nonlinear site amplification and soil-structure interaction on the seismic response of multi-span bridges founded on piles. Bulletin of Earthquake Engineering 2017; 15(11): 4963-4995.

Carbonari S, Dezi F, Leoni G. Seismic soil-structure interaction in multi-span bridges: application to a railway bridge. Earthquake Engineering and Structural Dynamics 2011; 40(11): 1219-1239.

Carbonari S, Morici M, Dezi F, Gara F, Leoni G. Soil-structure interaction effects in single bridge piers founded on inclined pile groups. Soil Dynamics and Earthquake Engineering 2017; 92: 52-67.

Carbonari S, Morici M, Dezi F, Leoni G. A Lumped Parameter Model for Time-Domain Inertial Soil-Structure Interaction Analysis of Structures on Pile Foundations. Earthquake Engineering and Structural Dynamics 2018; 47(11): 2147-2171.

Chen GW, Omenzetter P, Beskhyroun S. Operational modal analysis of an eleven-span concrete bridge subjected to weak ambient excitations. Engineering Structures 2017; 151, 839–860.

Cunha A, Caetano E. Experimental Modal Analysis of Civil Engineering Structures. Sound and vibration; 2006.

DeSalvo GJ, Swanson JA. ANSYS Engineering Analysis System User's Manual. Houston, Pa.: Swanson Analysis Systems, 1985.

Dezi F, Carbonari S, Morici M. A numerical model for the dynamic analysis of inclined pile groups. Earthquake Engineering & Structural Dynamics 2016; 45(1), pp. 45-68.

Dezi F, Carbonari S, Tombari A, Leoni G. Soil-structure interaction in the seismic response of an isolated three-span motorway overcrossing founded on piles. Soil Dynamics and Earthquake Engineering 2012; 41: 151-163.

Dohler E, Reynders F, Magalhaes et al. Pre- and Post - identification Merging for Multi-Setup OMA with Covariance-Driven SSI. Dynamics of Bridges 2010; Vol. 5, pp. 55-70.

Elgamal A, Yan L, Yang Z, Conte JP. Three-dimensional seismic response of Humboldt Bay bridge-foundation-ground system. Journal of Structural Engineering ASCE 2008; 134(7): 1165-76.

Faraonis P, Sextos A, Chatzi E, Zabel V. Model updating of a bridge-foundation - soil system based on ambient vibration data. UNCECOMP 2015, 1st ECCOMAS Thematic Conference on International Conference on Uncertainty Quantification in Computational Sciences and Engineering, Papadrakakis M, Papadopoulos V, Stefanou G (eds.) Crete Island, Greece, 25–27 May 2015.

Foti D, Gattulli V, Potenza F. Output-Only Identification and Model Updating by Dynamic Testing in Unfavorable Conditions of a Seismically Damaged Building. Computer-Aided Civil and Infrastructure Engineering 2014; 29, 659-675.

Kappos AJ, Manolis GD, Moschonas IF. Seismic assessment and design of R/C bridges with irregular configuration, including SSI effects. International Journal of Engineering Structures 2002; 24(10):1337–48.

Li Y, Astroza R, Conte JP, Soto P. Nonlinear FE model updating and reconstruction of the response of an instrumented seismic isolated bridge to the 2010 Maule Chile earthquake. Earthquake Engineering & Structural Dynamics 2017; 46:2699–2716.

Luco JE, Trifunac MD and Wong HL. Isolation of soil-structure interaction effects by full-scale forced vibration tests. Earthquake Engineering & Structural Dynamics 1988; vol. 16, 1-21.

Lupoi A, Franchin P, Monti G, Pinto PE. Seismic design of bridges accounting for spatial variability of ground motion. Earthquake Engineering and Structural Dynamics. 2005; 34, 327-348.

Magalhães F, Cunha A. Explaining operational modal analysis with data from an arch bridge. 2011; 1431-1450. Mechanical System and Signal Processing.

Makris N, Gazetas G. Dynamic pile□soil□pile interaction. Part II: Lateral and seismic response. Earthquake Engineering & Structural Dynamics 1992; 21: 145-162.

MATLAB, The MathWorks, Inc., Natick, Massachusetts, United States.

Mirshafiei F, McClure G. Modified three-dimensional seismic assessment method for buildings based on ambient vibration tests: extrapolation to higher shaking levels and measuring the dynamic amplification portion of natural torsion. Earthquake Engineering & Structural Dynamics 2016; 45:2011-2026.

Mylonakis G, Gazetas G. Seismic soil structure interaction: Beneficial or detrimental? Journal of Earthquake Engineering 2000; Vol. 4(3), pp. 277-301.

Mylonakis G. Elastodynamic model for large-diameter end-bearing shafts. Soil and Foundations 2001; 41(3): 31-44.

Omenzetter P, Beskhyroun S, Shabbir F, Chen GW, Chen X, Wang S, Zha A. Forced and ambient vibration testing of full scale bridges. A report submitted to Earthquake Commission Research Foundation (Project No. UNI/578), 2013

Omenzetter P, Butt F. Updating of an instrumented building model considering amplitude dependence of dynamic resonant properties extracted from seismic response records. Struct. Control Health Monit. 2016; 23:598–620.

Overschee V, De Moor B. Subspace identification for linear systems. Kluwer Academic Publishers, Leuven, Belgio, 1996.

Polanco NR, May G, Hernandez EM. Finite element model updating of semi-composite bridge decks using operational acceleration measurements. Engineering Structures 2016; 126, 264–277.

Prendergast LJ, Hester D, Gavin K. Determining the presence of scour around bridge foundations using vehicle-induced vibrations. J. Bridge Eng. 2016; 21(10): 04016065.

Rainieri C, Fabbrocino G, Manfredi G, Dolce M. Robust output-only modal identification and monitoring of buildings in the presence of dynamic interactions for rapid post-earthquake emergency management. Engineering Structures 2012; 34, 436–446.

Regni M, Arezzo D, Carbonari S, Gara F, Zonta D. Effect of Environmental Conditions on the Modal Response of a 10-Story Reinforced Concrete Tower. Shock and Vibrations 2018; vol. 2018, Article ID 9476146, 16 pages.

Roesset JM, Angelides D. Dynamic stiffness of piles; Numerical Methods in Offshore Piling. 1980; 75–82. London: Institution of Civil Engineers.

Şafak E. Detection and Identification of Soil-Structure Interaction in Buildings from Vibration Recordings. Journal of Structural Engineering 1995; 121(5), 899-906.

Sextos AG, Pitilakis KD, Kappos AJ. Inelastic dynamic analysis of RC bridges accounting for spatial variability of ground motion, site effects and soil-structure interaction phenomena. Part 1: Methodology and analytical tools. Earthquake Engineering and Structural Dynamics 2003; 32(4): 607-27.

Sextos AG, Pitilakis KD, Kappos AJ. Inelastic dynamic analysis of RC bridges accounting for spatial variability of ground motion, site effects and soil-structure interaction phenomena. Part 2: Parametric study. Earthquake Engineering and Structural Dynamics 2003; 32(4): 629-52.

Trifunac MD, Todorovska MI, Hao TY. Full-Scale experimental studies of soil-structure interaction. Proc. 2nd U.S. - Japan Workshop on Soil-Structure Interaction, 2001, Tsukuba City, Japan.

Ubertini F, Comanducci G, Cavalagli N, Pisello AL, Materazzi AL, Cotana F. Environmental effects on natural frequencies of the San Pietro bell tower in Perugia, Italy, and their removal for structural performance assessment. Mechanical Systems and Signal Processing 2017; 82, 307–322.

Wolf JP. Soil-structure interaction analysis in time domain. Prentice-Hall, Englewood Cliffs, N.J. 1988.

Xia Y, Chen B, Weng S, Ni YQ, Xu YL. Temperature effect on vibration properties of civil structures: a literature review and case studies. Journal of Civil Structural Health Monitoring 2012; Vol. 2, No. 1, pp. 29-46.

Xu YL, Chen B, Ng CL et al. Monitoring temperature effect on a long suspension bridge. Structural Control and Health Monitoring 2010; Vol. 17, pp. 632-653.

Zhang J, Prader J, Grimmelsman KA, Moon F, Aktan AE, Shama A. Experimental Vibration Analysis for Structural Identification of a Long-Span Suspension Bridge. Journal of engineering mechanics, 2013.

Zonta D, Glisic B, Adriaenssens S. Value of information: impact of monitoring on decision-making. Struct. Control Health Monit. 2014; 21:1043–1056.